

https://dspace.org/

Development of complex shaped alumina parts by gelcasting and additive manufacturing

Ndinisa, Sindi Sithembiso

2019

https://hdl.handle.net/10539/29363

Ndinisa, Sindi Sithembiso (2019) Development of complex shaped alumina parts by gel casting and additive manufacturing, University of the Witwatersrand, Johannesburg, https://hdl.handle.net/10539/29363

Downloaded from a DSpace repository. https://dspace.org/

DEVELOPMENT OF COMPLEX SHAPED ALUMINA PARTS BY GELCASTING AND ADDITIVE MANUFACTURING

Sindi Sithembiso Ndinisa

A dissertation submitted to the Faculty of Engineering and the Built Environment, University of the Witwatersrand, Johannesburg, in fulfilment of the requirements for the degree of Master of Science in Engineering.

Johannesburg 2019

DECLARATION

I declare that this dissertation is my own unaided work. It is being submitted for the Degree of Master of Science in Engineering in the University of the Witwatersrand, Johannesburg. It has not been submitted before for any degree or examination in any other University.

_____

(Signature of candidate)

19th day of September 2019.

ABSTRACT

Gelcasting is a fabrication method for achieving near net shape of complex alumina parts capable of high performance. The processes used in gelcasting are similar to processes often used in conventional ceramic forming process. However, the relative high costs involved in the fabrication of non-porous moulds required by the process makes it uneconomical for new developments and low volume productions. In this study, an inexpensive and efficient way involving negative additive manufacturing and gelcasting was used to achieve the fabrication of complex geometries of alumina parts that cannot be formed by conventional methods. Additive manufacturing through fused deposition modelling of ABS filament was used to produce moulds for investment casting. Low toxicity monomers were identified and from these, the rheological behaviour of suspensions was optimized to successfully fabricate complex geometries by ensuring satisfactory mould filling. The suspension contained a ceramic powder, dispersing medium and organic monomers was poured into the non-porous ABS mould and a gel formed. The mould was then dissolved away in acetone to obtain the complex shaped part. Different complex geometries of alumina with near full densities (≤99.6%RD) were achieved using a 40vol% solids loading and 0.3wt% co-polymer of Isobutylene and maleic anhydride monomer system. This fabrication process enables low cost production of complex shaped alumina parts. The alumina components produced exhibited properties similar to those that are produced using traditional processing techniques. The ceramic components had relative densities up to 99%.The hardness and fracture toughness were measured to be 18GPa and 3.8MPa.√m respectively after pressure-less sintering at 1650°C in air for 3hrs.

ACKNOWLEDGEMENTS

There were a great deal of people who have given me support and advice; without it, this dissertation would not have been possible.

- Many thanks go to my advisors, Dr. David J. Whitefield and Prof. Iakovos Sigalas.
- DST-NRF Centre of Excellence in Strong Materials and Prof Sigalas for providing me with the funding.
- Lukas Janse van Renseberg for 3D printing the moulds for this work and helping with the building of an environmental chamber.
- Thanks to Dr. Patrick Rockebrand and Dr. Nthabiseng Ntholeng.
- Thank you to the undergraduate students who assisted with some of the experimental work and helped me exercise my leadership skills.
- Thanks to the School of Chemical and Metallurgy (CHMT) for assistance.

DEDICATION

To my family

I greatly appreciate your encouragement, words of advice and prayers. My gratitude is undying for your constant support and belief in me.

Mzomba, Msibekeli

CONTENTS

ABSTRACT ii

ACKNOWLEDGEMENTS iii

CONTENTS v

LIST OF FIGURES ix

LIST OF TABLES xiii

NOMENCLATURE xv

Chapter 1 : Introduction 1

1.1. Background 1

1.2. Research Motivation 3

1.3. Aims and Objectives 4

1.4. Hypothesis and Limitations 5

1.5. Scope 6

1.6. Dissertation Outline 7

Chapter 2 : Literature Review 8

2.1. Overview 8

2.2. Ceramic Processing 12

2.3. Powder Forming 13

2.4. Colloidal forming methods 14

2.5. Gelcasting 15

2.6. Monomer Systems 16

2.7. Fabrication tooling/ Casting process 19

2.7.1. Additive Manufacturing 20

2.8. Sintering of ceramics 21
2.9. Summation of literature review 26
Chapter 3 : Experimental Procedure 27
3.1. Powder Characterisation 28
3.2. Gelcasting Process 29
3.2.1. Preparation of ceramic suspension 30
3.2.2. Milling / Mixing 34
3.2.3. Rheological Studies 35
3.2.4. De-airing 35
3.3. Net-shape Forming 36
3.3.1. Mould Design 36
3.3.2. Casting 38
3.4. Drying 38
3.5. Sintering & Binder burn-out 39
3.6. Characterisation Techniques 41
3.6.1. Density Determination 41
3.6.2. Sample Preparation 42
3.6.3. Mechanical Testing 43
3.6.4. Field Emission Scanning Electron Microscope (FE-SEM) 47
3.6.5. Grain size measurements 47
Chapter 4 : Results 48
4.1. Powder Characterisation 48
4.1.1. Particle Size Analysis 48
4.1.2. Scanning Electron Microscope 49

4.1.3. Powder X-Ray Diffraction 51
4.2. Optimisation of Slurry 51
4.2.1. Zeta Potential 52
4.2.2. Dispersant amount 54
4.2.3. Viscosity-Shear Relationship 56
4.3. Additive Manufacturing of Moulds and Casting 64
4.4. Gelation and Demoulding 67
4.5. Drying of Green Bodies 68
4.5.1. Shrinkage 69
4.1. Sintering and Characterisation 70
4.1.1. Effect of Sintering Temperature 70
4.1.2. Effect of Solids Loading 74
4.1.3. Effect of Monomer / Gel-Binder System 78
4.1.4. De-airing 81
4.1.5. Grain Growth Inhibitors 83
4.2. Complex Shaped Parts 86
4.3. Mechanical Behaviour 89
4.3.1. Hardness and Fracture Toughness 89
4.3.2. Transverse Rapture Strength 94
4.3.3. Fracture 97
Chapter 5 : Discussion 99
5.1. Powder Preparation 100
5.2. Preparation of Suspensions 100
5.2.1. Optimal Dispersion 101

5.2.2. Zeta potential 102
5.2.3. Viscosity- shear relationship 103
5.2.4. Effect of Monomer 105
5.3. Near Net Shape Forming 107
5.4. Optimization of sintering 109
5.4.1. Factors affecting densification 109
5.5. Mechanical Properties 112
5.5.1. Hardness 112
5.5.2. Fracture Toughness 113
5.5.3. Transverse Rupture Strength 114
Chapter 6 : Conclusion 117
Chapter 7 : Future Work 120
References 121
Appendices 129

LIST OF FIGURES

Figure 2-1: Ceramic forming techniques. 13
Figure 2-2: Stages of densification during solid state sintering of ceramics (26)..... 22
Figure 3-1: Gelcasting process (44) 29
Figure 3-2: Slurry preparation with HEMA-MBAM system..... 31
Figure 3-3: Slurry preparation using Isobam® system. 32
Figure 3-4: Slurry preparation using PVA-DHF system. 33
Figure 3-5: The process of 3D printing moulds [Lukas Janse van Renseburg]. 36
Figure 3-6: Photograph of a) ABS resin and b) the Ultimaker 3D printer..... 37
Figure 3-7: Image showing a) an environmental chamber and b) its controls..... 39
Figure 3-8: Binder burn-out and sintering profile used. 40
Figure 3-9: The Vickers indentation technique results in cracks of width 2*c* and an indentation of width 2*a*. A side view of the crack system is shown on the left and a surface view is shown on the right (46). 43
Figure 3-10: The ball on three balls test setup (48). 46
Figure 4-1: Particle size distribution for alumina powder. 49
Figure 4-2: SEM characterisation of the starting powder. 50
Figure 4-3: X-ray diffraction analysis of the alumina powder..... 51
Figure 4-4: The measure of Zeta potential as a function of pH. 54
Figure 4-5: Effect of APAA concentration on the viscosity of 50vol% alumina suspensions at a shear rate of $10s^{-1}$. 55
Figure 4-6: Effect of Isobam® concentration on the viscosity of 60vol% alumina suspension at a shear rate of $10s^{-1}$..... 56
Figure 4-7: The viscosity of alumina suspensions with varied solids loading using 1vol% APAA as a dispersant..... 57
Figure 4-8: The viscosity of alumina suspensions with varied solids loading using 0.3wt% Isobam® as a dispersant. 57

Figure 4-9: Determination of Cross parameters, behaviour index and viscosity at very high shear rates, respectively. 60
Figure 4-10: Fitting of the Cross model to the viscosity shear rate relationship of alumina suspension prepared using 50vol% solids loading. 61
Figure 4-11: Linearisation and fit of the Reddy model to determine maximum solids loading. 63
Figure 4-12: Illustration of the tooling method showing the CAD file of the ABS 3D printed mould and the product of the mould design. 65
Figure 4-13: Images illustrating the capabilities of the process used to fabricate simple and complex shaped parts with differing thicknesses 66
Figure 4-14: Cracks initiated due to fast drying as an effect of acetone. 67
Figure 4-15: Mass loss during drying of the green cast parts in a controlled environmental chamber. 68
Figure 4-16: Relative density and porosity of Al_2O_3 parts after sintering at various temperatures for 3hrs for HEMA-MBAM/APAA system. 72
Figure 4-17: SEM micrographs of the ceramic sintered at: 1450°C , 1550°C, 1650°C and 1700°C for three hours in air. 73
Figure 4-18: SEM micrographs of sintered alumina gelcast using varied solids loading and HEMA-MBAM system, sintered at 1650°C. 76
Figure 4-19: SEM micrographs of parts produced by Isobam® using varied solids loading and sintered at 1650°C. 77
Figure 4-20: Illustration of the processing steps for different polymer / gel forming systems for casting alumina. 78
Figure 4-21: Effect of monomer system on the sintered relative density of alumina using 40vol% solids loading. 80
Figure 4-22: Illustration of the effect of de-airing a)Image showing bubbles as a result of insufficient de-airing (RD=87.58%) and b) SEM image showing sufficient de-airing with a microstructure with minimal defects (RD=98.61%) 82
Figure 4-23: The effect of deairing time on the relative density of gelcast alumina parts sintered at 1650°C. 83

Figure 4-24: SEM-EDS results for MgO doped gel cast alumina ceramic part and elemental analysis. 85
Figure 4-25: SEM image of MgO doped gel cast alumina part, sintered at 1650°C. . 85
Figure 4-26: Illustration of complex shaped parts produced, a) as demoulded 6-blade impeller and b) a dried solid pyramid showing markings as a result of the resolution on 3D printed moulds. 87
Figure 4-27: Complex shaped parts produced using Isobam® system and sintered at 1650°C for 3 hrs (3-blade and 6-blade impellers as well as a solid 4 sided pyramid). 87
Figure 4-28: Illustration of different pyramid shapes (solid and hollow pyramids) and sizes that were produced by gelcasting using 3D printed moulds. 88
Figure 4-29: Optical micrograph showing Vickers indentation and cracks radiating from the corners of the indent of the alumina using an indentation load of 5kgf. 90
Figure 4-30: Dependence of Vickers hardness to solids loading and monomer. 92
Figure 4-31: Relationship between Vickers hardness and relative density of gelcast alumina sintered at 1650°C for 3hrs. 93
Figure 4-32: Relationship of monomer and solids loading on the fracture toughness of alumina sintered at 1650°C for 3hrs. 93
Figure 4-33: Dependence of Vickers hardness and fracture toughness on the average grain size for alumina prepared with Isobam® at different solids loading and sintered at 1650°C. 94
Figure 4-34: Relationship between the probability of survival and the transverse rapture strength. The strength at a probability of 0.37 is shown. 95
Figure 4-35: Determination of the Weibull modulus using the relation in equation 4-8. 96
Figure 4-36: Fracture patterns of Al_2O_3 discs tested using the ball on three balls test assembly a) 40vol%, b)50vol% and c) 60vol% solids loading using Isobam® . The circles show the area of the fracture origin. 97

Figure 4-37: SEM micrographs showing the microstructure of 60 vol% , 50 vol%, 40 vol% and (A_HM) HEMA-MBAM fractured gel cast alumina sintered at 1650°C. 98
Figure 5-1: SEM micrograph showing a sample with large elongated grains. 110
Figure A-1: Determination of flow behaviour index 129
Figure A-2: Determination of Cross parameter, the viscosity at very high shear rates. 132

LIST OF TABLES

Table 2-1: Materials and properties of common ceramic materials and their applications [16]. 10
Table 2-2: Characteristics of an optimal processing method for advanced ceramics [1]. 11
Table 3-1: Materials used. 27
Table 3-2: The milling parameters used when mixing ceramic powder and pre-mix solutions. 34
Table 3-3: Materials used for fuse deposition modelling of gelcasting moulds [10].. 37
Table 4-1: Determination of Zeta potential at the measured pH value. 53
Table 4-2: Viscosity as a function of solids loading at a shear rate of $1000s^{-1}$ 63
Table 4-3: Mould materials used for gelcasting alumina parts. 64
Table 4-4: Densities and shrinkages of gel cast alumina sintered at 1650°C. 69
Table 4-5: Densities of HEMA-MBAM gelcast and sintered ceramic parts as a function of the sintering temperature. 71
Table 4-6: Comparison of sintering properties at 1650°C at different solids loading when using HEMA-MBAM monomer. 75
Table 4-7: Comparison of sintering properties at 1650°C at different solids loading when using Isobam® monomer. 76
Table 4-8: Comparison between the different gel forming systems. 79
Table 4-9: The effect of different monomer system on the density and open porosity of gelcast parts using 40 vol% solids loading and sintered at 1650°C 80
Table 4-10: Effect of de-airing technique on the density of cast parts using Isobam®. 81
Table 4-11: Effect of MgO addition on the density, mechanical properties and grain size of alumina sintered at 1650°C using 50vol% solids loading. 84
Table 4-12: Properties of complex shaped parts produced and sintered at 1650°C in air. 86

Table 4-13: Mechanical properties of various gelcast alumina parts sintered at 1650 °C. 91
Table 4-14: Transverse rapture strength and Weibull modulus determined by using the ball on three balls (B3B) test. 96

NOMENCLATURE

Symbol/ Abbreviation	Description
3D	Three dimensional
B3B	Ball on three balls
SEM	Scanning electron microscope
XRD	X-ray diffraction
Ξ	Zeta potential
APAA	Ammonium poly acrylic acid
Isobam®	Isobutylene and maleic anhydride
HEMA-MBAM	Hydroxyethyl methacrylate cross-linked with methylenebisacrylamide
η	Viscosity
γ	Shear rate
Φ	Solids fraction

Φ_m	Maximum achievable solids fraction
FDM	Field deposition modelling
STL	Stereolithography
CAD	Computer aided design
PLA	Poly lactic acid
ABS	Acrylonitrile butadiene styrene
RH	Relative humidity
RD	Relative density
PVA-DHF	Polyvinyl alcohol crosslinked with dimethoxy dihydrofuran
IB	Isobam®
PD	PVA-DHF
DI H2O	De-ionised water
PYR-S / PYR-H	Pyramid (solid or hollow)
IMP-3B / IMP-6B	Impeller containing 3 or 6 blades

$\boldsymbol{\sigma}$	Transverse rapture strength
$\boldsymbol{\sigma_o}$	Transverse rapture strength at a probability of 0.37
m	Weibull modulus
$\mathbf{P_s}$	Probability of survival

Chapter 1 : Introduction

1.1. Background

Advanced ceramics play an important part in technologies such as energy, transport, communication, military and medical industries. The most commonly used ceramic materials are alumina, zirconia, carbides and nitrides. These materials possess superior mechanical properties, however, all of them struggle to compete with alumina on a commercial basis due to its low cost, biocompatibility and ability to be sintered pressureless to near full density. Although alumina and other ceramic materials play a critical role in technological advancement, they have a niche market due to the difficulties in their forming techniques, which can hopefully be resolved by gelcasting and 3D printing.

In a review of ceramic processing, Lange, (1989) concluded that most forming methods are not suitable for the production of advanced ceramics. This is due to the ceramics' high hardness, high melting point and low fracture toughness. Thus, advanced ceramics cannot be produced by traditional methods alone. For ceramics, the maximisation of the materials' properties is often in opposition with the need for a low cost processing technique [1]. Therefore, there is a need to find alternative solutions to the manufacturing challenges that require custom solutions to achieve production cost reduction whilst maintaining these superior properties.

Investigations into the colloidal processing of ceramics have been done and these methods have been found to improve the reliability of ceramic manufacturing [2]. Gelcasting is one of the colloidal forming methods investigated. It has proved to be an effective and low cost near net shape method in the fabrication of complex

three-dimensional ceramic parts [3]. This method has been widely adopted due to its versatility. It involves filling a non-porous mould with a well dispersed ceramic suspension of high solids loading and requires a reasonably low viscosity to facilitate filling of the mould. The suspension is then polymerised to form a gel with sufficient strength that can then be dried and sintered to form a dense ceramic part.

However, gelcasting has limitations to industrial usage [4, 5, 6], including;

i) cracking of the green bodies during drying,
ii) low densities due to entrapped air in the suspension,
iii) costly and often toxic organic additives,
iv) effect on the environment due to disposal of toxic solvents and
v) mould requirements.

Progress has been made in identifying low toxic organic additives such as Poly Vinyl Alcohol (PVA), a co-polymer of isobutylene and maleic anhydride (Isobam®) and acrylamides [2, 7, 6, 8]. Recent technological developments have widened the application of gelcasting as a ceramic forming method. Technologies such as additive manufacturing can be used to produce complex shaped moulds that can be used in an investment type of gelcasting fabrication procedure.

Additive manufacturing has proven capable of producing custom parts with complex geometries and has also been proven to be of specific use in the rapid production of functional prototypes. It can be used to achieve complexity in products without negatively affecting production rates or the quality of the products whilst still reducing production costs [9, 10]. This process allows for simple, rapid, and economic design alterations [9]. The simplicity of the process and low waste of material are its main benefits in comparison to traditional shaping methods [11].

The application of rapid prototyping to ceramic forming was motivated by recent advances in engineering ceramics that require custom made parts with complex shapes which would be difficult to produce by traditional methods. The mould can be fabricated by using cheap plastic. The materials for the mould can be either PVA or ABS plastics. These are both excellent materials as they are soluble in cheap solvents, such as, water and acetone. Thus, facilitating easier mould removal of complex shaped objects provided the gel cast is not itself susceptible to the solvents.

1.2. Research Motivation

The classical shaping of ceramic materials has been based on the dry pressing of powder compacts. This conventional method has been used over many decades and continues until today. However, this processing technique generally produces defects in the microstructure, such as porosity, grain boundaries and inclusions [12] due to inhomogenities in the green compact. These microstructural flaws reduce the strength and reliability of the ceramic components produced. To achieve high reliability in advanced ceramics, it must be ensured that the parts have a high relative density and low porosity [13].

A significant amount of research has been devoted to processing strategies, such as powder synthesis and processing, green structure achievements and low temperature sintering to achieve full densification. These processes are now well understood. However, new applications of advanced ceramics require improvements on the traditional processing techniques to achieve yet further improvements in the materials properties. There is a need to find alternative solutions to manufacturing challenges that require custom solutions to achieve

production cost reduction, the use of polycrystalline ceramic powders and the production of complex shaped parts, without the current defects that maybe encountered such as porosity.

1.3. Aims and Objectives

The aim of the current research project was to successfully produce alumina ceramics with a homogeneous microstructure, high hardness, and a sufficiently high density using gelcasting method and 3D printed moulds. This process would solve existing problems involving complex geometries and give a new method of manufacturing advanced complex shaped ceramics.

The objectives of this work were to determine the suitability of 3D printing and gelcasting techniques with ceramic powders to produce ceramic parts.

The processing parameters investigated were:

- The effect of 3D printed moulds on the resulting microstructure of ceramic parts.
- The effect of gelcasting parameters on the resulting ceramic components.
- The effect of sintering temperature, heating rate and sintering aids on the densification and grain growth of alumina components.
- And ultimately determine the feasibility and ease of fabricating complex shaped parts through the presented approach.

1.4. Hypothesis and Limitations

A novel combination of gelcasting and 3D printed moulds is hoped to give another ceramic manufacturing method for high quality parts.. Parts with uniform mechanical properties and minimum defects in the microstructure can be produced with savings in costs, producing less waste and ensuring accurate geometries.

Despite the great promise of gelcasting and 3D printing, these technologies have not been widely used in the ceramics industry because of the following limitations:

- Toxicity of the polymers used to achieve gelation of the suspension.
- Entrapped air bubbles in the suspension leading to porosity in the final part.
- The effect of the 3D printing process on the surface morphology of the cast parts is not yet understood.
- High cracking susceptibility due to non-uniform drying conditions.

1.5. Scope

The current study used alumina to manufacture different complex shapes using 3D printing technology, colloidal powder processing methods and pressure-less sintering in air.

The parameters investigated were:

- The solid loading in the ceramic suspension.
- Different monomer systems.
- De-airing techniques.
- The rate of drying.
- The sintering temperatures.
- Fabrication of parts with complex geometries.

1.6. Dissertation Outline

This dissertation is organised into 7 chapters as outlined below.

- **Chapter 1** defines the motivation and objectives, scope, aims and structure of the dissertation.
- **Chapter 2** reviews the background areas relevant to achieve the objectives of this research. It also covers the advantages and limitations of the processes used, identifies existing gaps from which the objectives were developed.
- **Chapter 3** summarises the research methodology, experimental and analysis techniques employed in this study as well as the equipment used.
- **Chapter 4** outlines the results obtained from the experiments conducted. The topics covered are: particle size analysis, rheological measurements, tooling manufactured by 3D printing, binder systems used, de-airing of the slurries, casting and gelation. The binder burn-out, sintering and analysis of the effect of temperature, characterisation of samples by measurement of density, hardness, fracture toughness, XRD, microstructural characterisation and porosity are also presented.
- **Chapter 5** discusses the results of the experiments that were conducted. The results are discussed in relation to the reviewed literature.
- **Chapter 6** draws conclusions from the obtained results,
- **Chapter 7** outlines recommendations for future research on this subject and lastly,
- **References** that were consulted during the study and in compiling this dissertation.

Chapter 2 : Literature Review

2.1. Overview

Technically advanced ceramics have a niche market of application; they are favoured in operations where metals would often fail. Ceramics are harder and stiffer, more heat and corrosion resistant and have a lower density than most metals and their alloys. Furthermore, their raw materials are less expensive. The low density, chemical inertness and high hardness of ceramics offer additional potential for extending performance limits beyond those offered by metals. Ceramics have excellent mechanical and functional properties that make them some of the most sort-after materials in our modern world. The widespread usage of ceramics has been limited by their brittleness and poor reliability of strength which are a result of current processing techniques. These conventional processing techniques are aged or outdated (some may say well established) and cannot keep up with the current demand and requirements for advanced ceramics. However, with novel 21st century processing techniques new markets can be opened to ceramic materials.

Scholars have made progress in the compositional and microstructural design of ceramics. It has been demonstrated that the final properties of ceramic materials are highly dependent on the processing route and its variables [14]. The performance of ceramics is linked to the control of the purity and composition of the starting powder and the microstructure. Characteristics such as, small defect size, homogeneous grain boundary composition and high relative density are essential [1]. To achieve these excellent properties, advanced ceramics must be fabricated in such a way that the desired microstructure is obtained.

Advanced ceramics can be classified into:

1) Oxide ceramics such as alumina and zirconia.

2) Non-oxide ceramics including carbides and silicates.

3) Composites which are a combination of oxides and non-oxides.

The common ceramic materials and their corresponding unique properties are summarised in Table 2-1. Alumina was chosen as the material for investigating because it can be tailored to meet a large range of requirements. Furthermore, alumina is a low cost ceramic material and is abundantly available.

Table 2-1: Materials and properties of common ceramic materials and their applications [16]**.**

Material	Alumina Al_2O_3	Zirconia ZrO_2	Silicon Nitride Si_3N_4	Silicon Carbide SiC
Density(g/cm^3)	3.99	6.1	3.2	3.2
Melting Temp.(°C)	2050	2400	1900	2500
Hardness (GPa)	19	12	16	26
Fracture Toughness ($MPa.m^{1/2}$)	3-5	5-10	4-6	3.4
Application	Medical devices, high temperature processes, engine parts, and armour.	Engine parts, chemical industries and medical devices	Engine parts, high temperature processes and machining operations	Engine parts, chemical industries and high temperature applications
Desired properties	Resistance to wear and corrosion, heat insulation, high temperature strength, biocompatibility and low density	Corrosion and wear resistance, thermal and electrical insulation, high temperature strength and biocompatibility	Resistance to wear and corrosion, heat and electrical insulation and high temperature strength	Resistance to wear and corrosion, heat and electrical insulation and high temperature strength

Advanced ceramics can be tailored to possess certain mechanical and functional properties. For tailored properties to be attained, old school fabrication techniques must be merged together with new fabrication technologies. A relationship between the microstructure, properties and the method of fabrication must be well understood and optimised to achieve the desired results. Sigmund, et al., (2000) summarised the requirements for an optimal processing method to achieve the desired microstructural characteristics as shown in Table 2-2.

Table 2-2: Characteristics of an optimal processing method for advanced ceramics [1]**.**

Materials properties	**Processing method characteristics**
High reliability	Near-net shape
Sufficient strength	Simple processing concept
Fewer defects	Minimal processing steps
	High flexibility
	Environmentally friendly

2.2. Ceramic Processing

The production of advanced ceramics involves the use of high purity raw materials together with precise control of the production process to ensure superior properties in the final part. Advanced ceramics are produced using a powder metallurgy technique which involves the following [17]:

- Preparation of the starting powders

  This process includes milling the powder to obtain a small particle size which leads to a high surface area that ensures better sinterability due to high Gibbs free energy between particles. A homogeneous unimodal size distribution is desirable as it allows for ease in filling voids and leaves less porosity during the densification process.

- Consolidation of the powder to form a desired shape

  The objective of the powder consolidation step is to form the desired shape of the final part, to obtain a high green density and allow for handling of the powder compact. Powder consolidation allows for green machining in the case of complex shaped parts, thus eliminating the post processing step after sintering and therefore reducing the fabrication costs.

- Sintering to achieve densification of the part

  Densification is an essential part of ceramic processing. Full densification is a requirement to achieve the superior properties of advanced ceramic materials. Sintering can be achieved by means of pressure-less or pressure assisted sintering.

2.3. Powder Forming

The techniques used for powder consolidation are summarised in Figure 2-1. Pressing involves pouring the powder into a die and applying pressure to consolidate the powder. Pressing can be performed dry or wet in the presence of a solvent or binder. The process can be done in a uniaxial press or by isostatic pressing in a rubber bag depending on the pressure applied. This results in a powder compact that can then be green machined and sintered or simply sintered to shape.

Colloidal forming involves the manipulation of van de Waals forces between the particles in an aqueous medium [4]. Colloidal forming has many advantages over pressing in that powder agglomerates that may result in flaws are broken down during milling. Furthermore, homogeneous green bodies and optimal particle packing are obtained [18].

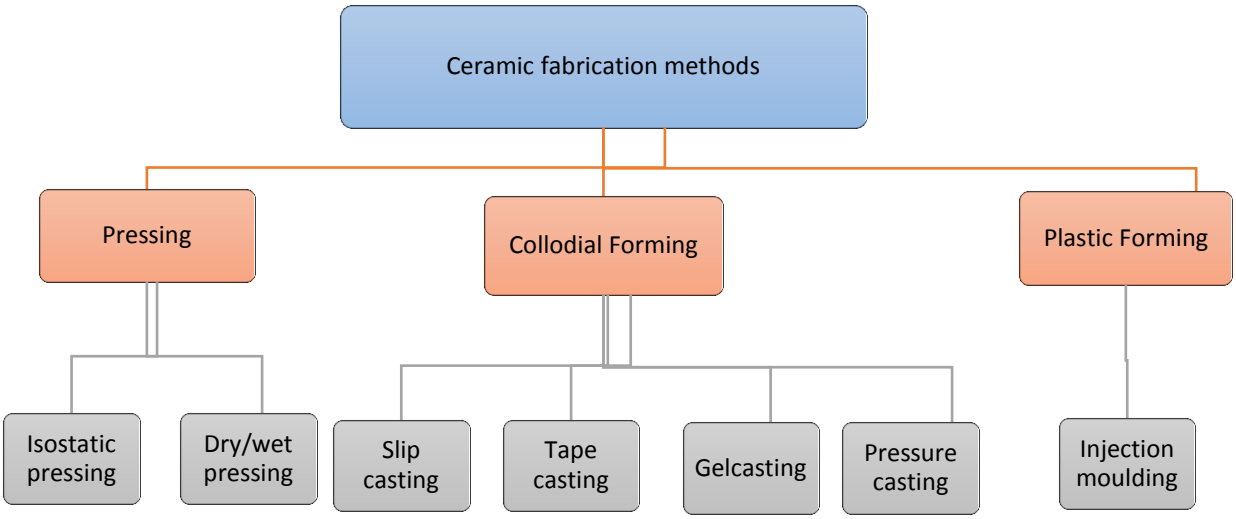

Figure 2-1: Ceramic forming techniques.

2.4. Colloidal forming methods

Colloidal forming can be defined as a liquid based forming technique [4]. It involves the preparation of a suspension by mixing a ceramic powder with a dispersant, a coagulating agent and a solvent. The suspension is poured into a mould to form the desired shape. The green body can then be dried and sintered to form a dense part. Colloidal forming processes include tape casting, slip casting and gelcasting. In this work gelcasting is the primary area of focus.

To utilise the advantages of colloidal processing methods, the process must satisfy the following requirements [4, 19]:

- A concentrated suspension must be created.

  A high solid loaded suspension produces green bodies with high densities. It allows close control of dimensions as the shrinkage of the part is determined by the solids content and organics added.

- Dispersant.

  The use of dispersants ensures the production of slurries with a low viscosity that will facilitate easy pouring of the slurry into a mould.

- Mould material and mould release agent.

  The appropriate mould material and release agent must be selected to ensure easy demoulding of the cast part and prevent cracking of the part before drying and sintering.

- Drying rate.

  The rate of water removal from the wet body is the rate limiting step of the colloidal forming processes. It must be carefully controlled to limit capillary stresses formed due to differential shrinkage and to avoid warping.

2.5. Gelcasting

Gelcasting is a near net shape colloidal forming process that is based on polymer science, colloidal chemistry and ceramic science. Gelcasting is a form of direct coagulation casting and uses a thermally or chemically induced in-situ phase transition (e.g. a gelling transition) of an organic and water-based suspension and enables casting of suspensions into non-porous molds (e.g. metal molds) to form a gradient-free microstructure. It has been widely used for a range of ceramics and metals by means of in-situ polymerisation of organic monomers and cross-linkers with a high solid loaded suspension [20]. The gelcasting process has the ability to produce components with high green strength and green density as well as acceptable green machinability. Other advantages include dimensional accuracy and complex shaping capabilities while reducing the cost of manufacturing [21].

Several polymeric components such as monomers, dispersants, cross-linker, and catalyst or initiator are used to create an in-situ solidification of particles through which a macromolecular network is created to hold the ceramic particles together [22]. The formed gel-binder system can then develop sufficient strength to support its own weight and can be handled without distortion or breakage [23]. Traditional gel-binder systems include acrylic acids, cellulose ethers, epoxy resins, acrylamides and polyvinyl alcohol. Often gel-binder systems are too expensive for large scale production and many also contain toxic and environmentally unfriendly chemicals.

Gelcasting has been frequently used to produce small complex shaped parts. However, larger complex shaped cast bodies often develop cracks because of the high internal stresses produced during drying of the green body. Another issue associated with gelcasting is the solid content in the suspension. A low solids loading leads to high shrinkage rates and uneven shrinkage with cracking, while a

high solids loading leads to the formation of flocculants or agglomerates which then act as flaws in the sintered body.

2.6. Monomer Systems

During gelcasting, the selection of the monomers plays an important role. A monomer solution contains a monomer and the appropriate cross-linker which is responsible for the formation of a gel. The selection of a monomer depends on its environmental friendliness, strength, stiffness and toughness of the gel, green machinability, reactivity, ease of use and the price. The most used monomer systems have been acrylamides, however, they have been found to have a high toxicity and are losing favour in the industry [2, 6].

Progress has been made in identifying low toxicity organic additives such as polyvinyl alcohol (PVA), a co-polymer of isobutylene and maleic anhydride (Isobam®) and methacrylamides and bisacrylamide [2, 7, 6, 8]. Using hydroxyethyl–methacrylate cross-linked with methyl-bis-acrylamide (HEMA-MBAM), it is often the norm that the ceramic suspensions contain about 10-20wt% of the monomers and these pose a difficulty during the binder burn out process. High amounts of binder take a longer time to decompose while leaving pores in the green compact.

The HEMA-MBAM system requires the use of an initiator and catalyst for the formation of the gel. The initiator acts as a chain forming substance through the reaction between the monomer and the cross-linker. A new system of isobutylene and maleic anhydride has been developed and it has been proven to produce high strength ceramic parts. This co-polymer has been favoured due to the use of only

a single reagent that acts as both the gelling agent and a dispersant when added in amounts up to 0.3wt% [24].

Dhara, et al., (2002) [25]highlighted the use of gelcasting to produce porous and complex shaped ceramics using the HEMA-MBAM solution and found that the essential steps that govern a successful gelcasting procedure are the drying process, the design and surface finish of the mould, de-airing process and the use of release agents. From this study it was noted that the drying process is the rate limiting step and can result in cracks or warping of the green body if drying is not accurately controlled. The de-airing process is essential to remove any entrapped gases as these may lead to flaws (porosity) that reduce the mechanical properties of the final part. The mould design and choice of mould material determine the complexity of the part that can be produced by gelcasting.

Liu, et al., (2002) [21] studied the effects of the rheological behaviour of prepared suspensions on the microstructure of sintered Al_2O_3-ZrO_2 ceramic parts and found that the mechanical properties were significantly influenced by the solids content of the suspension. The hardness, fracture toughness and relative density of the sintered parts were found to increase with an increase in the solids content up to 50vol% solids. However, as the solids loading increased above 50vol% the properties were adversely affected and flocculation or agglomerates occurred. Even though all suspensions exhibited a shear thinning behaviour that is in favour of the casting process, at high solids loading the suspensions exhibited a thixotropic hysteric behaviour that resulted in the formation of flocculation. The green bodies of parts cast from suspensions with a solid content less than 50vol% were found to have a homogeneous microstructure and close packing of particles which favoured the densification process. At higher solids loading, the formation of flocculants lead to non-uniform packing which acted as a source of flaws and resulted in low density of the final part.

Sun, et al., (2014) [26] developed a method of gelcasting high strength ceramics with low shrinkage that was favourable in the production of complex shaped parts. A co-polymer of Isobutylene and maleic anhydride (Isobam®) with a low molecular weight was developed and tested using alumina powder. In the study, bodies with green densities as high as 60% relative density were produced and the shrinkages of up to 14% after sintering were achieved. The co-polymer, Isobam® was also studied in a similar process by Sun, et al., (2015) [26] where the effect of particle size, surface area and the polymer content were studied in the production of transparent alumina. It was found that gelcasting resulted in a more homogeneous microstructure.

Zhang, et al., (2015) [28] in the study of the aqueous gelcasting of transparent magnesia-aluminate spinel using a co-polymer of isobutylene and maleic anhydride confirmed that gelcasting results in homogeneous microstructures. A spinel slurry with a solids content as high as 54vol% was prepared and found to possess a viscosity of 0.6Pa.s. The fractured surfaces of parts produced by casting the slurry prepared and parts produced by dry pressing were investigated and compared. It was found that the gelcast parts displayed a homogenous microstructure which is in agreement with the study performed by Sun, et al., (2015) [26].

It can be concluded that gelcasting is a superior ceramic forming method compared to traditional processes such as dry pressing as complex shaped parts with homogeneous microstructures can be easily produced.

2.7. Fabrication tooling/ Casting process

The selection of the fabrication tool or mould and its production are important factors during the gelcasting of ceramics. The commonly used moulds are glass, aluminium and polyethylene based. The setback in decreasing the operating costs by using colloidal forming methods is the need for a fabrication tool or a mould. The time and expense required in machining operations to form a mould increases the overall cost of colloidal methods.

Aluminium is the cheapest material and it can be easily machined, however it must be treated so that the surface is smooth to prevent the cast from sticking to the mould wall. Glass generally has a smooth surface for easy mould removal, however, the machining of glass to form complex moulds is difficult. Other moulds such as wax have been used to overcome the issue of demoulding. Demoulding from a wax mould can be achieved by burning off the mould at temperatures between 90 and 120°C [29]. However, at temperatures above 120°C the drying process starts and if the humidity is not controlled defects such as cracks and warping results.

With technological advancements, manufacturing processes such as CAD and 3D manufacturing have been utilised in this work to overcome the shortcomings of mould design and fabrication [30].

2.7.1. Additive Manufacturing

Additive manufacturing or 3D printing can be defined as a fabrication technique that builds parts layer by layer. The digital process would start with 3D scanning of the objects' geometry and modifications could then be made electronically, rather than physically [31]. The main advantage of this process is that the geometric freedoms offered by additive manufacturing provide a means for fabricating complex geometries that are difficult or impossible to fabricate by traditional means [10]. Other benefits of additive manufacturing include reduced post-production processing, higher design flexibility, as well as cost reductions in design, production, finishing, and re-use of non-sintered powder.

In reviewing the literature, it has been found that additive manufacturing is effective in manufacturing parts for tooling to be used in investment casting. Chimento, et al.,(2010) [31] have applied this technology in the forming of medical devices and they concluded that the 3D printed parts had the necessary strength and permeability and that the moulds easily integrated into current processing procedures. Yoo, et al., [32] used 3D printing to prepare structural ceramics from fine ceramic powders and obtained near fully dense ceramic parts with flexural strengths up to 324MPa. It was also observed that the parts had a smooth surface finish; however, an increase in the amount of binder had negative effect on the parts being produced.

A new 3D printing method, Layer-wise Slurry Deposition (LSD) has been applied in the additive manufacturing of alumina ceramics, Zocca, et al., (2017) [33] studied this method and concluded that complex shaped alumina parts could be printed and would exhibit a high green density and densities after sintering that are comparable with parts produced by traditionally accepted shaping technologies. Although, additive manufacturing has not been widely used in the

production of advanced ceramics, it is evident that this technology could enable engineers to overcome manufacturing limitations.

However, not enough is known about the effects of 3D printing on the resulting structure and properties of ceramic parts. Therefore, investigations need to be conducted to determine the effect on parameters such as dimensional tolerances, hardness, surface roughness, and production costs.

2.8. Sintering of ceramics

Ceramics have a high melting point; thus the production of ceramic components requires high sintering temperatures. Sintering can be defined as the process by which powder compacts are converted into dense ceramics by material transport mechanisms at temperatures just below the melting point of the starting powder [34, 17]. It is a process by which small particles of a material are bonded together by solid-state diffusion resulting in the transformation of a porous compact into a dense product. The process involves the densification of a powder compact by diffusion and other atomic transport mechanisms that removes pores. This results in a body that has 95-99% full density [34].

The process of sintering involves determining the required microstructure and design processing conditions that will be required to produce this microstructure. An increase in the density of the compact during sintering is useful for the development of properties, such as mechanical strength. The parameters that influence the resulting microstructure are the particle size of the starting powder, applied pressure, heating rate and the sintering temperature [19]. Sintering takes place at 0.7 to 0.9 of the melting point of the material through three steps, these

are; initial, intermediate and the final stage of sintering. Figure 2-2 indicates the stages that occur during the solid state sintering of ceramics.

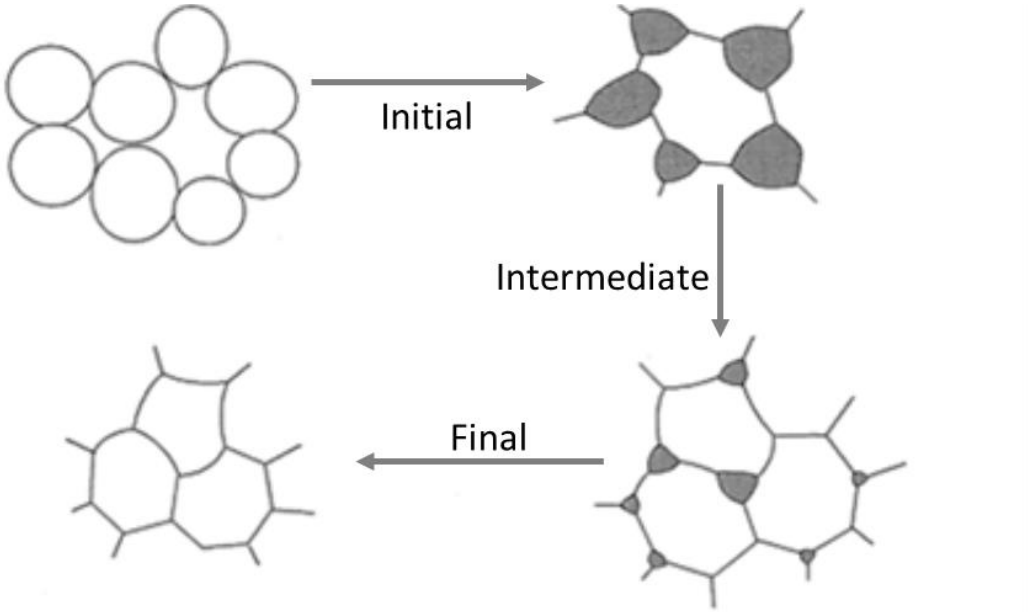

Figure 2-2: Stages of densification during solid state sintering of ceramics [35]**.**

The initial stage of sintering is where particle re-arrangement takes place and the particles are packed. During the second stage of sintering, densification and pore minimisation takes place due to grain boundary mobility. The final stage of sintering occurs when densification is accompanied by grain growth. However, in order to obtain the desired microstructure i.e. a pore free microstructure, abnormal grain growth must be controlled and/or minimized [34].

Grain growth and densification often occur simultaneously during sintering and are driven by grain boundary diffusion. Often, the occurrence of excessive grain growth stops the densification process as the pores are trapped inside the large grains [36]. Grain growth in ceramics can be controlled by controlling the structure of the starting powder, powder consolidation and sintering conditions.

Sintering methods have been used to achieve high densities with minimum grain growth such as pressure assisted sintering which uses pressure and heat to compact a powder to near full density at relatively low temperatures [37]. However, this method is mostly possible for simple shaped parts, while complex shaped parts are still mainly prepared by pressure-less sintering [38]. For high relative densities to be obtained by pressure-less sintering, high sintering temperatures are required, but at high temperatures, excessive grain growth occurs.

Extensive research has been conducted to find ways to overcome these drawbacks in ceramic forming methods. Strategies such as the addition of a secondary phase (sintering aids or grain growth inhibitors) and two step sintering methods have been utilised by scholars.

The Hall-Petch equation (Equation 2-1) states that the strength of a material is inversely proportional to the grain size of the material. Thus, a grain size reduction is a means to increase the strength and fracture toughness of a material.

$$\boldsymbol{\sigma_0 = \sigma_i + k/\sqrt{D}} \qquad \text{Equation 2-1}$$

Where;

σ_0 is the strength of the material (MPa),

σ_i is the frictional stress (MPa),

k is the stress intensity factor, and

D is the grain size (μm)

Thus, grain refining must be well understood to produce parts with the desired properties. Reducing the grain size gives rise to a range of desirable material properties. Grain refining can be achieved by one of two methods. The first method is by decreasing the particle size of the starting powder and by inhibiting the grain growth of the particles during sintering. However, the final stage of solid state sintering usually results in the occurrence of abnormal grain growth due to high driving forces that promote densification as well as decrease interfacial forces that lead to the formation of agglomerates.

Krell, et al., (2003) [39] suggested the use of sub-micron sized starting powder rather than nano-sized powders to overcome the formation of agglomerates during the final stage of sintering. These powders must be shaped such that the green body has a high relative density because of smaller and homogeneously distributed pores. When such powders are prepared by colloidal forming processes such as gelcasting where homogeneous packing of particles and high green strengths are realized, the sintering temperature and grain growth would be significantly minimized.

The second technique that can be used for the refining of grains to attain parts with superior mechanical properties is the prevention of grain growth by the addition of grain growth inhibitors. Grain growth inhibitors act by pinning grain boundaries. It is well known that achieving a high density in a polycrystalline body of alumina is dependent upon a number of factors [40]. To improve the mechanical properties and long term performance of polycrystalline ceramics, the addition of various sintering aids has been proposed by various scholars [40, 41, 42]. Sintering aids or grain growth inhibitors such as MgO and ZrO_2 have been proposed.

Coble, (1962) [40] proposed a method for forming an alumina body having the desired mechanical characteristics by compacting a mixture of finely divided alumina with minor additions of magnesia (MgO), and firing the compact for a predetermined period at a temperature not lower than 1700°C. According to Coble, (1962) [40], the addition of magnesia (MgO) limits grain growth by pinning the grain boundaries and preventing the boundaries from sweeping past included pores and trapping the pores within the grain body and minimising stress cracking.

Azhar, et al., (2010) [41] studied the influence of the addition of magnesia to zirconia-toughened alumina cutting inserts and concluded that the microstructural observations showed that the Al_2O_3 grain size was found to be significantly dependent on the amount of MgO additives. This is in contrast with the results obtained by Heraiz, et al., (2006) [42] where it was concluded that MgO additions promoted grain growth but improved the densities up to a certain optimum amount of MgO and any further increase in MgO addition led to a decrease in densities.

2.9. Summation of literature review

This research review's purpose was to help understand the different aspects posed by the research on the fabrication of complex shaped alumina parts. The different aspects of ceramic forming techniques including powder colloidal forming and sintering reviewed sheds light into the work conducted. It also proved to be beneficial in formulating the experimental procedures and providing potential answers to the research limitations.

Chapter 3 : Experimental Procedure

This chapter presents the experimental work undertaken during the fabrication of alumina ceramics by gelcasting onto 3D printed ABS plastic moulds. This chapter consists of the materials used as summarised in Table 3-1, the equipment and the description of the experimental setup.

Table 3-1: Materials used.

Material	Supplier	Function
Al_2O_3 powder	Alfa Aesar	Ceramic powder
MgO powder	Alfa Aesar	Dopant
Polyvinylpyrrolidone	Sigma Aldrich	Polymer
2-hydroxyethyl methacrylate	Sigma Aldrich	Monomer
N,n,n',n'-tetramethylenediamine	Sigma Aldrich	Catalyst
Ammonium persulfate	Sigma Aldrich	Initiator
Poly vinyl alcohol	Sigma Aldrich	Binder
Polyethylene glycol	Sigma Aldrich	Plasticiser

Poly acrylic acid	Sigma Aldrich	Dispersant
1-octanol	Sigma Aldrich	Antifoam
N,n-methylene bis-acrylamide	Sigma Aldrich	Cross-linker
Isobam®	Sigma Aldrich	Co-polymer
Acetone AR	Chemistry Stores, Wits	Demoulding solvent

3.1. Powder Characterisation

A commercially available α-alumina powder (Al_2O_3) was used in this study. The ceramic powder was first characterised prior to processing to determine the physical and chemical properties and to understand how these properties may change during processing and sintering and their influence on the resulting microstructure.

The particle size distribution of the powder was determined using a Malvern Mastersizer 2000. This was done by laser diffraction analysis where particles are passed through a focused laser beam. The particles scatter light at an angle that is inversely proportional to the particle size. A series of photosensitive detectors measure the angular intensity of the scattered light. The number and positioning of the detectors in the Mastersizer 2000 has been optimized to achieve maximum resolution across a particle size between 0.1μm to 1.0mm [43].

The samples were prepared by making up a suspension of the ceramic powder. Where, 1g of alumina power was mixed with 5ml distilled water and sonically resonated for 10minutes to remove agglomerates. The suspension was then added to 800ml distilled water and the particle size measured. The particle size was represented as a function of the volume fraction with the size measured in microns. The powder was further characterised for morphology by using scanning electron microscopy and the phases were characterised by XRD.

3.2. Gelcasting Process

The process includes several steps as summarized in Figure 3-1. The monomers and cross-linkers were dissolved in a dispersing medium before addition of the powder to prepare the suspension. An initiator and a catalyst were added to polymerize the slurry and the reaction started. The suspension was then cast into the desired moulds. The free radical reactions lead to the formation of a microgel network of monomer and cross-linker inside the suspension. Once the polymerization reaction takes place, the green body was demoulded, and dried before the binder burn out and the sintering steps.

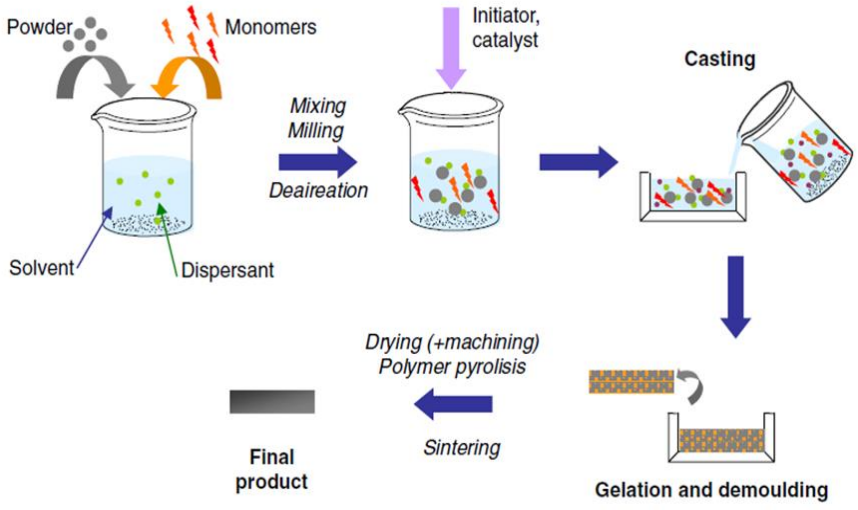

Figure 3-1: Gelcasting process [44]

3.2.1. Preparation of ceramic suspension

Slurries were prepared using different polymer systems. The monomers used were sourced from Sigma Aldrich. The first monomer tested; 2-hydroxyethyl methacrylate (HEMA) was used as a monomer and it was cross-linked with n, n'-methylene bis-acrylamide (MBAM) and the second was a co-polymer of isobutylene and maleic anhydride (Isobam®).

3.2.1.1. HEMA-MBAM System

The amounts of the additives were calculated as a weight percent of the starting powder. The appropriate amounts of monomer, cross-linker, plasticiser and dispersant were mixed with deionised water in a beaker as shown in Figure 3-2. The suspension was mixed using a magnetic stirrer for 2hrs to achieve complete mixing of the additives. The alumina powder was calculated as a volume percent of the final suspension. The powder additions used were between 40 and 70vol%.

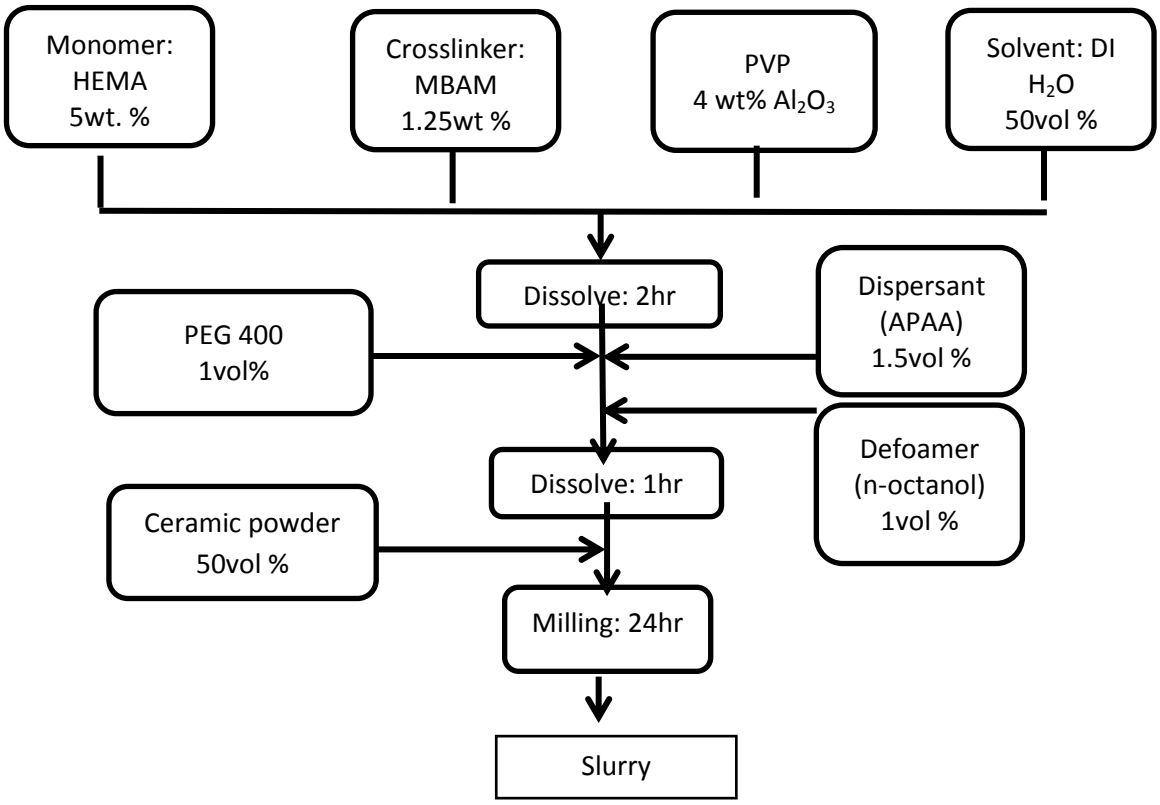

Figure 3-2: Slurry preparation with HEMA-MBAM system.

3.2.1.2. Isobam ® System

The calculated amount of the co-polymer of Isobutylene and maleic anhydride as a weight percent of alumina was mixed with deionised water in a beaker over a magnetic stirrer plate until Isobam® dissolved completely. Once dissolved the appropriate amount of alumina was added while gradually increasing the speed of the stirring bar as the mixture became more viscous. The mixture was then transferred into a zirconia lined milling pot together with alumina milling balls.

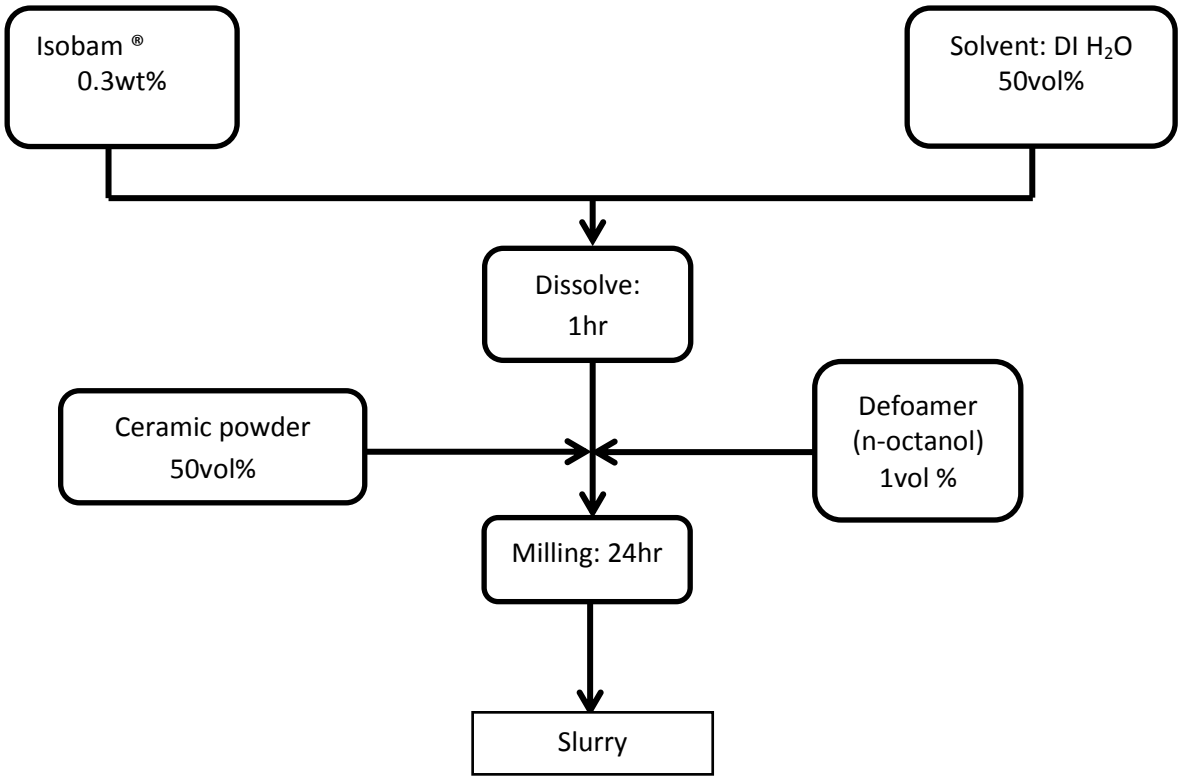

Figure 3-3: Slurry preparation using Isobam® system.

3.2.1.3. PVA-DHF System

The appropriate amounts of PVA, DHF, defoaming agent and ceramic powder were measured and the suspension prepared as shown in Figure 3-4. APAA and deionized water were mixed using a magnetic stirrer for an hour. The ceramic powder, DHF, PVA and the defoamer were then added before the suspension was milled in a ball mill for a period of 24hrs. The gelation process was achieved by heating the suspension.

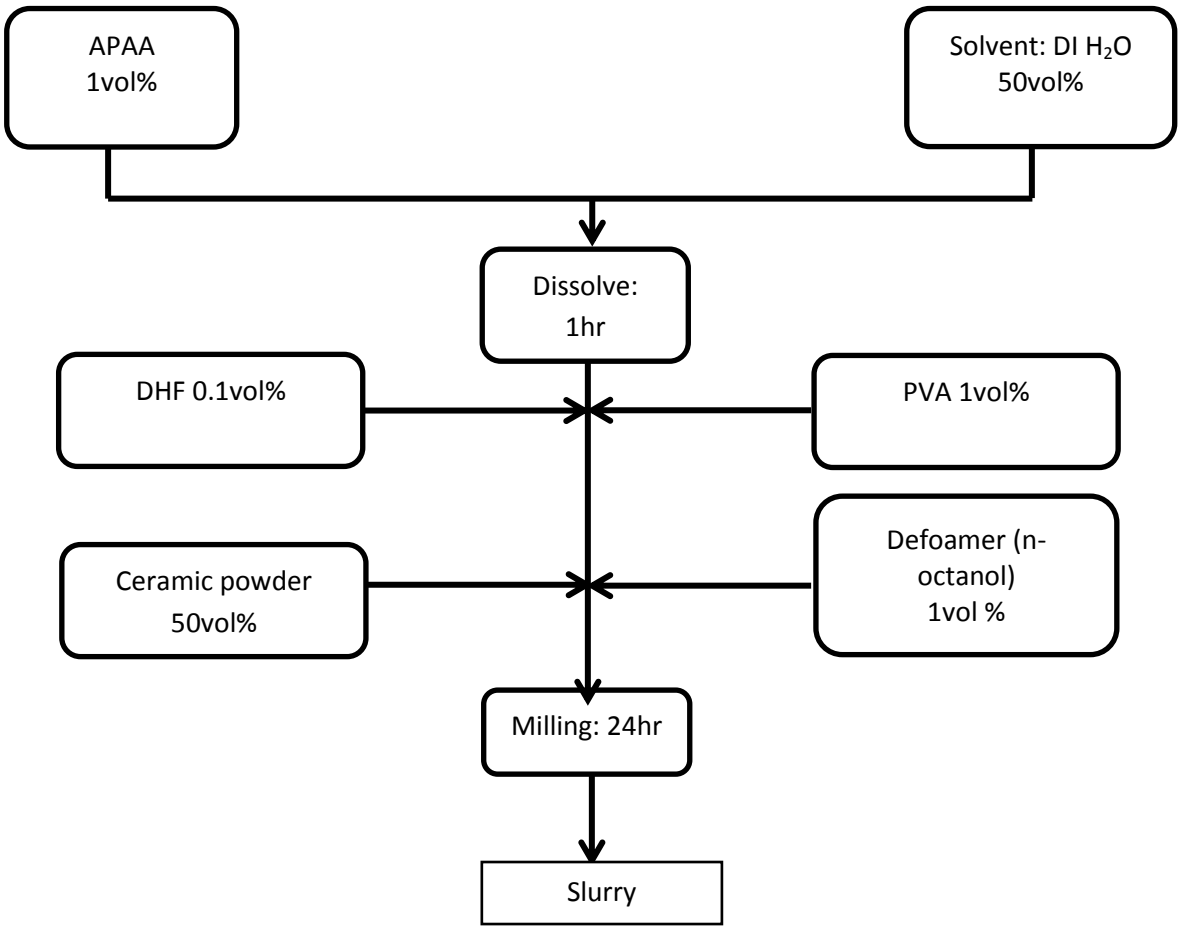

Figure 3-4: Slurry preparation using PVA-DHF system.

3.2.2. Milling / Mixing

The suspensions were prepared by mixing the polymers, coagulating agents, ceramic powder and a solvent as illustrated in Figure 3-2, Figure 3-3 and Figure 3-4. A Fritsch pulverisette 6 planetary mono ball mill was used for the milling and mixing of the alumina powder to achieve the alumina suspensions. The milling balls were cleaned prior to adding these to the mill using the following method. Alumina balls were added into a zirconia lined milling pot and washed by running the mill at a speed of 200rpm 3 consecutive times for 15 minutes until the balls were clean.

The milling parameters are summarised in Table 3-2. Slurries were mixed in a 250 ml stainless steel milling bowl with a zirconium oxide lining and an inside diameter of 7mm. Alumina grinding balls with a diameter of 2mm were used as the milling media. The powder and the milling balls used for the milling were carefully weighed to achieve a ball to powder mass ratio of 1:3. The slurries were milled for 24hrs to break up the agglomeration of the particles and ensure perfect mixing using a milling speed of 300rpm.

Table 3-2: The milling parameters used when mixing ceramic powder and pre-mix solutions.

Milling speed	300rpm
Ball-to-powder ratio	1:3
Milling time	24hrs

3.2.3. Rheological Studies

Slurry fluidity is an important aspect of gelcasting. A suspension with a low viscosity and high solids loading is preferable. To measure this, rheological studies need to be performed to determine the optimum additives additions.

The rheology of the slurry was determined using an advanced Physica MCR300 rheometer (Anton Paar Corp.) where the viscosity of the slurry was determined as a function of the shear rate. This uses the Rheoplus software and a concentric measuring cup that requires a 24ml suspension. The slurry was poured into the cup and the measuring cell inserted. The viscosity was measured as a function of shear rate in the range of 1 to $1000s^{-1}$. The solids' loading was varied between 35 and 70vol% alumina to determine the optimum solid loading at the lowest possible viscosity. The second variable investigated was the dispersant amount, which was varied between 0.5 to 1.2wt% for ammonium poly acrylic acid (APAA) and amounts between 0.1-0.8wt% for Isobam®.

3.2.4. De-airing

De-airing of the slurry was performed to remove air bubbles trapped in the slurry during the milling process. The suspension was first sieved to remove the milling balls. A deforming agent (n-octanol) was added to the slurry to assist with the de-airing process. The beaker containing the suspension was placed in a desiccator connected to a vacuum pump. The vacuum pump was set at partial vacuum and the slurry was left for a period of 4 hours.

3.3. Net-shape Forming

3.3.1. Mould Design

The moulds used for casting were produced by 3D printing, using an ABS material and a Stratasys® FDM 3D printer. The desired shape was designed using computer aided design (Ultimaker-CURA®), where an STL file of the negative of the desired shape was produced. The STL file was then sent to the printer and a mould was obtained as shown in Figure 3-5.

The mould fabrication method was based on fused deposition modelling (FDM) where a plastic melt is deposited on a platform and a part is built up layer by layer. The technology applies the melt extrusion method to fabricate an object, making use of layer by layer thermoplastic polymer. The monofilament is a commercial FDM apparatus which is moved by two rollers and activates a piston to drive the semi molten polymer through a nozzle. When each layer in the x-y plane is finished, the base platform (z-axis) is lowered and the procedure is repeated until the object is finished.

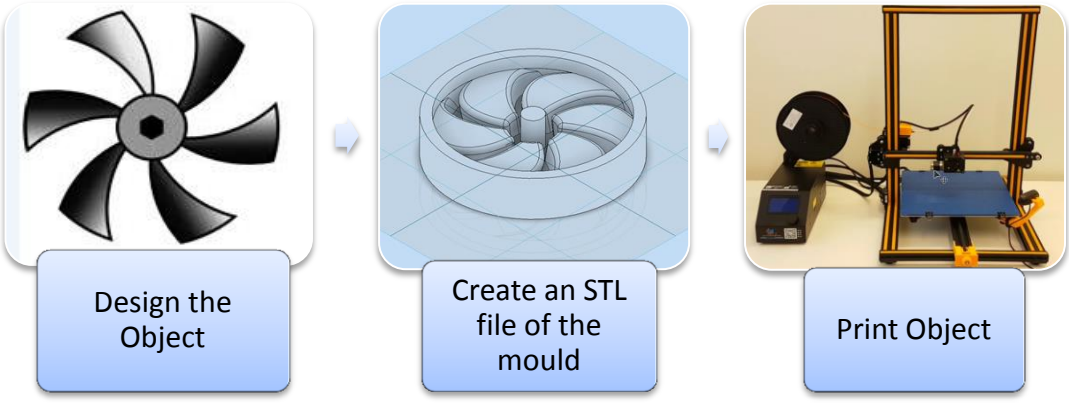

Figure 3-5: The process of 3D printing moulds [Lukas Janse van Renseburg].

Table 3-3 shows the materials used for 3D printing of the moulds. AutoCAD® software was used to design the desired shape and an STL file was created. The file was sliced using Cura® software to produce a negative of the part and this would act as the mould. Figure 3-6 shows the ABS filament used in the printing of dissolvable moulds. The mould was printed using an Ultimaker® printer as shown in Figure 3-6.

Table 3-3: Materials used for fuse deposition modelling of gelcasting moulds [10].

	PLA (Poly-Lactic Acid)	**ABS(Acrylonitrile Butadiene Styrene)**
Source	Lactic acid	Crude oil
Melting temperature (°C)	180-220	230
Glass transition temperature (°C)	60-65	105
Safety	No safety measures required	Must print in a well-ventilated area
Demoulding procedure	-	Dissolves in acetone

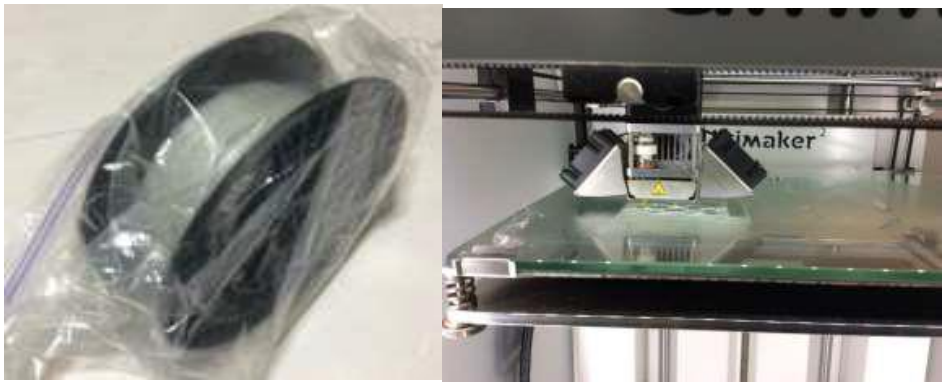

Figure 3-6: Photograph of a) ABS resin and b) the Ultimaker 3D printer.

3.3.2. Casting

An initiator and catalyst were added to the suspension prior to casting. The 3D printed moulds were first coated with a thin film of silicon spray or petroleum jelly to prevent wall interaction friction that could lead to cracks in the green body as it gelled and dried. The suspension was then cast into the moulds. After casting, the green body was allowed to set at room temperature for 4hrs allowing time for gelation to occur. The parts were then de-moulded by dissolving the ABS based moulds in acetone.

The acetone bath was placed in a bath containing hot water to speed up the reaction before the gel cast part could lose its strength. The moulds completely dissolved in acetone in approximately 3hrs leaving the gelled body, which was then removed from the acetone solution and further dried in a controlled environmental chamber.

3.4. Drying

The cast suspension forms into a gel that contains the alumina powder and the water. Therefore, the water must be removed by drying in a controlled environment to prevent differential shrinkage and cracking. The drying process is the rate controlling step of the process. The gelled suspension was first removed from the mould i.e. demoulding.

An environmental chamber [45] controlling humidity and temperature was used to dry the gelled part as shown in Figure 3-7. The chamber was designed to reach a relative humidity of 100%RH and a temperature of up to 60°C. The

microprocessor based humidity controller had one input probe and one relay output, where the user is able to program parameters including the set point, cycle time and ambient probe adjustment. The temperature controller was designed for both heating and cooling applications.



Figure 3-7: Image showing a) an environmental chamber and b) its controls.

The green bodies were dried in an environmental chamber under controlled humidity and temperature as follows:

- 95% humidity and a temperature of 40°C for 12hrs.
- 60% humidity and a temperature of 40°C for 8hrs.

3.5. Sintering & Binder burn-out

The organic material needs to be burnt off at 600°C prior to sintering. A muffle furnace with a maximum operating temperature of 1800°C was used for both the burn off and sintering of the gelcast samples. The furnace consists of molybdenum disilicide heating elements and is lined with durable fibre material.

A type B thermocouple is positioned in the heating chamber and used as a temperature sensor providing data for temperature readings. The samples were placed in alumina boats and positioned in the middle of the furnace. The heating, cooling and hold time cycles were programmed through the built in programmer. Binder burn out and sintering was performed in air. The sintering and binder burn out profile is shown in Figure 3-8, where T_S is the sintering temperature and T_B is the temperature for binder burn out.

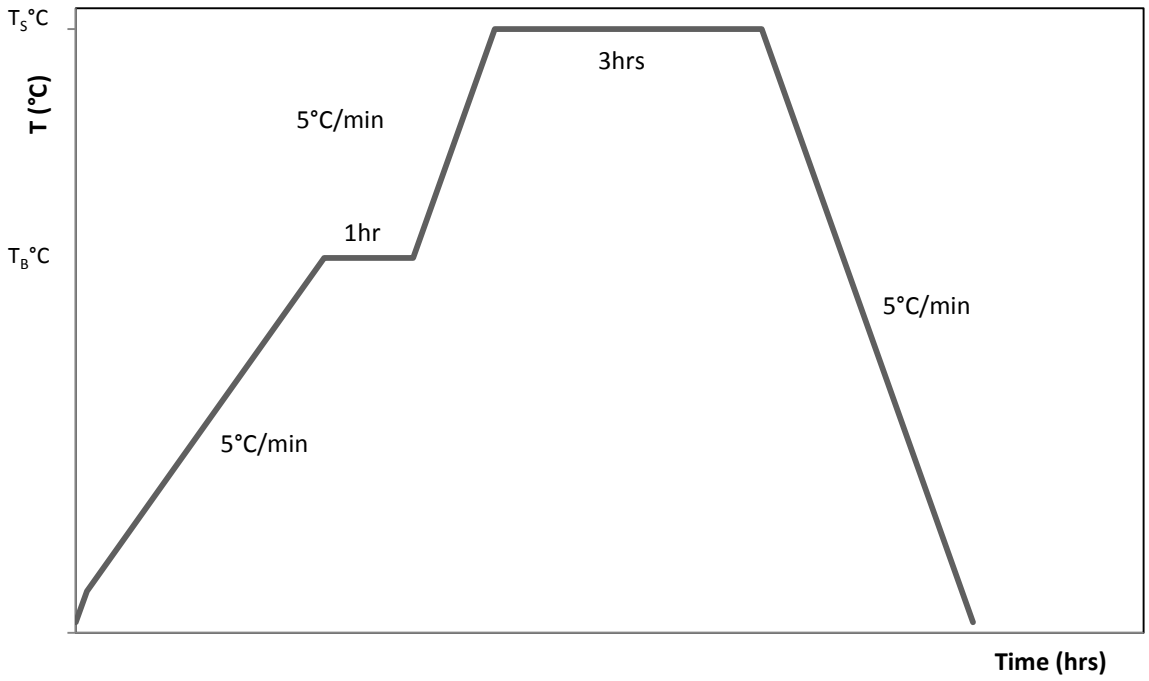

Figure 3-8: Binder burn-out and sintering profile used.

3.6. Characterisation Techniques

3.6.1. Density Determination

The density of the sintered samples was determined by using Archimedes' principle where the dry weight and wet weight of the sample were measured and compared to the volume of water displaced by the part. Measurements were taken by weighing the dry mass of the samples, where 5 measurements were taken for each sample. Wet and suspended weights were measured by first boiling the samples in distilled water for 3hrs after which the suspended weight and wet weight were measured 5 times per sample.

The density was determined by using the following equations:

$$\text{True volume} = \frac{w_1 - w_3}{\rho_w} \qquad \text{Equation 3-1}$$

$$\text{True density} = \frac{w_1 - \rho_w}{w_1 - w_3} \qquad \text{Equation 3-2}$$

$$\text{Bulk density} = \frac{w_1 - \rho_w}{w_2 - w_3} \qquad \text{Equation 3-3}$$

$$\%\ \text{porosity} = \frac{w_2 - w_1}{w_2 - w_3} \times 100 \qquad \text{Equation 3-4}$$

Where:

$w_1 =$ dry weight (g), measured by weighing the dry ceramic part.

$w_2 =$ wet weight (g), measured after boiling the samples in distilled water for 3 hours.

$w_3 = \text{suspended weight (g)}$, measured by suspending the part in water and measuring the weight of the water displaced by the ceramic part.

$\rho_w = \text{density of water } (g/cm^3)$

3.6.2. Sample Preparation

A Struers Secotom-10 cutter was used to cut the samples and this was operated at a wheel speed of 3000rpm, a feed speed of 0.015mm/s using a diamond cutting blade and water as a lubricant. The cut length was varied according to the size of the sample. The polished samples were mounted using poly fast resin while keeping the polished surface exposed.

Mechanical grinding and polishing preparation is the most common method of preparing surfaces for microscopic examination. The specific requirement of the prepared surface depends on the particular type of analysis or examination to be conducted. For Vickers hardness, fracture toughness and flexural strengths measurements as well as SEM analysis, a mirror finish is required for specimens. The basic process of specimen preparation is material removal, using abrasive particles in successively finer grits to remove material from the surface until the required mirror surface finish is achieved. The samples are first plane ground using a plate with a grit size of 220µm followed by fine grinding using a disk with a grit size of 1200µm. Water was used as a coolant for the grinding process and to remove abraded particles. Grinding is followed by polishing, which removes the damage introduced by the grinding operation. The disk particle sizes used for polishing were 9, 6, 3 and 1µm. Diamond slurry was used during the polishing process.

3.6.3. Mechanical Testing

Hardness and fracture toughness were measured by using indentation fracture mechanics method as illustrated in Figure 3-9. A Leco V-100-A2 Vickers hardness tester with diamond indentation was used to measure the hardness and fracture toughness of the sintered ceramic parts. A load of 49N was applied and maintained for 10sec. A total of 5 indentations per sample were used for statistical averaging purposes.

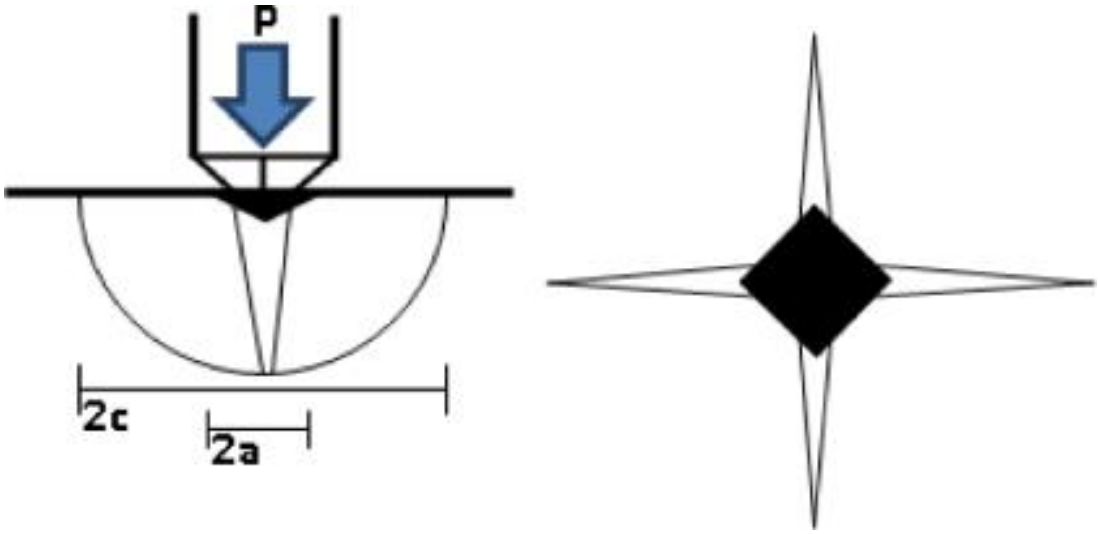

Figure 3-9: The Vickers indentation technique results in cracks of width 2*c* and an indentation of width 2*a*. A side view of the crack system is shown on the left and a surface view is shown on the right [46].

3.6.3.1. Hardness

The hardness tests were performed on polished surfaces. The following formula was used to calculate the hardness values.

$$HV = \frac{1.8544 \times P}{d^2}$$ Equation 3-5

Where;

HV = Vickers hardness number

P = Load applied (kg)

d = Mean length of diagonals of indentation (mm)

To convert the HV value to GPa units, the following formula was used:

H (GPa) = 0.009807 HV

3.6.3.2. Fracture Toughness

The fracture toughness of the samples was calculated using the 'half penny' crack method. The cracks were initiated during the Vickers hardness testing. The Anstis equation [47] was used to calculate the fracture toughness based on the length of the cracks observed.

$$K_{1c} = \xi \times \sqrt{\frac{E}{H}} \times \left(\frac{L}{C_{ave}}\right)^{1.5} \qquad \text{Equation 3-6}$$

Where;

K_{1c} = Fracture Toughness ($Mpa.m^{0.5}$)

E = Young's Modulus (GPa)

H = Hardness (GPa)

L = Load (N)

C_{ave} = Average crack length (m)

ξ = constant = 0.016

3.6.3.3. Transverse Rapture Strength

The biaxial flexural strength was measured using the ball on three balls (B3B) test, where a disc is supported by three balls and loaded by a forth ball as shown in Figure 3-10. In this case all four balls had a diameter of 11 mm. The test was conducted on 10 different specimens that differed in solids loading (40-60vol %) of the starting suspension and sintered at a temperature of 1650°C. The specimens had a relative density between 97 and 99%. The surfaces of all specimens were ground and polished to a 9μm grit size. The specimens had diameters of either 16 or 20mm and a thickness that was ≤ 2mm.

A universal testing machine (Tinius Olsen H50KT press) was used for load application. A pre-load of 10N was applied to hold the specimen between the four balls. The tests were conducted under a controlled loading rate of 100N/s. The tests were performed such that the load was increased to achieve failure at about ±30seconds and the fracture load, F, was used to calculate the maximum tensile biaxial stress in the specimen at the moment of fracture.

An interactive Web-Mathematica tool, developed by the Institute of Structural and Functional Ceramics, Montan University, Leoben [48, 49] was used to calculate the TRS values based on the equations below.

$$Q_{max} = f \times \frac{F}{t^2} \qquad \text{Equation 3-7}$$

Where:

$F = force\ (N)$

$t = thickness\ of\ disc\ (mm)$

$$f = \frac{3(1+\upsilon)}{4} \times \left[1 + 2 \times ln\frac{R_a}{b} + \frac{(1-\upsilon)}{(1+\upsilon)} \times \left(1 - \frac{b^2}{2 \times {R_a}^2}\right) \times \frac{{R_a}^2}{R^2}\right] \quad \text{Equation 3-8}$$

$$R_a = \frac{2 \times R_b}{\sqrt{3}} \quad \text{Equation 3-9}$$

$R_a = support\ radius\ (mm)$

$R_b = radius\ of\ balls, (mm)$

$\upsilon = Poisson's\ ratio$

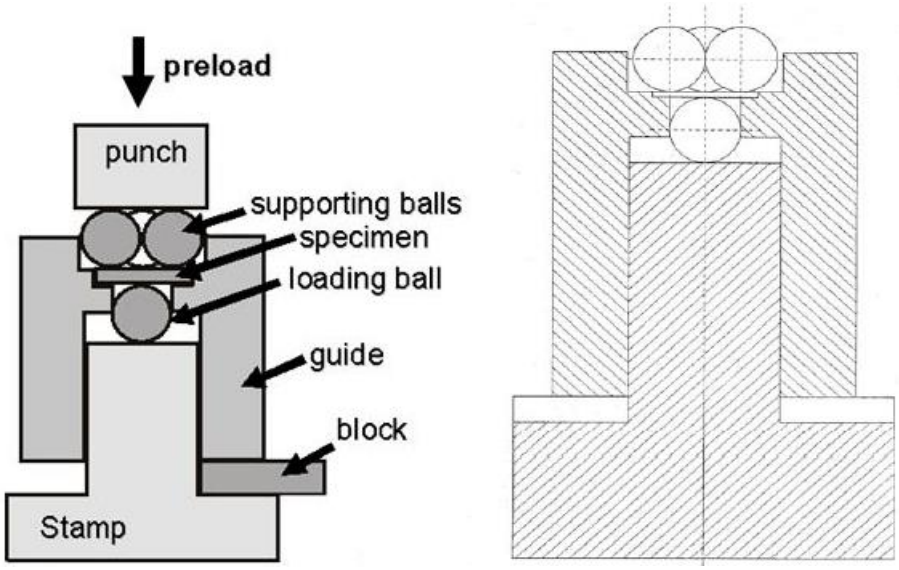

Figure 3-10: The ball on three balls test setup [48]**.**

3.6.4. Field Emission Scanning Electron Microscope (FE-SEM)

The sintered samples were thermally etched at 1350°C in air for 30minutes and coated using a carbon coater and a gold-palladium sputter coater prior to microstructural observations by Field Emission Scanning Electron Microscope (FE-SEM). The average grain size was estimated from the images of the fracture surfaces obtained from FE-SEM using the linear intercept technique.

3.6.5. Grain size measurements

The grain size is an important property of sintered ceramics as it affects the properties of the material, such as the hardness and fracture toughness. The grain size of the sintered parts was measured by using the linear intercept method to determine the average grain size from the SEM micrographs.

Chapter 4 : Results

This chapter reports on the overall results obtained from the experiments conducted. Results of powder characterisation, rheological measurements for ceramic suspensions, moulding using 3D printed moulds, and density measurement of ceramic materials from gelcasting are reported. It was found that there was a good balance between fluidity and solid content with rheological studies. These results enabled the casting of dense and complex shaped ceramic material. In addition, the green and sintered densities of alumina were obtained by density measurements. The results from Vickers indentation tests of ceramic components and ball on three balls (B3B) test are shown and the failure analysed.

4.1. Powder Characterisation

4.1.1. Particle Size Analysis

A Malvern Mastersizer 2000 was used to determine the particle size distribution of the starting alumina powder, Figure 4-1. The particle size d_{50} was found to be in the submicron range (0.5-1.0μm). The measured particle size distribution was in agreement with that provided by the supplier. An additional confirmation of the particle size was done by SEM.

d_{10} = 0.413µm d_{50} = 0.889µm d_{90} = 1.797µm

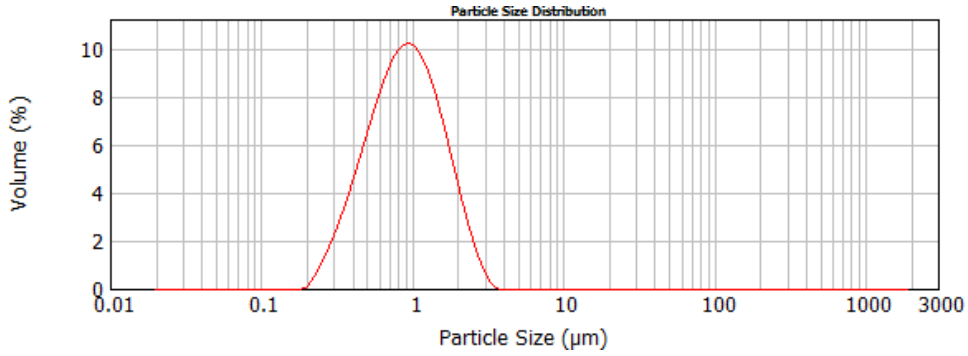

Figure 4-1: Particle size distribution for alumina powder.

4.1.2. Scanning Electron Microscope

The morphology of the as received powder was examined using SEM and the image was recorded at a magnification of 5 kX as shown in Figure 4-2. The figure shows that the majority of the particles have a diameter below 1µm, which agrees with the Malvern particle analysis. The particles were found to be irregular shaped.

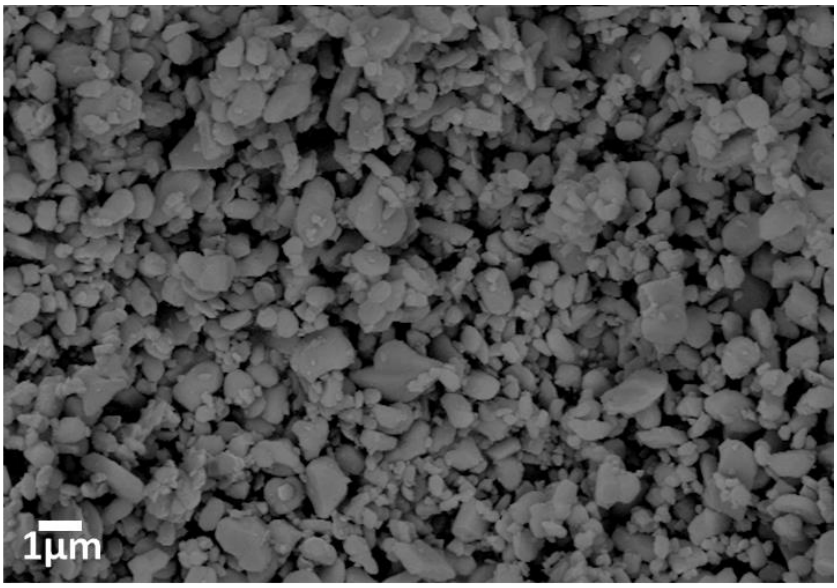

Figure 4-2: SEM characterisation of the starting powder.

4.1.3. Powder X-Ray Diffraction

The phases present in the starting powder and their corresponding crystal structure were determined using XRD analysis and the EVA software. The XRD pattern in Figure 4-3 displays a crystalline phase of 100% α-alumina with characteristic peaks.

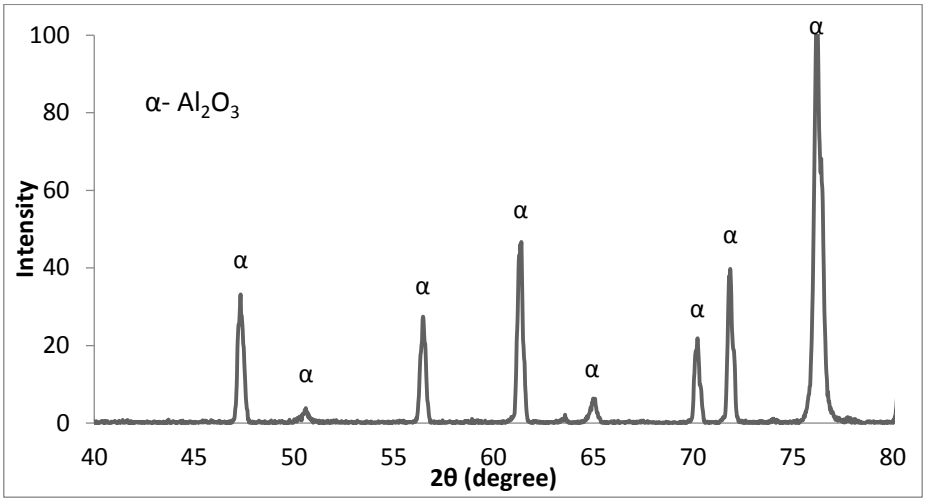

Figure 4-3: X-ray diffraction analysis of the alumina powder.

4.2. Optimisation of Slurry

The relationship between the rheological properties, dispersant concentration and the pH of the highly concentrated ceramic particles in an aqueous medium is of pronounced importance. These variables are key in controlling the stability of the ceramic suspension to ensure uniformity and to prevent flocculation. A high solids loading is desirable to reduce the shrinkage during drying and to ensure a high packing density. However, a low viscosity is necessary to ensure mould filling and adequate de-airing. Thus, a balance between these two opposing criteria, high solids

loading and slurry fluidity must be reached. The rheological behaviour of the colloidal suspension is influenced by two factors [50]:

i. Interparticle forces

   The interactions between charged particles in a solvent have an effect on the viscosity of the suspension and this can be stabilised by the use of dispersants.

ii. Particle characteristics

   The particle concentration and particle size has an effect on the rheological behaviour of the suspension.

The viscosity of the alumina suspensions prepared was determined using a rheometer (Anton Paar). The viscosity was plotted as a function of the shear rate, where the dispersant amount and the solids loading were varied and presented in the sections that follow.

4.2.1. Zeta Potential

The stability of colloidal systems is governed by the DVLO (Derjaguin-Landau-Vervey-Overbeek) theory [51]. Zeta potential is a measure of the stability of a colloidal suspension. The zeta potential indicates the pH at which the rate of flocculation is lower and the repulsion forces between the particles are large enough to overcome the Van der Waals attraction.

The variation of Zeta potential (ξ) of alumina suspension as a function of pH is shown in Table 4-1 and Figure 4-4. The isoelectric point or the characteristic pH of the suspension without a dispersant at which the net charge is zero was found at a pH of 7.8. Thus, at this pH the alumina particles in the solvent are unstable. It is clear that the zeta potential of alumina in the absence of a dispersing agent does not go beyond ± 30mV in the pH range of 2 to 10. Thus, the preparation of stable alumina suspensions by changing the pH alone requires selecting either a low or high pH as stability can be achieved beyond a Zeta potential of ± 30mV.

However, the addition of a dispersing agent moved the isoelectric point from a pH of 7.8 to 4.1 when 0.3wt% Isobam® was added and to a pH of 2.2 when 1vol% APAA was added. The zeta potential was at the pH of 7.8 was moved to -30mV for APAA addition and moved to -40.4mV when Isobam® was added. This indicates that both APAA and Isobam® are effective dispersing agents for α-alumina.

Table 4-1: Determination of Zeta potential at the measured pH value.

pH	**ξ [mV] pure Al_2O_3**	**pH**	**ξ [mV] Al_2O_3 with APAA**	**pH**	**ξ [mV] Al_2O_3 with Isobam**
1.5	51.60±0.50	1.4	5.17±1.26	2.5	40.10±1.53
2	48.96±0.60	2.5	-1.52±1.53	3.8	20.40±0.65
2.7	26.49±0.80	4.26	-18.10±0.65	4	4.07±3.10
4	27.52±0.66	8.8	-34.56±3.11	4.5	-6.21±0.40
5.5	24.03±0.50	11.2	-45.03±1.40	5.7	-18.01±1.40
6	16.40±0.05	12.1	-35.65±3.37	6.2	-30.30±3.30
7.56	7.43±0.40			7	-40.10±0.97
8	-18.40±0.56			9.2	-50.20±1.92
9	-20.90±0.80			10.2	-48.40±2.42
10	-28.80±0.50			11.5	-43.20±1.06
11	-39.10±0.63				
11.6	-41.50±0.41				

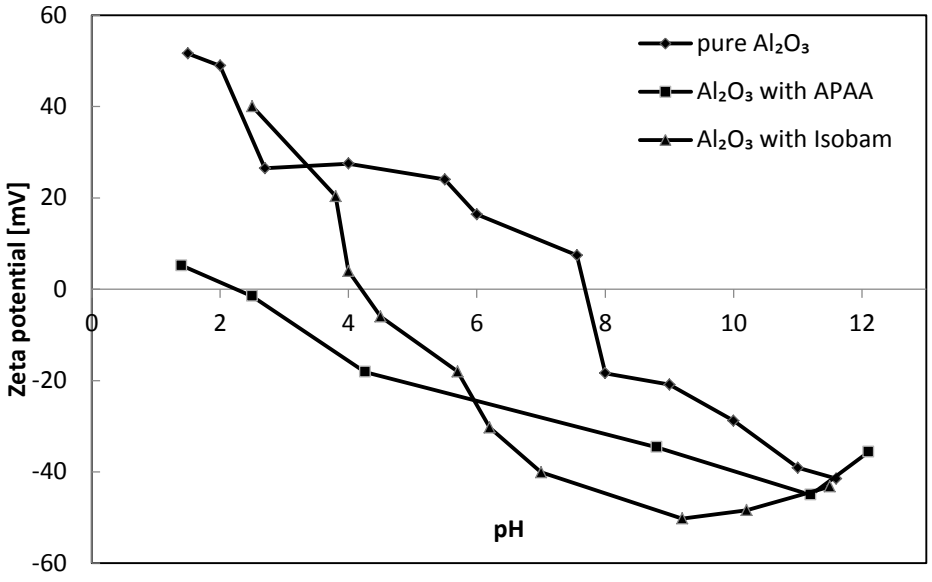

Figure 4-4: The measure of Zeta potential as a function of pH.

4.2.2. Dispersant amount

In colloidal forming processes, it is essential that enough dispersant is added to the ceramic slurry to ensure complete coverage of all the powder particles. The absorption of the dispersant onto the powder surfaces creates a large repulsive electric double layer that can overcome the attractive Van der Waals forces that are present [52]. This allows for the preparation of highly loaded and stable suspensions.

4.2.2.1. Effect of Ammonium Poly-Acrylic Acid (APAA)

Ammonium poly acrylic acid was used as a dispersant for the HEMA-MBAM gel-binder system. The amount of APAA was varied from 0.5 to 1.5vol% of the Al_2O_3

powder. Figure 4-5 illustrates the effect of the dispersant (APAA) concentration as a function of the viscosity at a shear rate of $100s^{-1}$. It was observed that the lowest viscosity was obtained at a dispersant concentration of 1vol%.

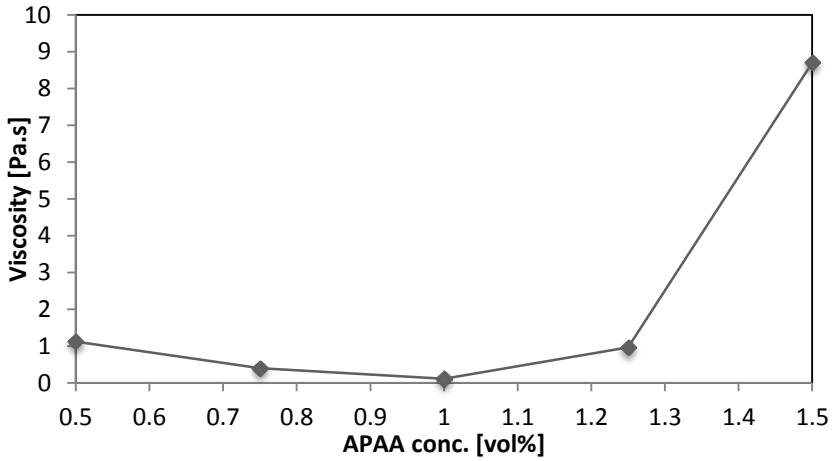

Figure 4-5: Effect of APAA concentration on the viscosity of 50vol% alumina suspensions at a shear rate of $10s^{-1}$.

4.2.2.2. Effect of Isobam® Dispersant

The dispersant (Isobam®) was varied between 0.1 and 0.7wt% of the Al_2O_3 powder. Figure 4-6 shows the viscosity of the suspension as a function of dispersant concentration for a 60vol% solids loading. The optimum Isobam® concentration giving the lowest viscosity was observed at a dispersant concentration of 0.3wt%.

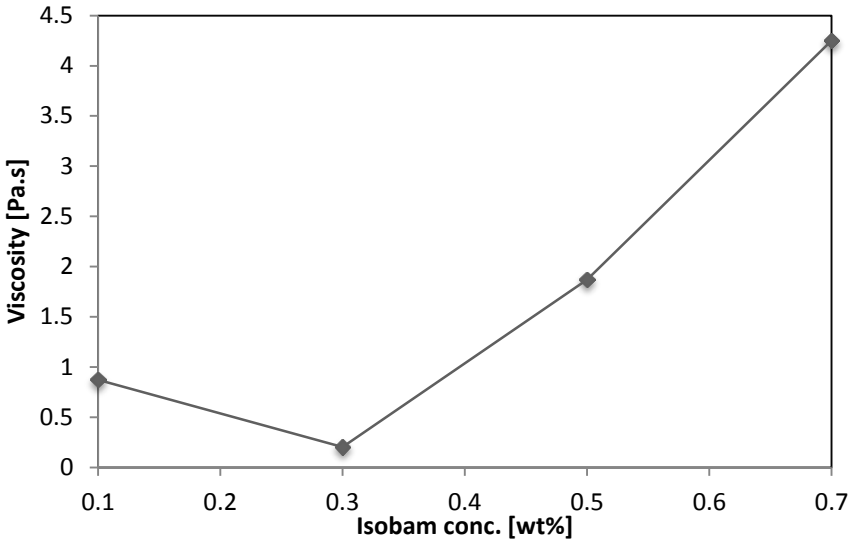

Figure 4-6: Effect of Isobam® concentration on the viscosity of 60vol% alumina suspension at a shear rate of $10s^{-1}$.

4.2.3. Viscosity-Shear Relationship

The viscosity flow curves for HEMA-MBAM and Isobam® based suspensions as a function of shear rate are shown in Figure 4-7 and Figure 4-8 respectively. It was observed from these curves that the suspensions exhibit a significant shear thinning behaviour over a wide range of shear rate. At higher solids loading thixotropic behaviour can be observed for both HEMA-MBAM and Isobam® systems. This behaviour was followed by a tendency to Newtonian plateau at very high shear rates ($1000s^{-1}$). The viscosity trend was expected as the viscosity of colloidal suspensions increases with an increase in solids loading and decreases as the shear rate decreases as reported by Bergstrom [4].

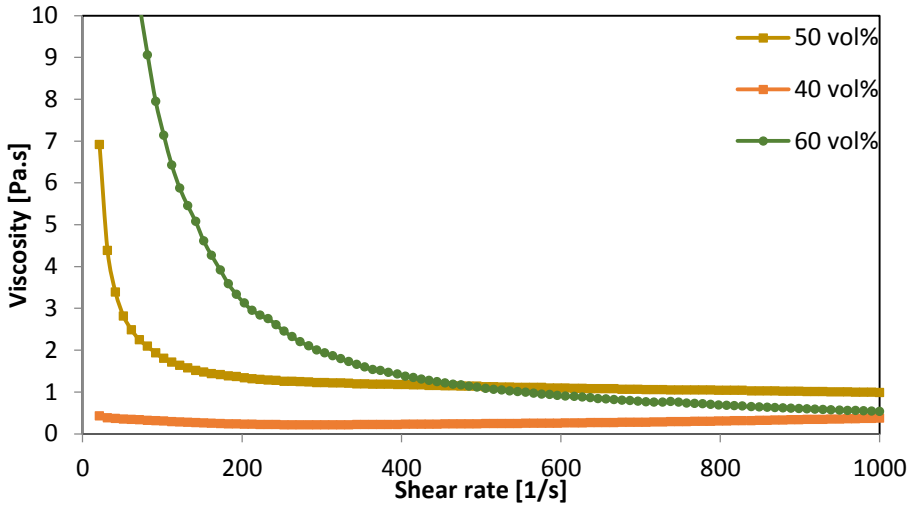

Figure 4-7: The viscosity of alumina suspensions with varied solids loading using 1vol% APAA as a dispersant.

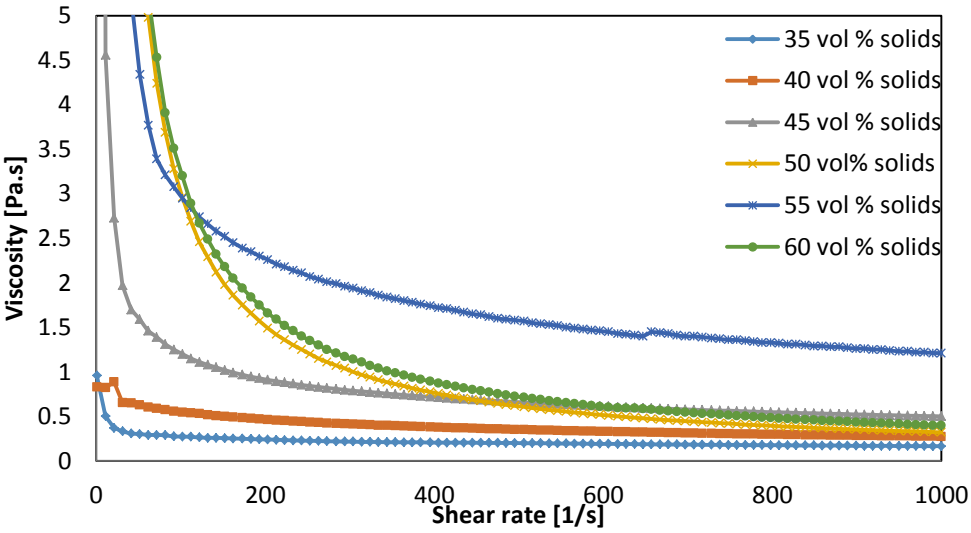

Figure 4-8: The viscosity of alumina suspensions with varied solids loading using 0.3wt% Isobam® as a dispersant.

4.2.3.1. Rheology Modelling

The effect of shear on the suspension structure can be conceptually demonstrated using models. The Cross model [52] and the Reddy model [53] were used to model the shear thinning behaviour and the effect of solids loading on the rheology of the suspensions.

4.2.3.2. The Cross Model

The Cross model was developed to study the relationship between deformation and stress for non-Newtonian suspension's behaviour [52]. The Cross model involves determining four parameters that are required to predict the general flow behaviour. The Cross model is quantified by Equation 4-1 [52].

$$\boldsymbol{\eta - \eta_{\infty} = \frac{\eta_0}{\alpha \gamma^n}} \qquad \text{Equation 4-1}$$

Where:

η = effective viscosity as measured by a rheometer (Pa.s),

η_{∞} = viscosity at a very high shear rate (Pa.s),

η_0 = viscosity at a low shear rate, close to zero (Pa.s),

α = consistency index

γ = shear rate as measured by a rheometer(s^{-1}), and

n = flow behaviour index.

The viscosity and shear rate relationship was used to model the pseudo-plastic behaviour of the suspensions. At high shear rates $\alpha\gamma^n >> 1$, the Cross equation can be reduced to Equation 4-2 to determine the behaviour index n. For shear thinning suspensions, the viscosity at a high shear rate tends to zero, thus the relationship between log η and log γ shows a linear relationship with n as the slope (Figure 4-9(a)). The Cross equation can then be converted to Equation 4-3 to determine the viscosity at very high shear rates. This value can be determined graphical as the intercept of the relationship between η and γ^n (Figure 4-9(b)). The graphical determination of the Cross parameters for Isobam® can be found in Appendix A.1.

Equation 4-4 was then used to determine the viscosity of the suspension at rest, which is at a shear rate of zero according to Hammad and Vradis [54]. The final obtained values for the four parameters of the 50vol% alumina suspension prepared using a) APAA and b) Isobam® are shown in Figure 4-10.It can be observed that the viscosity and shear rate relationship using the estimated parameters is in reasonable agreement with the values obtained experimentally.

$$\log(\eta - \eta_\infty) = log\left(\frac{\eta_0}{\alpha}\right) - nlog(\gamma) \qquad \text{Equation 4-2}$$

$$\eta = \eta_\infty + \frac{\eta_0}{\alpha}\gamma^{-n} \qquad \text{Equation 4-3}$$

$$\eta_0 = 1000\eta_\infty \qquad \text{Equation 4-4}$$

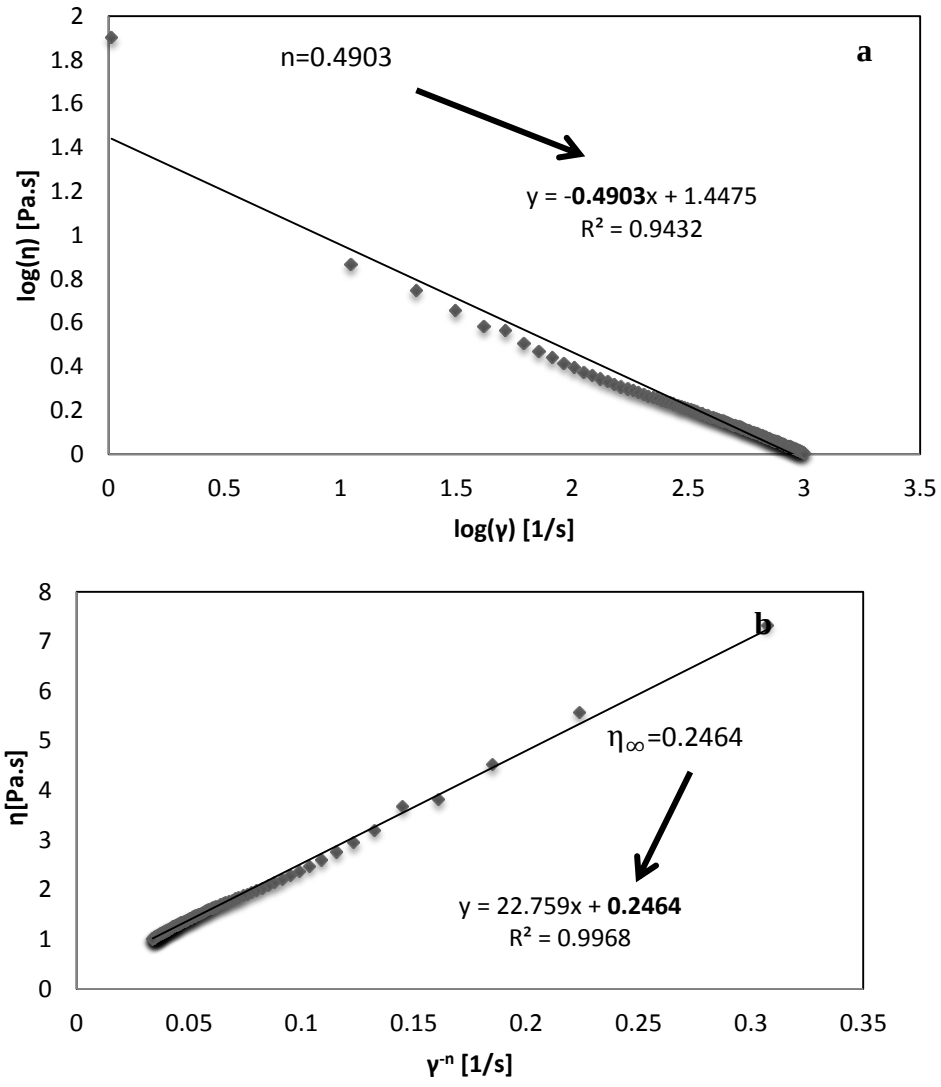

Figure 4-9: Determination of Cross parameters, behaviour index and viscosity at very high shear rates, respectively.

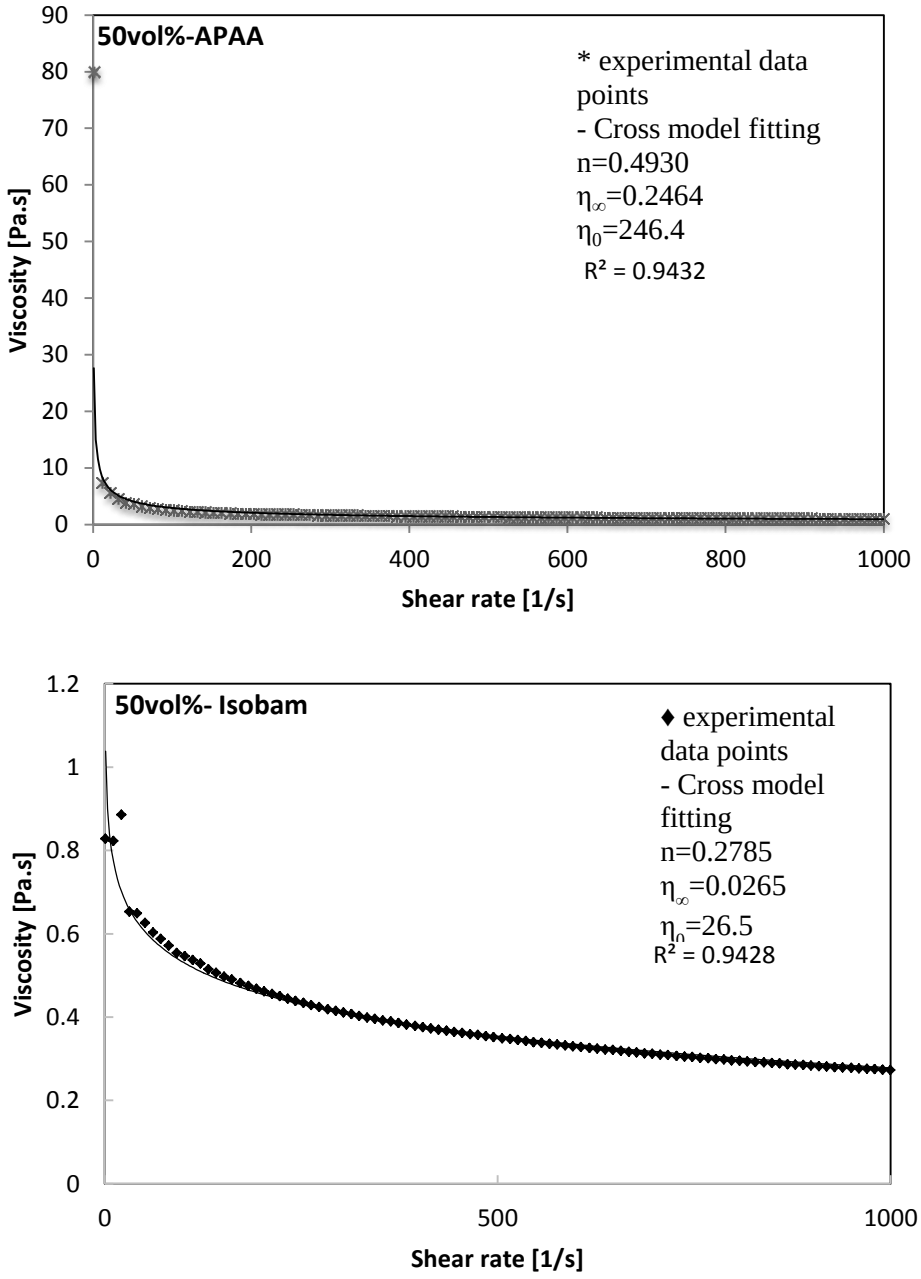

Figure 4-10: Fitting of the Cross model to the viscosity shear rate relationship of alumina suspension prepared using 50vol% solids loading.

4.2.3.3. The Reddy Model

Figure 4-7 and Figure 4-8 show the effect of alumina content on the rheological behaviour of suspensions prepared using APAA and Isobam®, respectively. As the solids loading increases the Van der Waals forces increase [50], thus an increase in viscosity was observed. The correlation between the relative viscosity of the suspensions and the solids loading can be approximated using the Reddy model based on the rule of mixtures Equation 4-5 [53].

$$\eta = \eta_0 \left(\frac{\phi_m}{\phi_m - \phi}\right) \qquad \text{Equation 4-5}$$

Where:

η = the intrinsic viscosity as measured using a rheometer (Pa.s),

η_0 = the viscosity of the medium taken as 1Pa.s for water (Pa.s),

ϕ = the volume fraction of solids,

ϕ_m = the maximum achievable solids loading.

The Reddy model was selected to model the suspension's viscosity because of its simplicity and versatility. The viscosity of the suspensions were found to show a shear thinning behaviour as shown in Figure 4-7 and Figure 4-8. Table 4-2 gives the results of the varied solids loading as prepared by using ammonium poly acrylic acid and Isobam® as dispersants. The maximum solids loading was determined from the slope of the linear relationship between the viscosity (η) and a product of the viscosity and solids fraction ($\eta\phi$) as shown in Figure 4-11 and it was found to be 60vol% for APAA dispersant and 55vol% for Isobam®.

Table 4-2: Viscosity as a function of solids loading at a shear rate of 1000s^{-1}

ϕ(%)	Viscosity, Pa.s (APAA)	Viscosity, Pa.s (Isobam®)
0	0	0
40	0.336	0.274
50	0.526	0.321
60	0.982	0.399

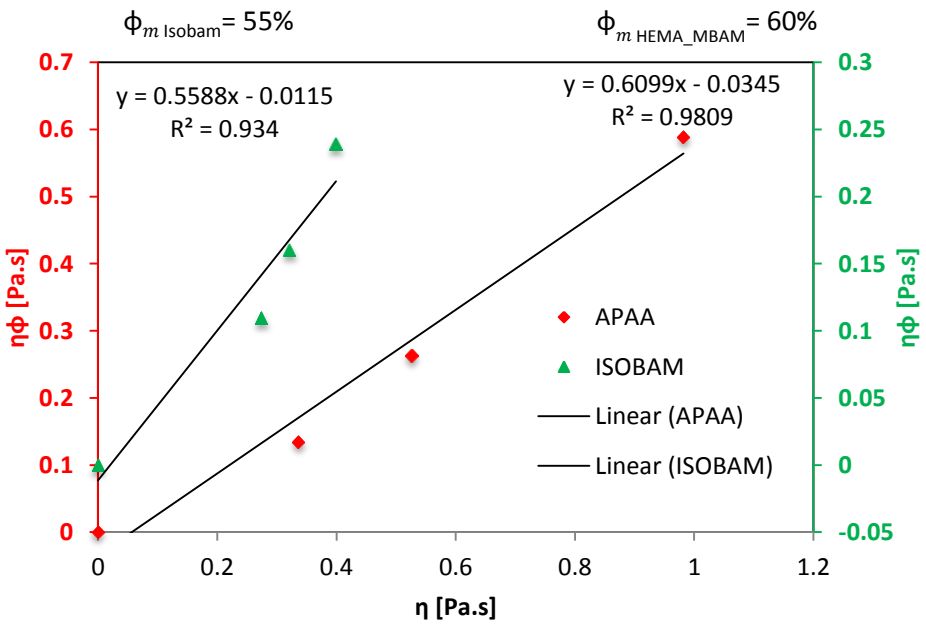

Figure 4-11: Linearisation and fit of the Reddy model to determine maximum solids loading.

4.3. Additive Manufacturing of Moulds and Casting

The ceramic slurries were cast into different shaped mould materials that have been prepared using 3D printing techniques rather than moulds produced from materials such as stainless steel. The moulds tested are shown in Table 4-3. The moulds were coated with a thin layer of release agent to reduce the interaction of the gelled part with the mould surface so that the cast part could be easily removed. Different release agents such as petroleum jelly and silicone spray were tested. It was found that petroleum jelly facilitated the easiest demoulding and the parts did not adhere to the mould. The green cast part and the dried body are shown in

Figure **4-12** and Figure 4-13; this illustrates the capability of the process to produce complex shaped parts. Several different mould materials were tried, but the best removal of the casting was found to be from the ABS resin.

Table 4-3: Mould materials used for gelcasting alumina parts.

Mould Material	Comment
Rubber mould	Good mould release {not pursued}
3D printed PLA mould	Swelling of mould as it absorbs water (soluble in water) {not pursued}
3D printed ABS mould	Good mould release {used in this work} (soluble in acetone)

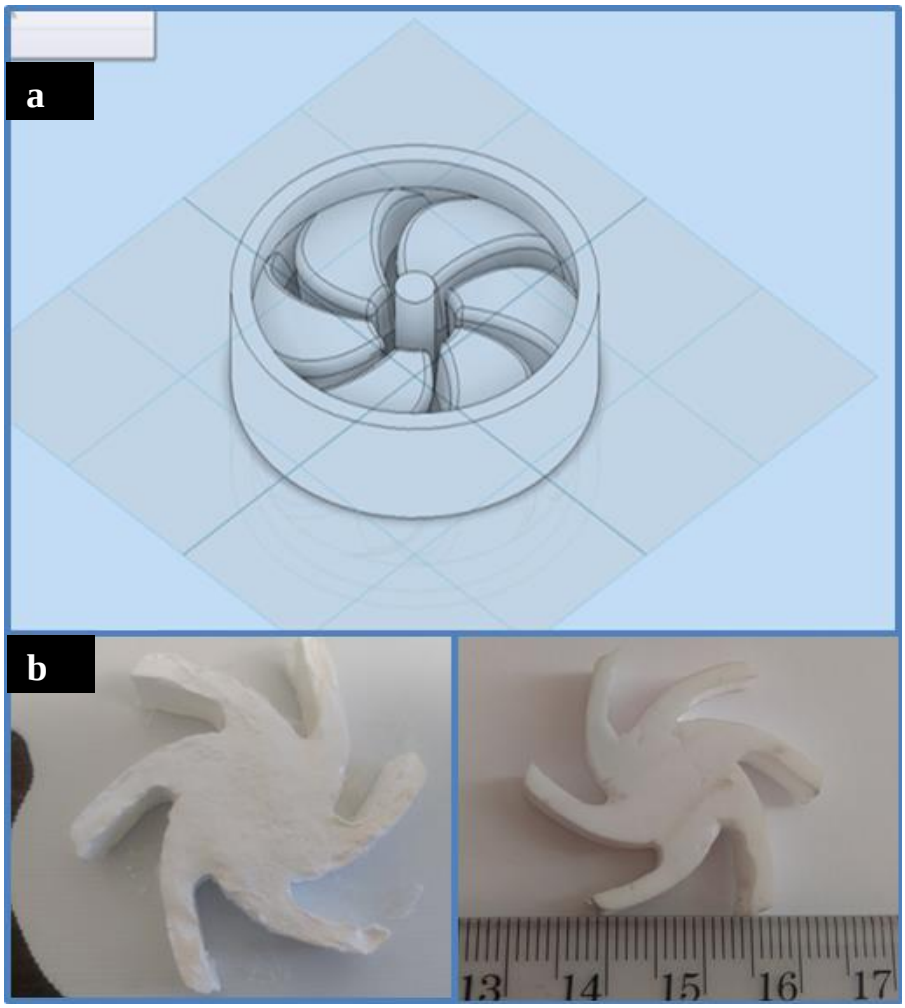

Figure 4-12: Illustration of the tooling method showing the CAD file of the ABS 3D printed mould and the product of the mould design.

Mould Used	Produced Part	Description
		Cylindrical shapes were used for characterisation purposes
		
	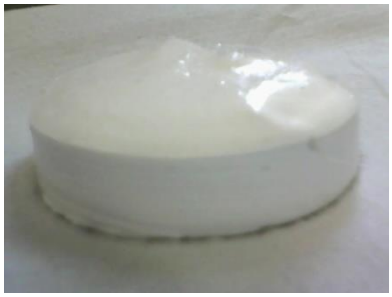	
	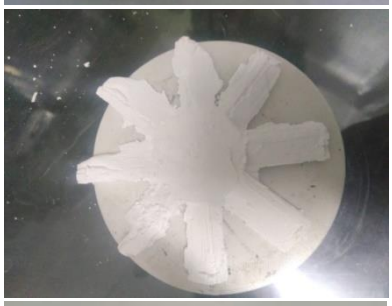	A complex shaped was used to determine the capabilities of the process to produce complex shapd parts.
	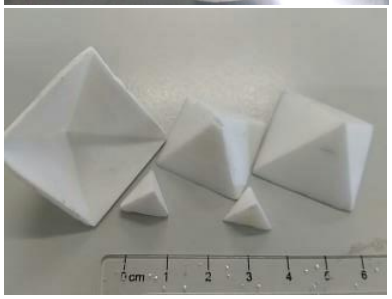	

Figure 4-13: Images illustrating the capabilities of the process used to fabricate simple and complex shaped parts with differing thicknesses

.

4.4. Gelation and Demoulding

For complex shaped gelcast parts, it is essential to demould the parts while avoiding cracking due to internal stresses that may form as the solvent is removed or evaporated from the wet body. A demoulding process was developed. This involved dissolving the ABS mould in acetone. The mould was found to dissolve in ±110 minutes at room temperature. However, longer exposure of the part to the acetone was found to adversely affect thin parts and complex angular shaped parts. Due to the drying effect of acetone, cracks were initiated in the parts as shown in Figure 4-14 (the green solvent is due to the colour of the ABS filament used). However, when the solvent (acetone) was heated to approximately 35°C, no cracks were observed on the parts. The moulds completely dissolved in acetone after approximately 65 minutes giving a part that was still rigid and strong enough for handling.



Figure 4-14: Cracks initiated due to fast drying as an effect of acetone.

4.5. Drying of Green Bodies

After gelation, the cast samples were demoulded and set to dry. Drying is a critical step in the gelcasting procedure. Fast drying results in sample distortion and cracking of the part as a result of differential drying. Drying of the cast samples was carried out in a drying chamber with controlled temperature and humidity. Figure 4-15 compares the drying efficiencies of samples drying at different temperatures and a relative density of 95%. Under these conditions, both thick and thin parts dried without cracking. However, at low relative humidity, the parts tend to crack.

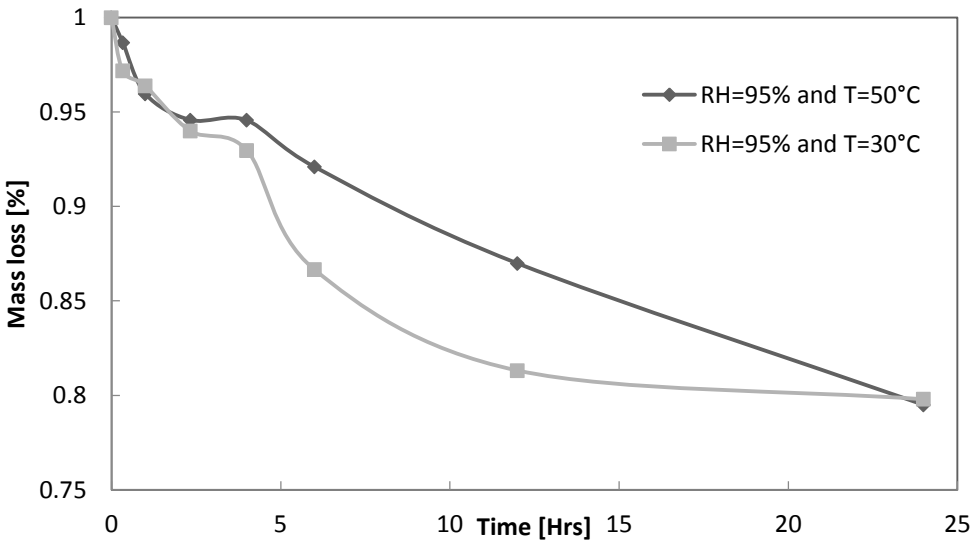

Figure 4-15: Mass loss during drying of the green cast parts in a controlled environmental chamber.

4.5.1. Shrinkage

Dimensional shrinkage is a typical phenomenon related to the casting processes caused by volumetric shrinkage during the drying process. The shrinkage of the green samples was calculated using equation 4-6. The dimensions of the mould and the dried samples were used to determine the drying shrinkage, while the shrinkage after sintering was determined using the dimensions of samples before and after sintering.

$$\%\ dimensional\ shrinkage = \left(\frac{L_d - L_i}{L_i}\right) \times 100 \qquad \text{Equation 4-6}$$

Where: L_d =dimension of dried sample (mm) and

L_i= dimension of mould cavity (mm).

The drying shrinkage was found to be 4% for both the 50 and 60vol% solids loading, differing from the alumina gelcast using 40vol% that had 14% shrinkage as shown in Table 4-4. The sintering temperature was the same for all solid loadings giving the shrinkage of 18-19% with an outlier of 16.81% which as yet cannot be explained.

Table 4-4: Densities and shrinkages of gel cast alumina sintered at 1650°C.

Solid loading	Green density (%)	Drying shrinkage (%)	Sintered density (%)	Sintering shrinkage (%)
40vol%	53.64	14.3	98.25	19.5
50vol%	63.31	4.7	98.51	16.81
60vol%	62.75	4.5	97.95	18.01

4.1. Sintering and Characterisation

The gelcast parts underwent binder burn out to remove the organic constituents prior to sintering at 600°C in air. The parts were then sintered in a muffle furnace at temperatures ranging from 1450 to 1700°C in air for 3 hours. Complex and cylindrical shaped parts were produced. The cylindrical shaped parts were used for analysis.

4.1.1. Effect of Sintering Temperature

After binder burn-out the green bodies were sintered at various temperatures to find the temperature that would give the required mechanical properties. The temperatures tested were 1450°C, 1550°C, 1650°C and 1700°C for a sintering time of three hours. The resulting sintered ceramic was characterised by the Archimedes density technique, and further analysed by SEM. The SEM micrographs were obtained for the sintered samples from which the microstructure and the grain size were analysed. Samples prepared using the HEMA-MBAM binder system were selected to analyse the effect of the sintering temperature, summarised in Figure 4-16.

4.6.1.1. **Densities and Porosity of the Sintered Ceramics**

Table 4-4 shows the green density, sintered density and open porosity of the sintered ceramics prepared using HEMA-MBAM and sintered for three hours at various temperatures in air. The green density was found to increase with an increase in the

solids content in the starting powder. However, the sintered density is depended on the sintering temperature. The relative density was calculated based on the theoretical density of α-alumina of 3.97 g/cm^3.

Table 4-5: Densities of HEMA-MBAM gelcast and sintered ceramic parts as a function of the sintering temperature.

Sample	**Green Density (g/cm^3)**	**Relative green Density (%)**	**Set Sintering temperature (°C)**	**Sintered Density (g/cm^3)**	**Relative sintered density (%)**	**Porosity (%)**
A40HM	1.82±0.06	45.61	1450	2.82±0.01	71.03	29.07
			1550	3.69±0.06	92.95	4.51
			1650	3.79±0.02	95.47	3.43
			1700	3.71±0.02	93.45	7.02
A50HM	2.04±0.02	51.13	1450	2.75±0.04	69.27	30.83
			1550	3.68±0.03	92.70	7.83
			1650	3.76±0.02	94.71	5.26
			1700	3.70±0.01	93.20	7.27

The sintering temperature effect on the densification of the gelcast alumina prepared by using HEMA-MBAM monomer were varied as shown in Figure 4-16. The sintered density was observed to increase with an increase in the sintering temperature from 1450 to 1650°C followed by a decrease at temperatures of 1700°C. This was due to grain growth as an increase in the sintering temperature is accompanied by a high degree of grain growth [34]. Thus, 1650°C was selected as the optimum sintering temperature for the alumina parts and parts sintered at this temperature were further analysed.

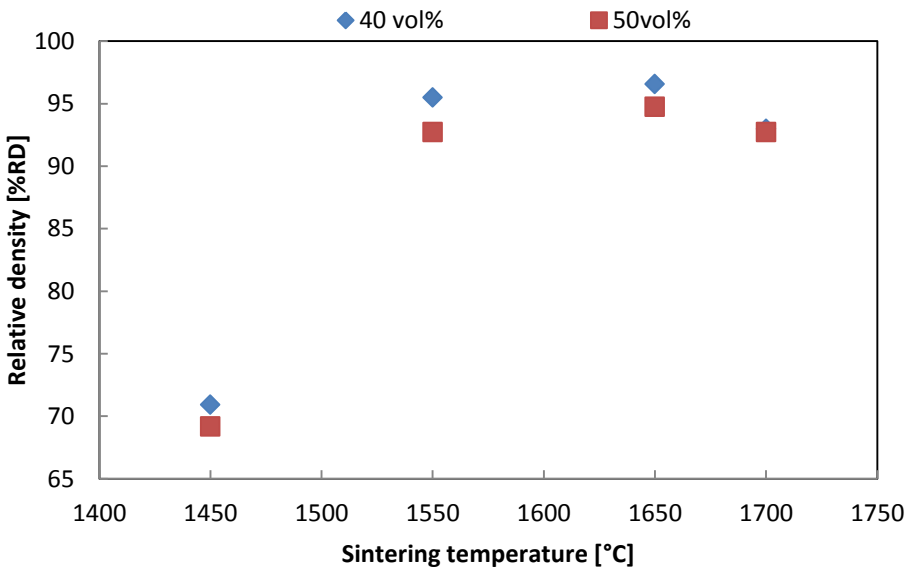

Figure 4-16: Relative density and porosity of Al_2O_3 parts after sintering at various temperatures for 3hrs for HEMA-MBAM/APAA system.

4.6.1.2. SEM Micrographs of the ceramic sintered at various temperatures

Figure 4-17 shows the SEM micrographs of the ceramic parts prepared using 50vol% solids loading, HEMA-MBAM monomer system and sintered at various temperatures. The SEM micrographs show the grain size of parts sintered at 1700°C which gave the largest grains, while a sintering temperature of 1650°C gave parts with homogeneous grains.

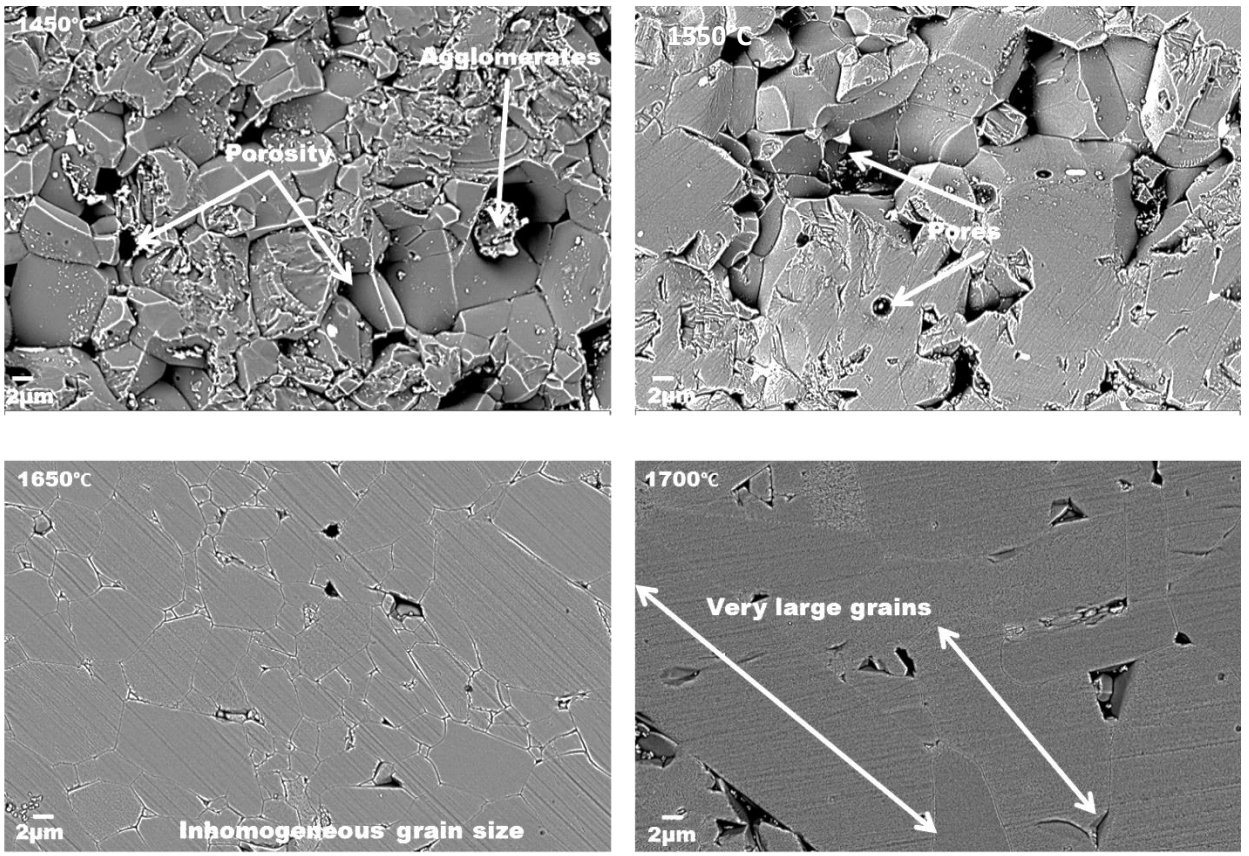

Figure 4-17: SEM micrographs of the ceramic sintered at: 1450°C , 1550°C, 1650°C and 1700°C for three hours in air.

4.1.2. Effect of Solids Loading

In the gelcasting of ceramic suspensions, the degree of densification is primarily related to the particle packing, the solids loading in the starting gelcasting suspension and the ratio of the surface energy of the powder particles to the interfacial energy of the sintered body [34]. The higher the ratio, the more densified the compact becomes during sintering.

4.1.2.1. Densities and Porosity of the Sintered Ceramics

Table 4-6 and Table 4-7 show the effect of the solids loading in the alumina suspensions on the relative density of the green and sintered alumina parts prepared by HEMA-MBAM and Isobam®. The effect of the solids content was varied from 40 to 70vol% for HEMA-MBAM and up to 60vol% for Isobam to determine the optimum solid content. An increase in the solids content in the suspensions from 40vol% causes the green densities to increase while the sintered densities increase and then decrease slightly at solids loading above 50vol% for HEMA-MBAM and 55vol% for Isobam®. This was attributed to high viscosity as the solid loading was increased. A high viscosity leads to insufficient de-airing and hinders the flow of the slurry thus allowing the formation of defects which hinder the densification process.

Figure 4-18 and Figure 4-19 shows the microstructures of ceramic parts gelcast using a solids loading varying from 40 to 70vol% for HEMA-MBAM and to 60vol% for Isobam®. A high degree of porosity was observed at low solids content. While, agglomeration can be observed at very high solids loading such as 70vol% for the

HEMA-MBAM system, while a cluster of grain sizes was observed for Isobam®. The 70vol% loaded suspension was not further pursued due to cracking and agglomeration at this solids loading.

Table 4-6: Comparison of sintering properties at 1650°C at different solids loading when using HEMA-MBAM monomer.

Solid loading	40vol%	50vol%	60vol%	70vol%
Density of green body(g/cm^3)	1.82±0.06	2.04±0.02	2.23±0.01	2.43±0.02
Density of sintered body(g/cm^3)	3.79±0.01	3.76±0.04	3.89±0.02	3.57±0.03
% Relative density	95.47	94.71	98.19	89.92

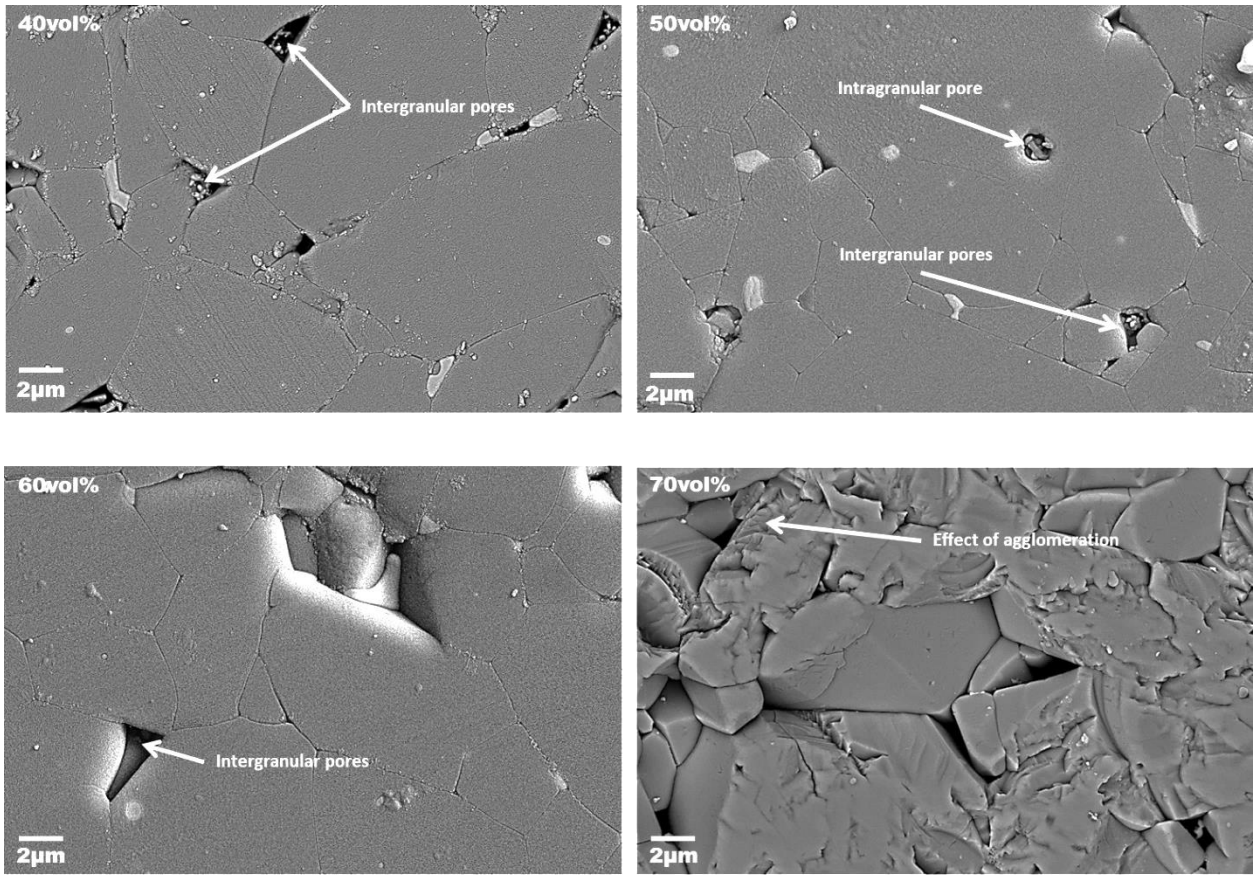

Figure 4-18: SEM micrographs of sintered alumina gelcast using varied solids loading and HEMA-MBAM system, sintered at 1650°C.

Table 4-7: Comparison of sintering properties at 1650°C at different solids loading when using Isobam® monomer.

Solid loading	40vol%	50vol%	55vol%	60vol%
Density of green body(g/cm^3)	1.84±0.06	1.91±0.03	2.08±0.01	2.33±0.07
Density of sintered body(g/cm^3)	3.89±0.02	3.87±0.05	3.94±0.02	3.83±0.04
% Relative density	98.84	98.48	99.27	96.59

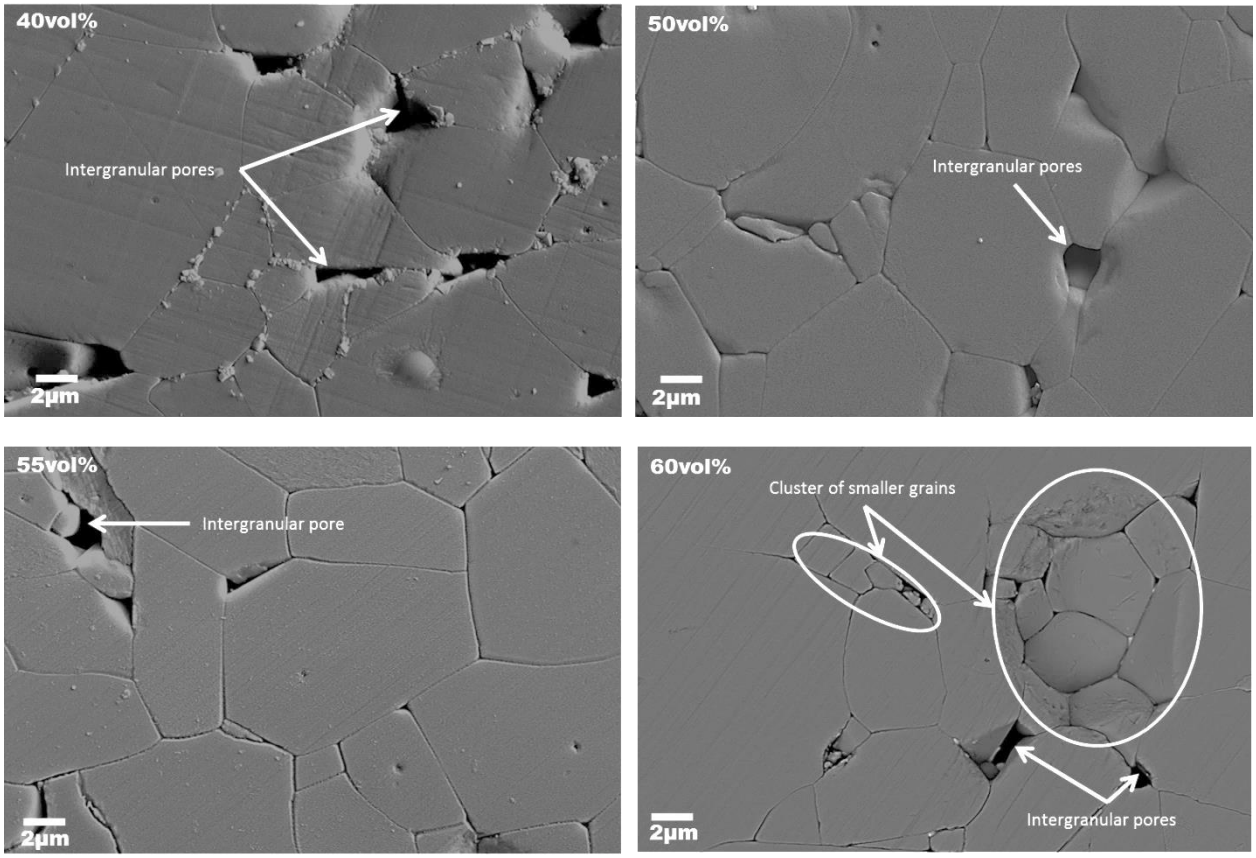

Figure 4-19: SEM micrographs of parts produced by Isobam® using varied solids loading and sintered at 1650°C.

4.1.3. Effect of Monomer / Gel-Binder System

There are numerous complex steps involved in the gelcasting of ceramics using the HEMA-MBAM system. Figure 4-20 illustrates the process steps involved in the suspension preparation and gelcasting when using HEMA-MBAM gel-binder systems together with examples of PVA-DHF and Isobam®. The Isobam® gel binder system has the least processing steps and is environmentally friendly, Table 4-8.

Table 4-9 and Figure 4-21 shows the densities obtained during the casting of 40vol% alumina content using the different monomer systems. From the data, the part cast using Isobam® exhibited the highest relative density of 97.74%. Therefore Isobam® and HEMA-MBAM were selected due to their environmentally friendliness and ability to produce parts with a uniform solid packing and high density.

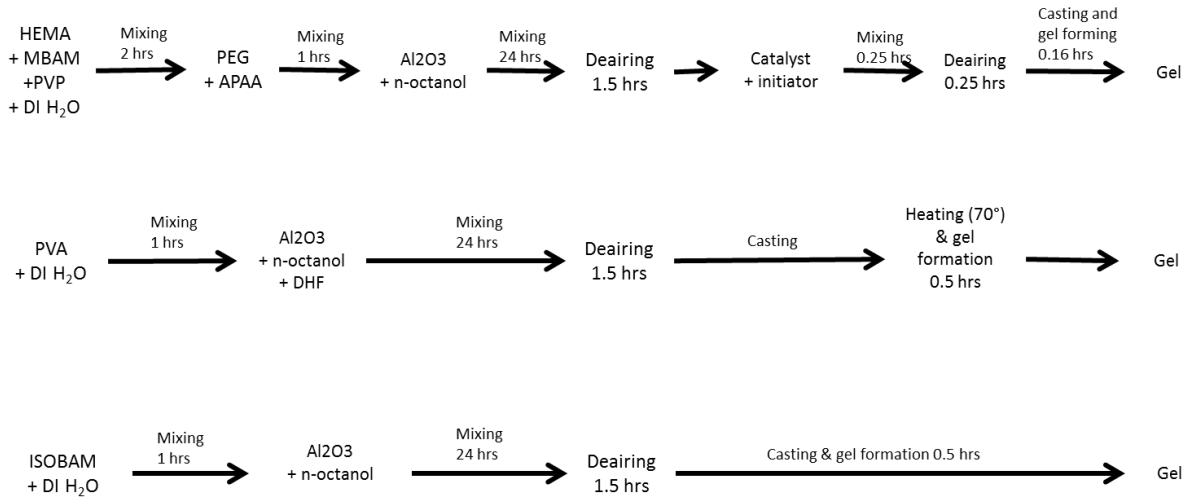

Figure 4-20: Illustration of the processing steps for different polymer / gel forming systems for casting alumina.

Table 4-8: Comparison between the different gel forming systems.

Gel former	HEMA-MBAM	PVA-DHF	Isobam®
Time requirement (hrs)	29	27	27
No. of additives	8	3	2
Gel formation requirement	Catalyst & initiator	Heat (70°C)	Room temperature
Safety consideration	Initiator toxic if inhaled	DHF is toxic a protective measures required	Environmentally friendly
Polymer content (wt%)	10	3.8	0.3
Advantage	Widely used and process has a track record.	PVA is widely used as a binder in ceramic forming	Water soluble copolymer, results in low shrinkage

Table 4-9: The effect of different monomer system on the density and open porosity of gelcast parts using 40 vol% solids loading and sintered at 1650°C

Sample	HEMA-MBAM	PVA-DHF	Isobam®
% Relative density of green body	42.57	42.71	46.25
Density of sintered body (g/cm^3)	3.83±0.12	3.78±0.09	3.88±0.11
% Relative density	96.84	95.16	98.84

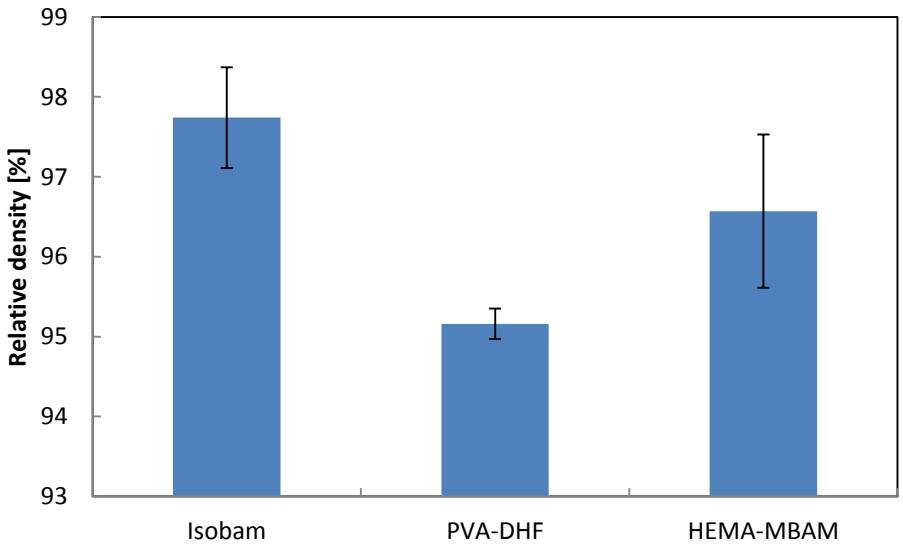

Figure 4-21: Effect of monomer system on the sintered relative density of alumina using 40vol% solids loading.

4.1.4. De-airing

Colloidal processing techniques exhibit one inherent problem, the presence of pores that are a result of entrained air bubbles in the suspension. These entrapped air bubbles are the result of the solvent used and the vigorous mixing procedures. Various techniques such as the addition of a de-airing aid or de-foaming agent, mechanical vacuum pump and ultrasonic vibration were used with the aim to reduce entrained air bubbles as shown in Table 4-10.

Table 4-10: Effect of de-airing technique on the density of cast parts using Isobam®.

De-airing technique	**After casting**	**Prior to casting**	
Casting technique	**Bottom feed**		**Top feed**
% relative density of green body	42.74	55.01	54.76
% relative density of sintered body	87.58	98.61	98.1
Porosity (%)	5.79	0.15	0.12

The SEM microstructures of the sintered gelcast samples made from suspensions that had undergone insufficient de-airing are shown in Figure 4-22. These images indicate the presence of elliptic shaped pores that were caused by trapped air bubbles as shown in Figure 4-22(a). Figure 4-22(b) shows the SEM microstructures of sintered gelcast samples whose suspensions were de-aired using a de-foaming aid, n-octanol, and have undergone sufficient de-airing. The bubbles were practically removed from the slurries, and therefore the structures appear homogeneous.

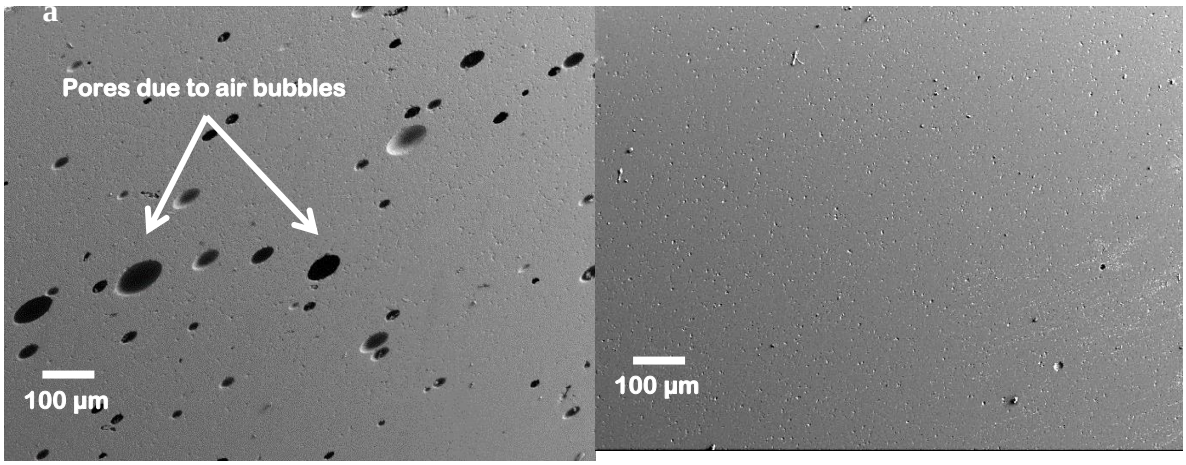

Figure 4-22: Illustration of the effect of de-airing a)Image showing bubbles as a result of insufficient de-airing (RD=87.58%) and b) SEM image showing sufficient de-airing with a microstructure with minimal defects (RD=98.61%) .

4.1.4.1. Effect of Deairing Time

The effect of the deairing time was varied between 15 and 120 minutes to study the effect on the final density of the cast parts prepared by Isobam®. Figure 4-23 shows the effect of the deairing time on the relative density of the sintered alumina parts. The relative density increases as the deairing time increases up to 120 minutes.

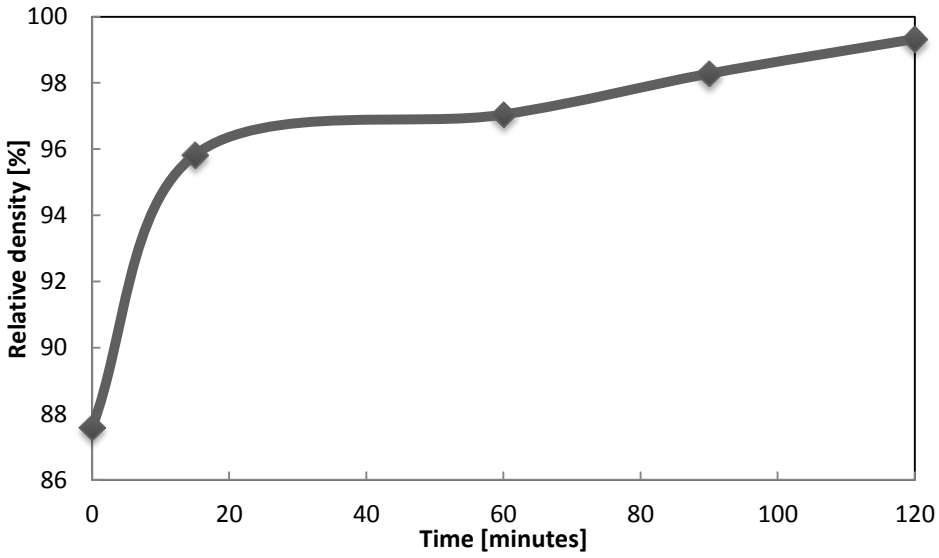

Figure 4-23: The effect of deairing time on the relative density of gelcast alumina parts sintered at 1650°C.

4.1.5. Grain Growth Inhibitors

Sintering is driven by the Gibb's free energy, which is a function of temperature [17]. During the sintering of ceramics, an increase in temperature leads to grain growth. However, the mechanical properties of ceramics are highly depended on its microstructure and grain size. A grain growth inhibitor was added to the starting powder as an attempt to minimise grain growth during the sintering of alumina. Magnesium

oxide was used as a grain growth inhibitor. The grain size was determined using the linear intercept technique on SEM images taken from all the sintered samples.

The results obtained are summarised in Table 4-11. Figure 4-24 and Figure 4-25 illustrate the EDS characterisation of MgO doped alumina samples which confirmed that the part contained both Al_2O_3 and MgO in the proportions used in the starting powder. Figure 4-25 shows the grains of the sintered parts which were observed to be both elongated and spherical.

Table 4-11: Effect of MgO addition on the density, mechanical properties and grain size of alumina sintered at 1650°C using 50vol% solids loading.

Monomer	**Isobam®**	**HEMA-MBAM**
Relative density (%)	98.08±0.24	97.52±0.80
Hardness (GPa)	17.03±1.23	14.87±0.51
Fracture toughness (MPa.√m)	3.23	1.33

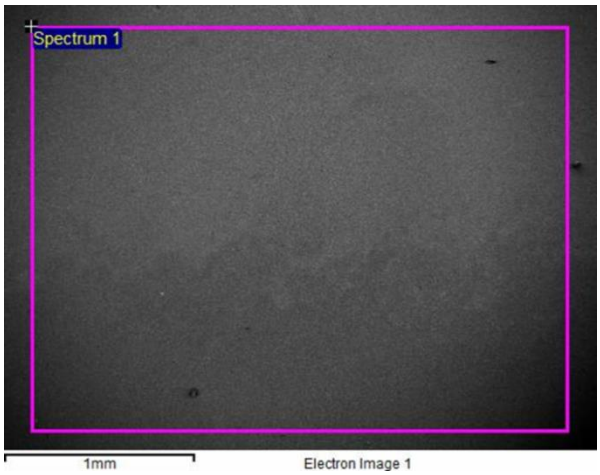

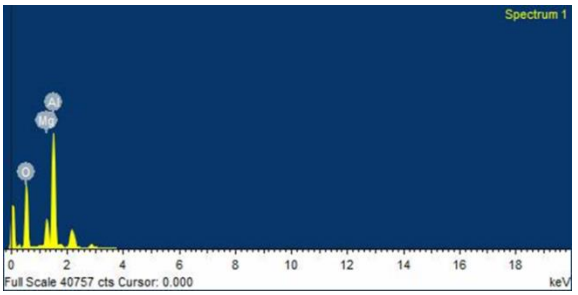

Element	Weight%	Atomic%
O	43.08	55.62
Mg	9.64	8.19
Al	47.28	36.19
Totals	100.00	

Figure 4-24: SEM-EDS results for MgO doped gel cast alumina ceramic part and elemental analysis.

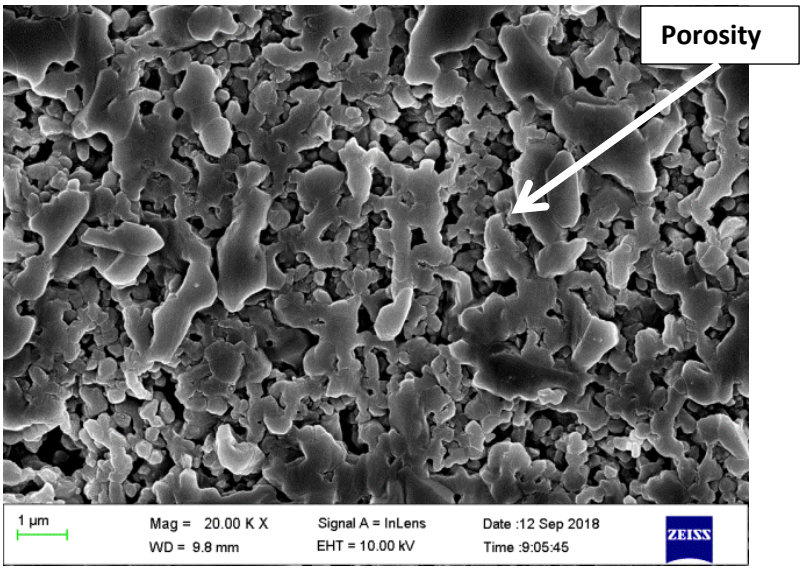

Figure 4-25: SEM image of MgO doped gel cast alumina part, sintered at 1650°C.

4.2. Complex Shaped Parts

Complex shaped parts were produced using the data obtained from previous tests. The Isobam® and HEMA-MBAM gel binder systems were used to produce the complex shapes. The solids loading used were those that ensured easy and porosity free filling of the mould; these were 40 and 50 vol%. All produced parts were dried and then sintered at 1650°C in air. The density of the produced parts was analysed by Archimedes' Principle and the results summarised in Table 4-12.The parts produced are shown in Figure 4-26, Figure 4-27 and Figure 4-28. The images illustrate the effect of the 3D printing process which leaves marks on the surface of the cast parts, these marks were almost invisible after the part was sintered. The parts produced vary in size.

Table 4-12: Properties of complex shaped parts produced and sintered at 1650°C in air.

Sample #	Density (g/cm^3)	Relative density (%)
A40IB-PYR-Solid	3.95±0.07	99.60
A50IB-PYR-Solid	3.94±0.04	99.29
A50IB-PYR-Hollow	3.08±0.06	95.94
A40IB-IMP-3Blades	3.93±0.09	99.09
A50HM-IMP-3Blades	3.26±0.12	82.14
A50HM-IMP-6Blades	3.76±0.17	94.74

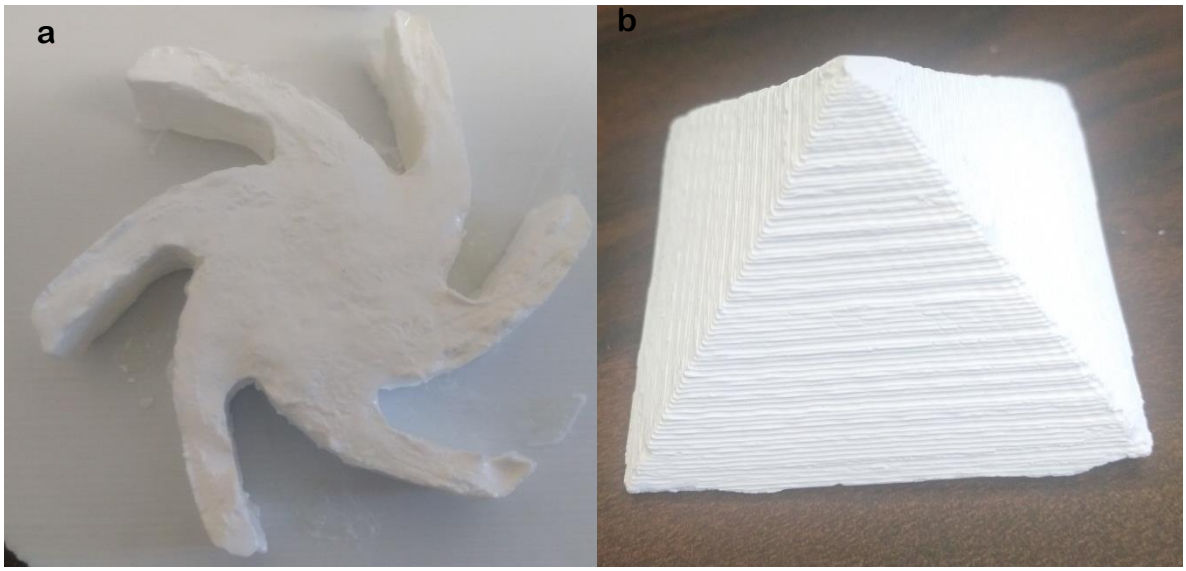

Figure 4-26: Illustration of complex shaped parts produced, a) as demoulded 6-blade impeller and b) a dried solid pyramid showing markings as a result of the resolution on 3D printed moulds.

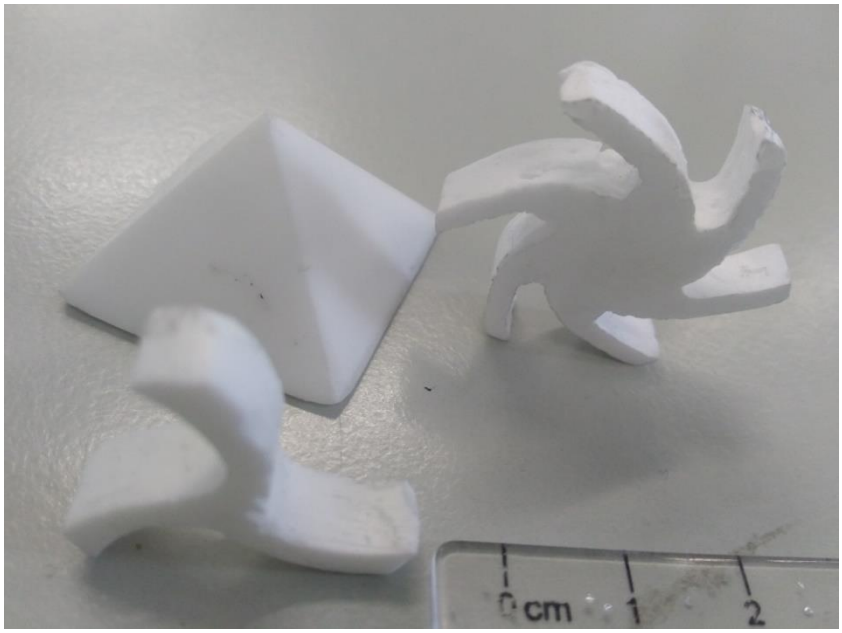

Figure 4-27: Complex shaped parts produced using Isobam® **system and sintered at 1650°C for 3 hrs (3-blade and 6-blade impellers as well as a solid 4 sided pyramid).**

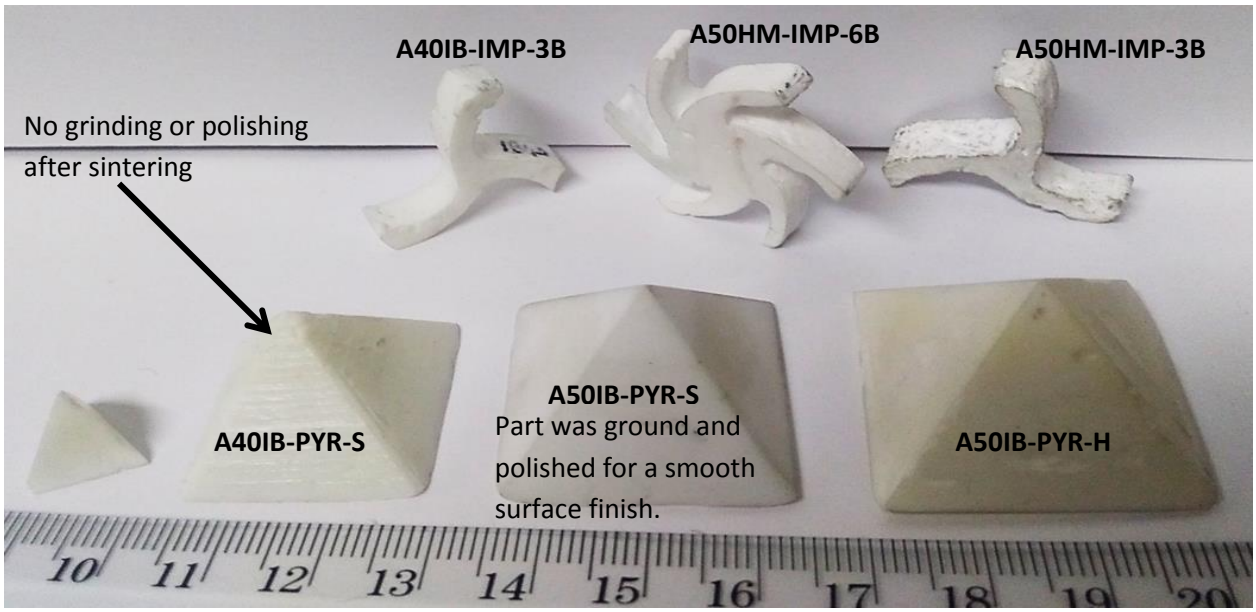

Figure 4-28: Illustration of different pyramid shapes (solid and hollow pyramids) and sizes that were produced by gelcasting using 3D printed moulds.

4.3. Mechanical Behaviour

The mechanical properties of ceramic materials are dependent on the existence of and size of microstructural inhomogenities, such as pores and grain size. The Vickers indentation technique was used to measure the hardness and fracture toughness. The ball on three balls test was used to determine the transverse rapture strength of the sintered materials. A correlation between the mechanical properties and physical and microstructural characteristics was established.

4.3.1. Hardness and Fracture Toughness

The hardness of the sintered gelcast parts was determined and it was compared for parts gelcast using 40, 50 and 60vol% solids loading using different gel binder systems. Figure 4-29 illustrates an indentation by a Vickers tester, medial and secondary cracks can be observed. The results for the Vickers hardness and fracture toughness tests for the various fabricated materials are presented in

Table **4-13.**

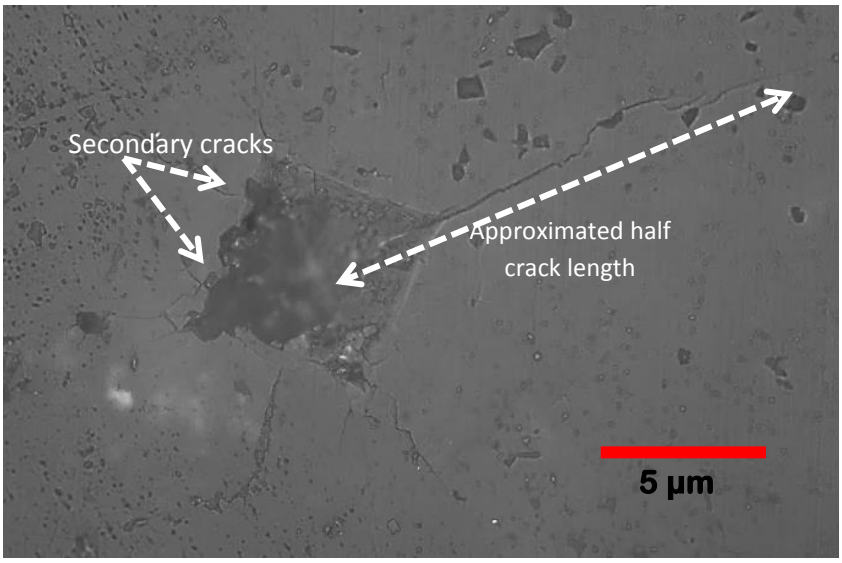

Figure 4-29: Optical micrograph showing Vickers indentation and cracks radiating from the corners of the indent of the alumina using an indentation load of 5kgf.

Table 4-13: Mechanical properties of various gelcast alumina parts sintered at 1650 °C.

Monomer	Solids loading (vol%)	Relative density (%)	Hardness (GPa)	Fracture toughness (MPa.√m)
Isobam®	**40**	98.60±1.00	18.38±1.13	3.93±0.69
	50	98.76±0.24	16.17±1.99	4.24±0.54
	55	99.19±0.08	16.28±0.69	3.83±0.80
	60	98.35±0.47	15.39±2.15	5.35±0.67
HEMA-MBAM	**40**	96.25±0.87	13.85±0.11	2.16±0.61
	50	96.84±1.51	11.29±1.81	1.97±0.43
	60	98.19±0.35	15.09±0.88	2.99±0.96

Figure 4-30 shows the dependence of the Vickers hardness (GPa) as a function of the solids content for both Isobam® and HEMA-MBAM monomer systems. The hardness decreases as the solids loading is increased from 40 to 60vol% for Isobam® samples while the HEMA-MBAM monomer system had the highest hardness at 60vol% solids loading. This may be due to particle packing and the stability of the alumina particles in the suspensions because the stability is highly depended on the dispersant used.

Moreover the hardness was plotted against the relative density in Figure 4-31, where the hardness exhibits a directly proportionality relationship.

The fracture toughness of the parts fabricated using Isobam® monomer shows a contradictory relationship that that of the hardness when plotted against the solids loading. The fracture toughness was found to increase as the solids loading is increased from 40 to 60vol% as shown in Figure 4-32. This relationship was also true for HEMA-MBAM samples. Figure 4-33 shows the relationship between the hardness and fracture toughness against the average grain size. Both the hardness and fracture toughness increase as the grain size is increase to 5µm, however for grain sizes as high as 9µm, both the hardness and fracture toughness decreases. These results were expected as an increase in grain size negatively affects the mechanical properties of ceramics.

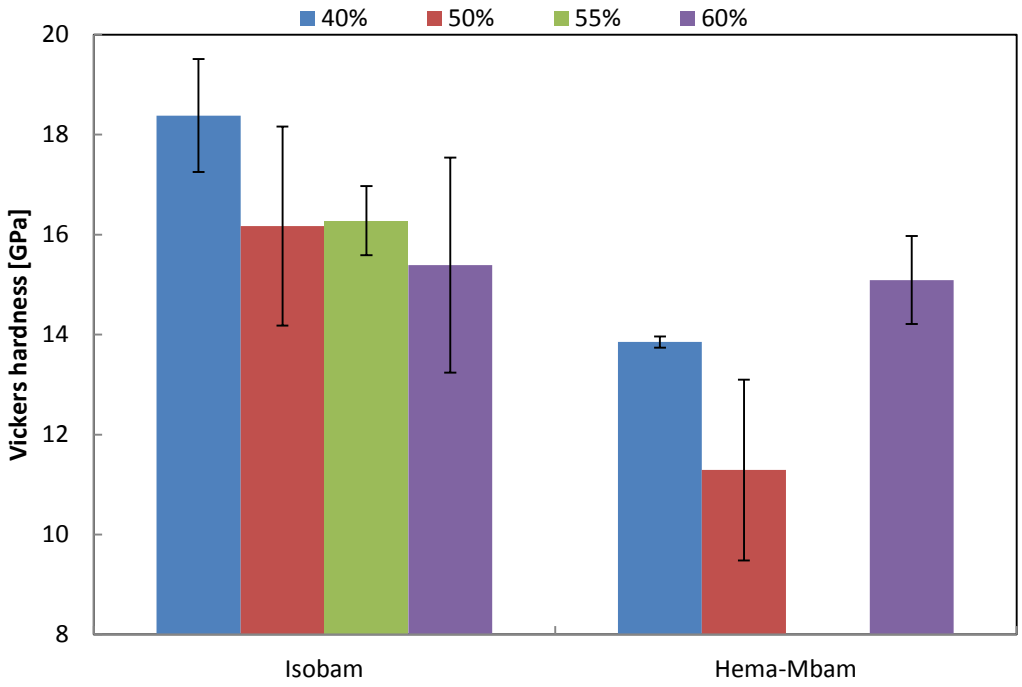

Figure 4-30: Dependence of Vickers hardness to solids loading and monomer.

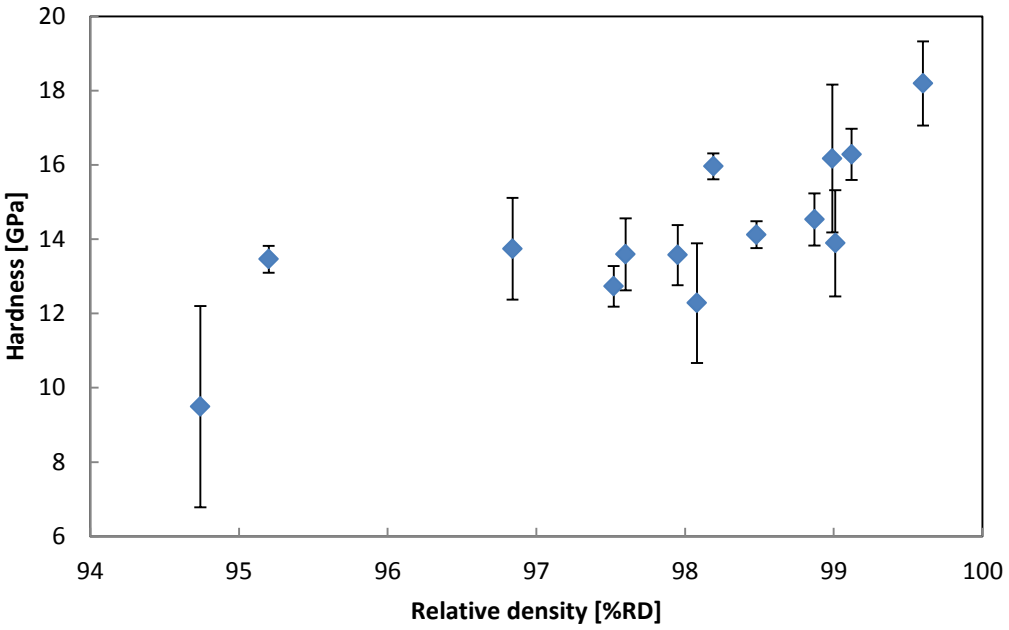

Figure 4-31: Relationship between Vickers hardness and relative density of gelcast alumina sintered at 1650°C for 3hrs.

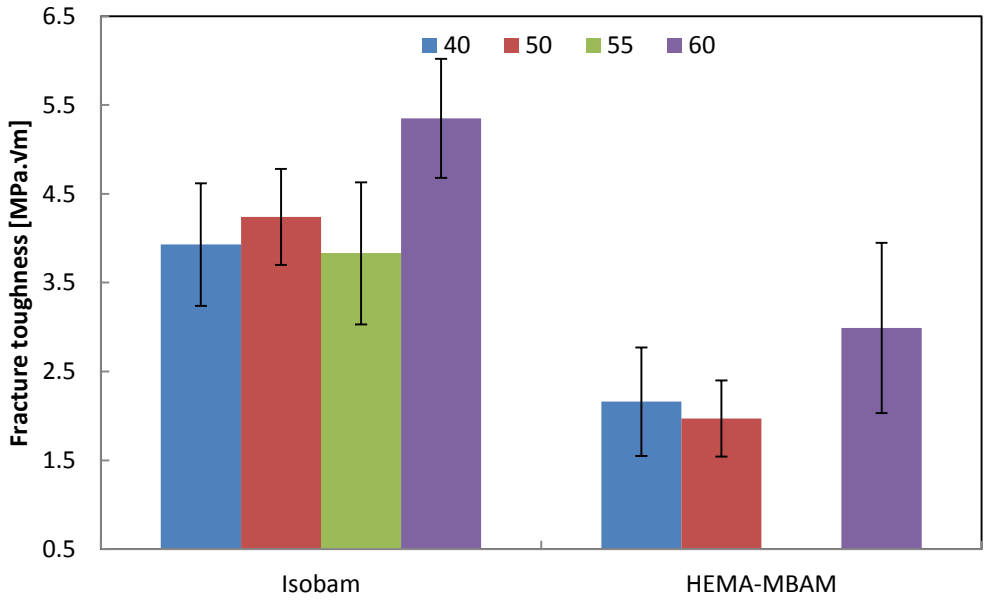

Figure 4-32: Relationship of monomer and solids loading on the fracture toughness of alumina sintered at 1650°C for 3hrs.

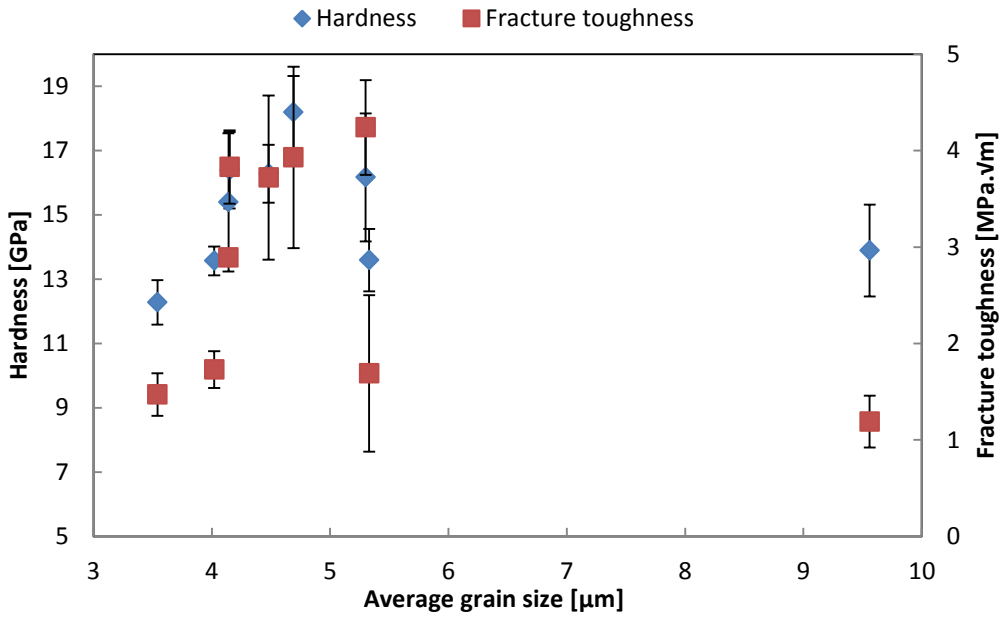

Figure 4-33: Dependence of Vickers hardness and fracture toughness on the average grain size for alumina prepared with Isobam® **at different solids loading and sintered at 1650°C.**

4.3.2. Transverse Rapture Strength

The ball on three balls tests (B3B) was used to determine the transverse rupture strength of the sintered gelcast parts. Samples were selected from those prepared by using HEMA-MBAM and those prepared using Isobam® as shown in Table 4-14. The statistical analysis of the strength measurements were performed according to EN 843-5 [55]. The representative mean (σ_{mean}) and characteristic strength (σ_0) were determined using Weibull distribution and the probability of survival (Ps) being indicative of that at which the sample would have a probability of survival (Ps) of 37 % and is presented in Figure 4-34. The Weibull parameters (σ_0) and Weibull modulus, m (Figure 4-35), were determined graphically using the probability of survival and the Weibull distribution as described by Equations 4-7 and 4-8.

$$Ps(\sigma) = exp\left[\left(\frac{\sigma}{\sigma_0}\right)^{-m}\right]$$ Equation 4-7

$$\ln\left\{ln\left[\frac{1}{Ps}\right]\right\} = mln\left(\frac{\sigma}{\sigma_0}\right)$$ Equation 4-8

Where:

σ = transverse rupture strength (MPa),

$\sigma_{0 =}$ characteristic strength found at a probability of survival of 37% (MPa),

P_s = Probability of survival and

m = Weibull modulus

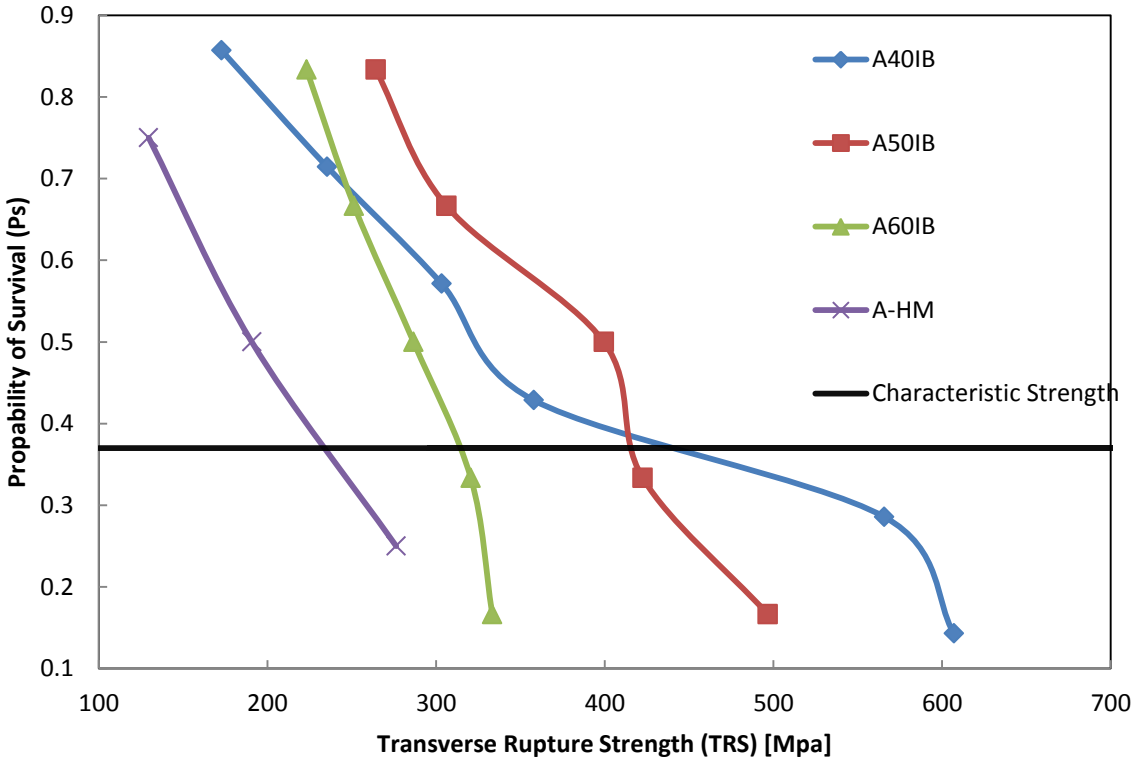

Figure 4-34: Relationship between the probability of survival and the transverse rapture strength. The strength at a probability of 0.37 is shown.

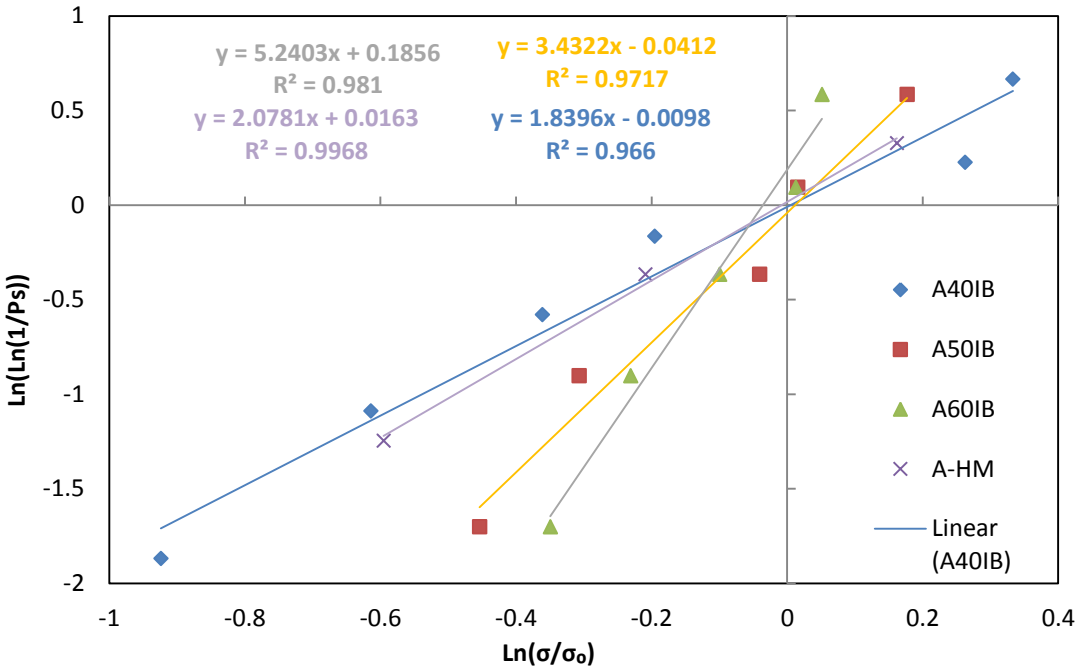

Figure 4-35: Determination of the Weibull modulus using the relation in equation 4-8.

Table 4-14: Transverse rapture strength and Weibull modulus determined by using the ball on three balls (B3B) test.

Composition	Relative density (%)	Fracture strength (MPa)	Critical flaw size (µm)	Fracture toughness (MPa.√m)	Vickers hardness (GPa)
A40IB	98.13	373.66±65.84	35.23	3.93	18.89
A50IB	98.85	377.79±33.97	9.38	4.24	16.17
A60IB	97.94	282.98±16.86	14.21	5.34	15.39
A-HM	95.84	198.86±34.74	12.79	2.99	15.09

4.3.3. Fracture

The samples tested all fractured into three pieces as shown in Figure 4-36. The fracture initiated at the centre on all the tested samples and all samples fractured into three pieces. Figure 4-37 shows the images obtained from the SEM of fracture surfaces of the samples. The arrows on the fractured surfaces indicate the points where the fracture initiated. Both intergranular and intragranular fractures were observed on the SEM images as the crack propagated through the samples.

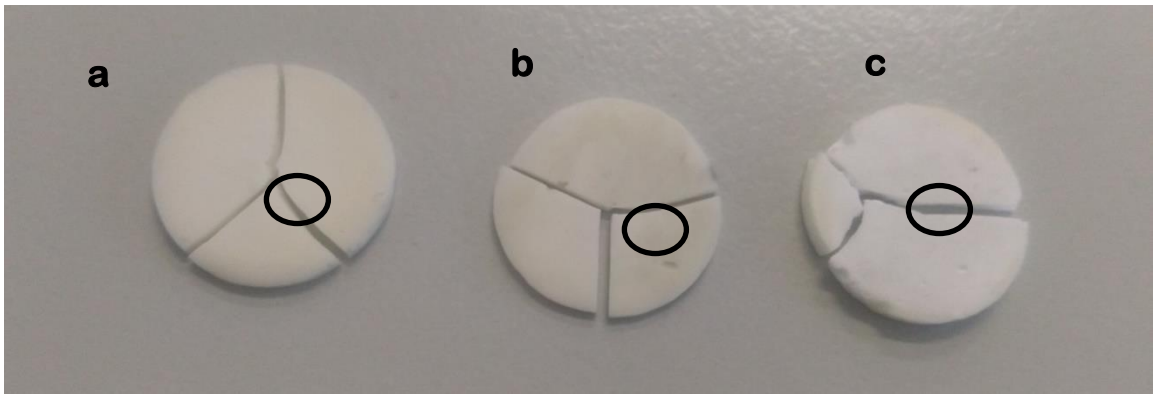

Figure 4-36: Fracture patterns of Al_2O_3 discs tested using the ball on three balls test assembly a) 40vol%, b)50vol% and c) 60vol% solids loading using Isobam® . The circles show the area of the fracture origin.

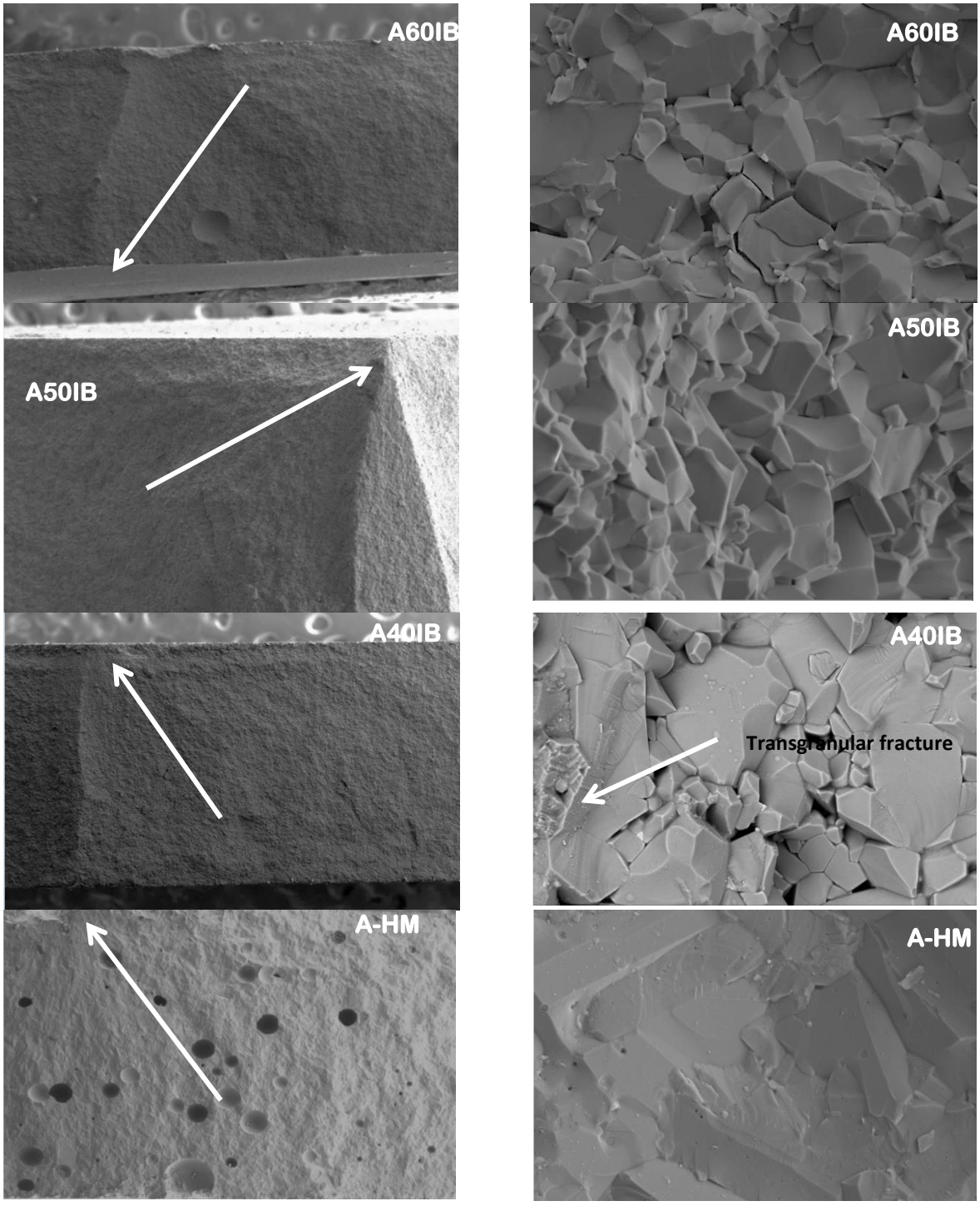

Figure 4-37: SEM micrographs showing the microstructure of 60 vol% , 50 vol%, 40 vol% and (A_HM) HEMA-MBAM fractured gel cast alumina sintered at 1650°C.

Chapter 5 : Discussion

The main goal of this investigation was to determine the practicality of combining additive manufacturing and gelcasting to produce complex shaped alumina parts. This was achieved by investigating the near net shape forming of gelcasting using additive manufactured moulds and varying the following parameters:

1. Monomer systems that result in the highest sintered density (>99% relative density). The monomer systems were chosen with regards to low toxicity, ease of suspension preparation, ability to handle high solids loading and environmental friendliness.
2. The de-airing techniques to remove air bubbles trapped in the prepared ceramic suspensions were investigated.
3. The sintering temperature was varied and the optimum temperature that lead to a relative density as high as 99.6% was selected.
4. Characterisation was done on the sintered samples, to determine their physical and mechanical properties and how this procedure may be useful in the advanced ceramics industry.

This chapter details the correlation between the processing parameters and the mechanical properties of the final ceramic components that can be produced using this technique. The obtained results were compared with those that exist in literature and conclusions drawn from these. The strength, limitations and weaknesses of the proposed fabrication technique are presented and their implications on current processing of complex shaped ceramics are detailed. From this discussion, conclusions and recommendations were drawn.

5.1. Powder Preparation

The starting alumina powder consisted of particles with a size shown by the D_{10}, D_{50} and D_{90} (Figure 4-1). The measured D_{50} particle size was similar to the particle size as stated by the powder supplier. There were some larger particles but these were the result of agglomeration. These large agglomerates were broken up during the milling process. The D_{50} was used as the mean particle size and taken to be representative of the overall powder sample used for production of parts. The particle size distribution obtained by Malvern laser analysis was confirmed by SEM (Figure 4-2). X-ray diffraction was done on the alumina powder (Figure 4-3) to identify the crystal structure. The XRD peaks were found to correlate to α-alumina peaks when using the brucker database.

5.2. Preparation of Suspensions

The preparation of colloidal suspensions must ensure the highest level of preservation of microscopic properties of the starting powder. The most critical factor in colloidal processing of ceramics is the production of stable suspensions with a high solids loading and low viscosity that will ensure flowability of the slurry [56]. This is achieved by controlling the solution chemistry and manipulation of the interparticle forces to create a stable suspension, where every particle is separated from one another. A stable colloidal suspension is achieved by adding a dispersant that will ensure a low viscosity and a zeta potential that is greater than +30 or less than -30mV.

5.2.1. Optimal Dispersion

In the preparation of stable colloidal suspensions, the addition of a dispersant imparts low viscosity and ensures that the powder particles do not settle [57]. There exists a critical amount of electrolyte that needs to be added to achieve a good stability of the suspension and ensure a low viscosity. An excess of the electrolyte results in an increase in viscosity. Therefore the saturation limit of the dispersant or an optimum of dispersant to be added to the suspension was determined and was presented in Figure 4-5 and Figure 4-6 for ammonium polyacrylic acid (APAA) and Isobutylene maleic-anhydride (Isobam®) dispersants, respectively. The point of minimum viscosity for both systems was determined to be 1vol% and 0.3wt% in relation to the ceramic powder added, respectively.

This result is in agreement with those found by [25], where stable suspensions were created by using a concentration of 1mL/100g Al_2O_3 powder using ammonium polyacrylic acid salt as a dispersant. For the Isobam® copolymer, the dispersant amount was in agreement with that found by scholars; Qin, et al., (2014) [24] and Sun, et al., (2014) [26]. Sun, et al., (2015) [26] found that an addition of 0.3wt% Isobam® to 45vol% alumina powders gave a viscosity as low as 1.4Pa.s at a shear rate of $100s^{-1}$. However, the polymer addition is depended on the nature of the powder and the particle size. Zhang, et al. (2015) [28] studied the effect of the copolymer addition on MgO-Al_2O_3 spinel and found that the optimum dispersant amount was 0.7wt%. It was reported that the co-ordination number of the -COO- group from the hydrolysis of Isobam® on the surface of the spinel caused a change in the zeta potential. In this study, the amount of Isobam® addition was kept at 0.3wt% for all powders. This lead to a low solids content when MgO was added to the Al_2O_3 powder, thus a low densification was reported.

5.2.2. Zeta potential

The zeta potential is the measure of the forces applied on each particle when it is submersed in an aqueous medium. Suspension stability rests on the alteration of the surface chemistry of the particles to ensure that all particles repel each other sufficiently to create a stable suspension. The zeta potential of alumina suspensions was studied and is shown in Figure 4-4. In the absence of a dispersing agent the zeta potential changes from 51.6mV at a pH of 1 to a zeta potential of -35.65mV at a pH of 12. Thus, the preparation of a highly stable alumina suspension by altering the pH can only be realized at high or low pH. The Isoelectric Point (IEP) of alpha alumina occurs at a pH of 8 to 9, and is in agreement with those found in literature.

In Figure 4-4, it is evident that the addition of a dispersing agent shifts the IEP point to a pH of 2.2 and the suspension was found to be stable at a pH above 8. Therefore, ammonium poly acrylic acid provides a more negative zeta potential value. This suggests that both poly acrylic acid and Isobam® are effective at creating repulsive electrostatic forces between the grains of material. The APAA dispersant absorbs into the surface of the alumina particles and provides electrostatic stabilisation, thus reducing the interaction between particles and prevents the formation of agglomerates.

5.2.3. Viscosity- shear relationship

Figure 4-7 and Figure 4-8 shows the viscosity-shear relationship of alumina suspensions at different solids content and different monomer systems. All suspensions showed a shear thinning behaviour at a wide range of shear rate. The shear thinning behaviour of suspensions is an important characteristic. When the suspension is at rest the viscosity is high and this prevents the alumina particles from settling and ensures a homogeneous distribution of all components of the suspension. An increase in shear rate leads to a decrease in viscosity ensuring a steady flow of the suspension into the mould during the casting process. Thus, shear thinning facilitates the pouring and ensures the precise control of the net shape during casting. This phenomenon was also reported by Jabbari, et al. (2016) [58].

Bergstrom (1998), reported that for a shear thinning suspension at rest, its structure is close to equillibrium at low shear rates and viscous forces affect the suspension structure at high shear rates and shear thinning then occurs. This corresponded to the high shear form of the Cross equation as proposed by Cross and modelled in Figure 4-10.

The solids packing fraction in ceramic colloidal forming governs the shrinkage, cracking/ warping and the green relative density of the formed parts. Thus, an increase in the solids fraction decreases the shrinkage rate, increases the relative green density and prevents excessive cracking during drying of the gelcast parts. Therefore, a high solids fraction is desirable in the production of complex shaped advanced ceramics to achieve the desired mechanical properties.

However, high solids loading leads to an increase in the viscosity, the particles jam up due to continuous contact of all particles in the suspension. This phenomenon is detrimental to the resulting microstructure. With very high solids loading, the flowability of the suspension is affected, thus the homogeneity of the suspension is compromised and ultimately the final product.

At low solids loading, the densification during sintering is difficult due to low green densities. Other defects that results due to low solids loading are cracks and warpage that form during the drying process. This is due to the excessive amounts of solvent that needs to be removed from the green body. The strength of the gel is also affected. Gelation takes longer to occur due to a longer distance between polymer and powder particles. The polymer attaches to the surface of the powder particle and forms a gel when the suspension is at rest. The interparticle separation is greater when the amount of solvent is greater than that of the particles in the suspension by volume.

The maximum packing of a colloidal suspension is closely related to the crystal structure of the ceramic powder. For a hexagonally closed-packed alumina powder, the maximum solid loading ranged between 52 to 74vol% [50]. The maximum packing is also affected by:

1. The particle size distribution
2. The particle size
3. Flocculation tendency

The Reddy equation was used to model the solids packing for the HEMA-MBAM and Isobam® monomer systems and the maximum packing fraction was found to be 0.609 and 0.559 respectively as illustrated in Figure 4-11. The maximum achievable

solids fraction for the alumina powder is comparable to the expected value for hexagonally closed packed structured powders.

The particle size distribution as shown in Figure 4-1 also played an important role on the maximum solids loading, as the particle size is broad in the range of 0.4 to 1.8μm, thus leading to a high solids fraction. However, the particle shape had a negative effect. Barnes et al. (1989) [50] stated that any deviation from spherical particles results in an increase in viscosity for the same solids loading. Figure 4-2 shows the SEM micrograph of the alumina particles, and it is clear that the particles deviate from spherical and have an irregular shape and is this in agreement with the work by Barnes et al.

5.2.4. Effect of Monomer

The effect of monomer was investigated by comparing two different gel binder systems, i.e. hydroxyethylene-methacrylate (HEMA) cross-linked with methylenebisacrylamide (MBAM) [HEMA-MBAM] and a co-polymer of Isobutylene maleic anhydride (Isobam®). The monomer content in the suspension is a critical factor, because after polymerisation the polymer networks are responsible for holding the ceramic particles together and providing mechanical strength [59].

The HEMA-MBAM system required approximately 20wt% organic content to be added to the suspension. However, more organic content in the suspension requires a longer binder removal time. A high organic content makes it difficult to get full densification during sintering because as the binder is removed, pores are likely

created. This is supported by comparing the densities between parts created using HEMA-MBAM and Isobam®. The relative sintered density was found to be higher for Isobam® which only required 0.3wt% organics to be removed.

The HEMA-MBAM system had a disadvantage compared to Isobam®, whereby an initiator and catalyst are required for the polymerisation to occur. The initiator and catalyst are essential to start the polymerisation process. The amounts of these additives control the idle time that allows for the pouring of the suspension into a mould and the start of polymerisation. Too little initiator and catalyst leads to a longer idle time and the suspension starts to dry prior to polymerisation leading to defects such as pores in the final part. While excess amounts of initiator and catalyst leads to shorter idle time, where the polymerisation occurs during the mixing stage and make pouring into the mould difficult. Polymerisation leads to a rapid increase in the viscosity of the suspension and this leads to agglomerates and pores dominating in the cast part and unfilled spaces are found in the mould.

Careful consideration of the idle time is essential, the idle time should not be too short to accommodate mixing, de-airing and pouring because if it is too short this leads to defects that affect the mechanical properties of the final part. High initiator content leads to the creation of too many free radicals that start polymerisation and end with a lot of short polymer chains, however, the creation of fewer long polymeric chains is ideal [59].

5.3. Near Net Shape Forming

Near net shaping means forming a part with dimensions as close to the final dimensions, while minimising post sintering processing. Gelcasting allows for the near net shape fabrication of ceramics across a wide range of complex geometries. Gelcasting involves the formulation of a suspension. The process also involves the design and production of a customised mould that will allow for close dimensional tolerance specifications.

For complex shapes 3D modelling is preferred [30], this allows for the fabrication of tooling that can be adjusted electronically rather than physically. The design of a mould forms an integral part of the forming process. The mould must allow for shrinkage to occur during the gelation process and minimise stresses on the cast part. Therefore softer mould materials are preferable for complex shaped parts, as these can deform under stress [25].

In this study, the fabrication of complex shaped parts was achieved by casting alumina suspensions onto 3D printed ABS plastic moulds. Where, the 3D design was achieved by using AutoCAD® which has the ability to produce tooling with features such as undercuts and sharp corners. The 3D printed ABS moulds were selectively dissolved in acetone at 35°C during the demoulding process. This allowed for the complex shaped part to dry without restrictions from the mould material and internal stresses were minimised.

Contrary to Dhara, et al., (2002) who found that the presence of vents in closed moulds were beneficial as they facilitated the release of trapped air during casting. The presence of vents prevents the collapse of air bubbles onto the slurry, thus preventing excess porosity.

Compared with traditional moulds used in a gelcasting process, combining gelcasting with 3D printing is efficient in fabricating complex ceramic parts, and it is more suitable for new product development and low-volume production of complex-shaped ceramic parts. This process can be tailor made for a specific purpose at a relatively low cost because the moulds are designed and modified using CAD.

5.4. Optimization of sintering

5.4.1. Factors affecting densification

The effects of the sintering temperature on the densification of the gelcast alumina parts was investigated, with the aim of achieving densification greater than 99% relative to the theoretical density of alumina taken as 3.97g/cm^3. The sintering temperature was varied from 1450 to 1700°C by pressure-less sintering in a muffle furnace in air. The densification increased with increased temperature from 1450 to 1650°C and decreased at 1700°C due to excessive grain growth which was expected during pressure-less sintering at high temperatures [17].

The samples sintered at low temperatures (1450-1550°C) had poor densification with high amounts of open porosity, and this was confirmed by their microstructures that had many pores (Figure 4-17). The low densification was caused by incomplete sintering at low sintering temperatures when pressure or a protective atmosphere was not applied [17]. The highest density was achieved at 1650°C. The decrease in density at the sintering temperature of 1700°C suggesting that further temperature increases would produce no improvements in densification.

During pressure-less sintering, the degree of densification is controlled by surface or volume diffusion [17]. These processes allow for a reduction in surface energy of the system and control the densification and produce either normal or abnormal grain growth [60]. Although densification above 99% was achieved for samples prepared with Isobam® when sintering at 1650°C, porosity was observed in all the sintered

samples (Figure 4-18). Corresponding to the increased densification, the amount of porosity decreased, however, this was accompanied by excessive grain growth along with pore growth on the triple boundary points. This was observed in Figure 5-1, where the densification reached 99.4% when sintering 60vol% solids loading at 1650°C resulting in the largest grains (9.2µm) and several pores in excess of 3µm.

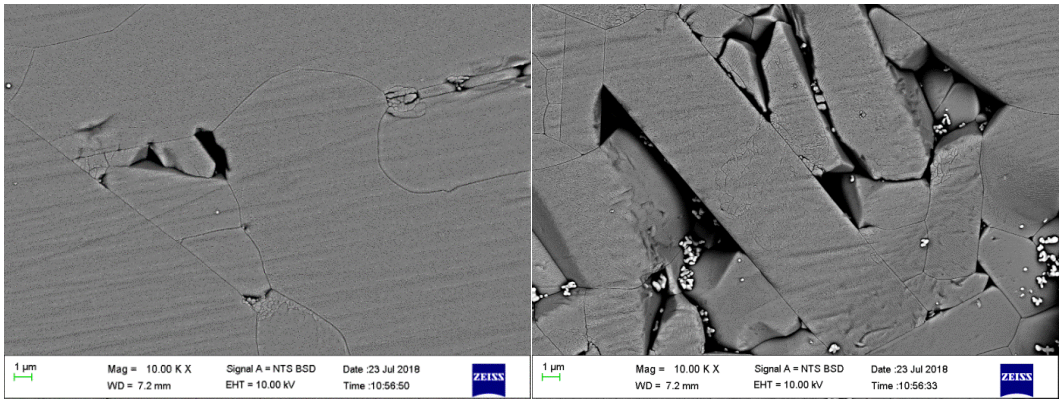

Figure 5-1: SEM micrograph showing a sample with large elongated grains.

The addition of 600 ppm MgO as a sintering aid slightly improved the densification (Table 4-11) [39]. Although the addition of 600 ppm MgO in the samples achieved higher densification compared to those samples without MgO, their final density was still less than the desired 99%. A further addition of MgO from 600ppm to 1vol% to achieve the formation of a spinel, resulting in a body with a high porosity (Figure 4-25). This was due to the use of an inhomogeneous colloidal suspension and low solids loading (32vol%). This indicated that dense ceramic bodies with good properties cannot be obtained from sintering green bodies with agglomerates and pores, this was shown in can be seen in the microstructures (Figure 4-25).

To improve the densification, longer de-airing times, defoaming agents and optimisation of solids loading to minimise trapped air bubbles in the suspension were applied. This was achieved by:

i) The addition of a defoaming agent which lowers the interfacial energy between water and air, thus decreasing the turbulence during mixing,

ii) Longer de-airing times up to 120 minutes over a mechanical shaker that prevents the collapse of the air bubbles in the suspension [5],

iii) Applying a demoulding agent (petroleum jelly) to eliminate the surface tension on the mould and reduce the formation of bubbles during pouring. This was accompanied by mechanical shaking of the mould to ensure complete filling and eliminate bubbles as casting was carried out in air.

The improved control of the processing parameters by applying these techniques, i.e. increasing de-airing time and improved casting method, facilitated the elimination of porosity and increased shrinkage, leading to good densification (>99%) in the alumina samples (Figure 4-23 and Table 4-10). Elimination of porosity in the sintered parts by improved de-airing was confirmed by SEM images (Figure 4-22).

5.5. Mechanical Properties

5.5.1. Hardness

In this work Al_2O_3 powder was gelcast and sintered using pressure-less sintering at 1650˚C, in air for 3 hours. The Vickers hardness of the Al_2O_3 sample was measured in GPa for a 5 kg load. The hardness behaviour of the produced alumina parts (Table 4-13) differed significantly between the different monomers and solids loading, as shown in Figure 4-30. The sample prepared by using Isobam® co-polymer and 40vol% solids loading had the highest hardness of 18.89GPa at a relative density of 99.6%RD The results obtained in this study were compared with the results obtained by other authors [8, 26].

The maximum hardness was observed for a sample gelcast using Isobam® and 40 vol% solids loading (18.2GPa) this was due to the high relative density of 99.6% and no grain growth was observed. Unlike the 60vol% solids loading where a relative density of 99.01% was achieved with a hardness of 13.89GPa where the resulting low hardness was observed to be due to pre-existing cracks in the material as well as the large grain size of 9μm.

The hardness for all the gelcast components was increased with increasing densification, and was expected to show a correlation to the solids loading of the starting suspension. It was found that the hardness decreases as the solids loading is increased in Figure 4-30 for both Isobam® and for HEMA-MBAM fabricated samples, the hardness increases as the solids loading is increased. These results are in

agreement with those obtained by Liu, et al., (2002) where an increase in the mechanical properties for solids loading upto 50vol% was observed.

5.5.2. Fracture Toughness

The average values of the fracture toughness at different solids loading and relative density are reported in Table 4-13. The fracture toughness decreases with an increase in the solids loading for both the monomer systems tested (Figure 4-32). The fracture toughness shows a considerable scatter for both monomer systems, this was evident from the 40vol% solids loading for both monomers and 60vol% solids loading for HEMA-MBAM. The average fracture toughness of all the components tested in this study varies considerably from 1.2 to 5.5 MPa.√m. This shows the importance of understanding the influence of processing parameters that influence the microstructure, which are useful in fabricating materials with unique mechanical properties.

The correlation between the fracture toughness and the average grain size is summarised in Figure 4-33 together with the influence of grain size on the Vickers hardness. A trend where both the fracture toughness and hardness increase with an increase in grain size for fine grained alumina (<5μm) and slightly decreases for coarser grains (>5μm). This behaviour is in agreement to the general behaviour of brittle materials as stated by the Hall-Petch relationship, where an increase in grain size is detrimental for mechanical properties.

Toughening of ceramics is characterised by:

- Micro cracking around the crack tip,

- Crack deflection and
- Grain bridging.

Microstructural observations of the Vickers indentation (Figure 4-29) confirm that intergranular fracture is a characteristic feature of the materials manufactured in this work. This feature is associated with crack deflection and crack bridging toughening mechanisms as stated by Nicolletto et al., (1996) [61].

5.5.3. Transverse Rupture Strength

The parts produced using the Isobam® gel former had higher TRS than those produced by HEMA-MBAM, with 50vol% solids loading using Isobam® having the highest value followed by 40vol% Isobam® (Table 4-14). The higher TRS of the 50vol% Isobam® sintered samples was due to the composition being close to the optimum solids loading of 55vol% as determined using the Reddy model (Figure 4-11), this led to decreased porosity and a better packing of the ceramic particles in the green body [62].

The larger grain size in the 40vol% Isobam® (Figure 4-37(c)) than in the 50 and 60vol% Isobam® sample (Figure 4-37(a) and (b)) could have acted as internal defects that could have prematurely initiated the fractures, therefore, slightly lowing the TRS even though the sample had the highest hardness and fracture toughness. Large and hard grains are easier to fracture. The 60vol% Isobam® samples had a lower TRS than all the Isobam® samples due to the residual pores found in the microstructure (Figure 4-37(a)), mainly on the triple boundaries and within grains. The high solids loading led to difficulties in de-airing the suspension, which increased the volume of

trapped air, causing porosity. Pores were most likely the origin of fracture and resulted in low TRS.

All ceramic parts produced by gelcasting using HEMA-MBAM had lower TRS, because of a number of defects that resulted during the processing of the green body. These defects maybe due to the higher organic content compared to the Isobam® content. A high organic content makes it difficult to get full densification because more pores (Figure 4-37(d)) are created during binder burn-out [59]. HEMA-MBAM samples have an organic content of 10% (Table 4-8), thus the higher monomer content resulted in higher porosity after binder burn off.

The possible defects that can cause fracture in ceramic materials produced by this gelcasting method include the following:

i. Residual pores and grain growth which is a result of poor densification due to difficulties in densifying without pressure and expected grain growth during pressure-less sintering.
ii. Trapped air bubbles and agglomerates formed by inhomogenities. Although defoaming aids and de-airing techniques reduce the occurrence of air bubbles in colloidal suspension, however they cannot be completely removed and thus act as strength limiting defects.
iii. Surface defects were also found to contribute to the reduction in transverse rapture strength. These include grinding marks but more often were associated with the layer by layer nature of the 3D mould production. The nature of the mould production leaves marks on the surface of gelcast parts. If these marks are larger than the critical defect size then they too will act as strength limit defects [63]. In the case of the 50vol% Isobam® sample, no internal flaws

were detected, thus the mode of failure can be attributed to surface flaws as a result of the mould marks or grinding marks.

Chapter 6 : Conclusion

A reliable method for fabricating complex shaped alumina based ceramics by combining additive manufacturing and gelcasting was demonstrated. The mould required for gelcasting the ceramic suspension was fabricated by additive manufacturing. PLA and ABS plastic resins were used as the printing material. The experiments conducted revealed that ABS plastic provides easier demoulding by dissolution in acetone and thus facilitated easier fabrication of complex geometries. The parts produced had high densities and no surface features that could have resulted from the negative printing were observed. The properties of the produced alumina parts were highly depended on the preparation of the gelcasting suspension.

The effects of the powder properties, suspension solid content and sintering parameters on the rheological properties, properties of the green body and the properties of the resulting alumina parts were investigated. It was found that the dispersion of alumina in the premix solution containing deionised water and a monomer was highly influenced by the pH of the suspension and the amount of the dispersant added. Suspensions with a wide range of viscosity were prepared by varying the solids loading and/or the monomer content. Highly loaded suspensions were found to be beneficial in minimising the shrinkage and thus preventing cracking and warping during drying. However, inherent issues such as difficulties in de-airing, poor flowability and agglomerates were discovered. These were caused by high viscosity which was due to small inter-particle spacing caused by a high volume of ceramic particles as opposed to the wetting and dispersing agents available in the system.

The solids loading that met casting requirements and mould filling was found to be as high as 70vol% and 60vol% for HEMA-MBAM and Isobam monomers, respectively. However, the Reddy model predicted a maximum allowable solids loading of 60vol% for HEMA-MBAM and 55vol% for Isobam. This was supported by the highest relative density of 99.6% obtained at a solids loading of 40vol% for Isobam monomer. The results from the Reddy model are in agreement with the properties of the sintered parts, as the solids loading increase above the maximum allowable volume percentage the properties tend to decrease. Thus, the solid loading has a critical effect on the properties of both the green and sintered bodies. The de-airing technique and solids loading played a critical role on the final relative density and mechanical properties.

The densities and mechanical properties of the parts produced are comparable to parts fabricated by using conventional methods. Relative densities ranged between 86% and 99% depending on the solids loading, sintering temperature and deairing.

Complex shaped parts such as an impeller and a pyramid with relative densities above 99% were obtained. The formed parts made had sections that were both thick and thin. This illustrates the successful capabilities of the combined 3D printing and gelcasting method. Thus, the forming of an object by gelcasting is only limited by the availability of the mould.

It can be concluded the overall process is affected by a number of factors; such as, deairing, mould filling and demoulding, solids loading and the sintering process. The main factor being the solids loading and the choice of monomer. The efficiency of the deairing process, the mould filling and demoulding are strong functions of the solids

loading. Isobam® monomer system as the gel former was found to be the superior monomer as opposed to those tested, provided the solids loading in the starting suspension is less and/or equal the maximum allowable content for the specific ceramic powder.

Thus, negative additive manufacturing techniques used in this work combined with gelcasting using Isobam® agrees in part with the work by Sigmund, et al., (2000). The process has demonstrated that it can produce parts with high reability, sufficient strength and fewer defects. Whereas, the process is itself simple with minimal processing steps and is environmentally friendly.

Chapter 7 : Future Work

Future work needs to be conducted to investigate:

i. Whether the process will be feasible on a wide range of ceramic powders.

ii. The dimensional shrinkage needs to be investigated and incorporated to real world scenarios to enable the industrialisation of the process.

iii. The effect of the grain size on the rheology and the final microstructure must be investigated to ensure adequate control of the mechanical properties.

iv. The effect of the 3D printing process on the resulting physical appearance of the sintered parts must be investigated, in terms of the strength and fracture toughness of the ceramics fabricated.

References

[1] W. M. Sigmund, N. S. Bell and L. Bergstrom, "Novel powder processing methods for advanced ceramics," *Journal of the Americal Ceramic Society,* vol. 83, no. 7, pp. 1557-1574, 2000.

[2] F. Chabert, "Cross-linked polyvinyl alcohol as a binder for gelcasting and green machining," *Journal of the American Ceramic Society,* vol. 91, no. 10, pp. 3138-3146, 2008.

[3] A. A. Babaluo, M. Kokabi and A. Barati, "Chemorheology of alumina-aqueous acrylamide gelcasting systems," *Journal of the European Ceramic Society,* vol. 24, pp. 635-644, 2004.

[4] L. Bergstrom, "Colloidal Processing of Ceramics," in *Handbook of Applied Surface Chemistry and Colloid Chemistry*, John Wiley & Sons, 2001, pp. 201-217.

[5] M. Kokabi, A. Pirooz and M. N. Haghighi, "Gelcasting of engineering ceramics," *Iranian Polymer Journal,* vol. 7, no. 3, pp. 169-175, 1998.

[6] M. A. Janney, O. O. Omatete, C. A. Walls, S. D. Nunn, R. J. Ogle and G. Westmoreland, "Development of low toxicity gelcasting systems," *Journal of the American Ceramic Society,* vol. 81, no. 3, pp. 581-591, 1998.

[7] K. Kumela, I. Nagashima, S. Matsui and K. Mizoguchi, "Crosslinking reaction of poly(vinyl alcohol) with poly(acrylic acid) (PAA) by heat treatment: Effect of neutralization of PAA," *Journal of Applied Science,* vol. 90, pp. 2420-2427, 2003.

[8] C. A. Moorehead, V. L. Blair and J. W. Adams, "Characterisation of novel gelcasting systems to make complex shaped aluminum oxide (Al2O3) parts," US Arms research laboratory, Department of defence, Washington, 2016.

[9] J. Klein, M. Stern, G. Franchin, M. Kayser, C. Inamura, S. Dave, J. C. Weaver , P. Houk, P. Colombo, M. Yang and N. Oxman, "Additive manufacturing of optically transparent glass," *3D Printing and Additive Manufacturing*, vol. 2, no. 3, pp. 92-105, 2015.

[10] B. Utela, D. Storti, R. Anderson and M. Ganter, "A review of process development steps for new material systems in three dimensional printing (3DP)," *Journal of Manufacturing Processes*, vol. 10, pp. 96-104, 2008.

[11] A. Zocca , C. M. Gomes, E. Bernardo, R. Muller, J. Gunster and P. Colombo, "LAS glass-ceramic scaffolds by three-dimensional printing," *Journal of the European Ceramic Society*, vol. 33, pp. 1525-1533, 2013.

[12] R. Johnson, P. Biswas, P. Ramavath, R. S. Kumar and G. Padmanabham, "Transparent Polycrystalline Ceramics: An Overview," *Transactions of the Indian Ceramic Society*, vol. 71, no. 2, pp. 73-85, 2012.

[13] G. Sundararajan, P. Biswas and N. Eswara-Prasad, "Mechanical Properties of Transparent Polycryastalline Alumina Ceramics Processed Using an Environmentally Benign Thermal Gelcasting Process," *Experimental Mechanics*, vol. 53, pp. 123-129, 2013.

[14] I. Ganesh, G. Sundararajan, S. M. Olhero, P. M. Torres and J. M. Ferreira, "A novel colloidal processing route to alumina ceramics," *Ceramics International*, vol. 36, no. 4, pp. 1357-1364, 2010.

[15] W. M. Sigmund, N. S. Bell and L. Bergstrom, "Novel powder-processing methods for advanced ceramics," *Journal of the American Ceramic Society*, vol.

83, no. 7, pp. 1557-1574, 2000.

[16] "Application examples of ceramics," 2018. [Online]. Available: http://www.sanyu-tokusyu.com. [Accessed 17 05 2018].

[17] M. Barsoum, Fundamentals of Ceramics, Chap. 10, New York: McGraw-Hill, 1997.

[18] F. F. Lange, "Powder processing science and technology for increased reliability," *Journal of the American Ceramic Society,* vol. 72, pp. 3-15, 1989.

[19] J. S. Reed, Principles of Ceramics Processing, New York, USA: John Wiley & Sons Inc., 1995.

[20] R. Xie, D. Zhang, X. Zhang, K. Zhou and T. W. Button, "Gelcasting of alumina ceramics with improved green strength," *Ceramics International*, vol. 38, no. 8, pp. 6923-6926, 2012.

[21] X. Liu, Y. Huang and J. Yang, "Effect of rheological properties of the suspension on the mechanical strength of Al2O3-ZrO2 composites prepared by gelcasting," *Ceramics International*, vol. 28, no. 2, pp. 159-164, 2002.

[22] K. Prabhakaran, R. Sooraj and A. Melkeri, "A new direct coagulation casting process for alumina slurries prepared using poly(acrylate) dispersant," *Ceramics international*, pp. 978-985, 2009.

[23] J. Yang, J. Yu and Y. Huang, "Recent developments in gelcasting ceramics," *Journal of European Ceramic Society*, pp. 2569-2591, 2011.

[24] X. Qin, G. Zhou, Y. Yang, J. Zhang, X. Shu, S. Shunzo and S. Wang, "Gelcasting of transparent YAG ceramics by a new gelling system," *Ceramics International*, vol. 40, no. 8, pp. 745-750, 2014.

[25] S. Dhara, R. K. Kamboj, M. Pradhan and P. Bhargava, “Shape forming of ceramics via gelcasting of aqueous particulate slurries,” *Bulletin Materials Science,* vol. 25, no. 6, pp. 565-568, 2002.

[26] Y. Sun, S. Shimai, X. Peng, M. Dong, H. Kamiya and S. Wang, “A method for gelcasting high-strength alumina ceramics with low shrinkage,” *Journal of Materials Research ,* vol. 29, no. 2, pp. 247-251, 2014.

[27] Y. Sun, S. Shimai, X. Peng, G. Zhou and S. Wang, “Gelcasting and vaccum sintering of translucent alumina ceramics with high transparency,” *Journal od Alloys and Compounds,* vol. 641, pp. 75-79, 2015.

[28] P. Zhang, P. Liu, Y. Sun, J. Wang, Z. Wang, S. Wang and J. Zhang, “Aqueous gelcasting of the transparent MgAl2O3 spinel ceramics,” *Journal of Alloys and Compounds,* vol. 646, pp. 833-836, 2015.

[29] A. G. Cooper, S. Kang, J. Stampfl and F. B. Prinz, “Fabrication of ceramics parts for a miniture jet engine application using mold SDM.,” *Ceramic Transactions,* vol. 108, pp. 389-398, 2000.

[30] T. O. Henriksen, “Near net shaping of ceramic components- Plant tour of a custom manufacturer,” *American Ceramic Society Bulletin,* vol. 94, no. 3, 2015.

[31] J. Chimento, M. J. Highsmith and N. Crane , “3D printed tooling for thermoforming of medical devices,” *Rapid Prototyping Journal,* vol. 17, no. 5, pp. 387-392, 2010.

[32] J. Yoo, M. J. Cima, S. Khanuja and E. M. Sachs, “Structural Ceramic Components by 3D Printing”.

[33] A. Zocca, P. Lima and J. Gunster, “LSD-based printing of alumina ceramics,” *Journal of Ceramic Science and Technology ,* vol. 8, no. 1, pp. 141-148, 2017.

[34] R. M. German, Sintering theory and practice, New York: John Wiley & sons, 1996.

[35] J. L. Shi, "Relation between coarsening and densification in solid state sintering of ceramics: Experimental test on superfine Zirconia powder compacts," *Journal of Materials Research,* vol. 14, no. 4, pp. 1389-1397, 1999.

[36] S. I. Bae and S. Baik, "Critical concentration of MgO for the prevention of abnormal grain growth in alumina," *Journal of the American Ceramic Society,* vol. 77, no. 10, pp. 2499-2504, 1994.

[37] W. R. Matizamhuka, "Spark plasma sintering (SPS) - an advanced sintering technique for structural nanocomposite materials," *The Journal of the Southern African Institute of Mining and Metallurgy,* vol. 116, pp. 1171-1179, 2016.

[38] M. N. Rahaman, Sintering of Ceramics, Taylor and Francis, 2007.

[39] A. Krell, P. Blank, H. Ma, T. Hutzler and M. Nebelung, "Processing of high-density submicrometer Al2O3 for new applications.," *Journal of the American Ceramic Society,* vol. 86, pp. 546-553, 2003.

[40] R. L. Coble, "Transparent alumina and method of preparation," 20 March 1962. [Online]. Available: https://www.google.com/patents/US3026210. [Accessed 09 January 2018].

[41] A. Z. Azhar, H. Mohamad, M. M. Ratnam and Z. A. Ahmad, "The effects of MgO addition on microstructure, mechanical properties and wear perfomance of zirconia-toughened alumina cutting inserts," *Journal of Alloys and Compounds,* vol. 497, pp. 316-320, 2010.

[42] M. Heraiz, A. Merrouche and N. Saheb, "Effect of MgO addition and sintering parameters on mullite formation through reaction sintering kaolin and alumina,"

Advances in Applied Ceramics, vol. 105, no. 6, pp. 285-290, 2006.

[43] M. Mastersizer, "Malvern Mastersizer Manual," [Online]. Available: www.malvern.co.uk/ms2000. [Accessed 24 05 2017].

[44] C. Tallon and G. V. Franks, "Recent trends in shape formingfrom colloidal processing: A review," *Journal of the Ceramic Society of Japan,* vol. 119, no. 3, pp. 147-160, 2011.

[45] L. Janse van Rensburg, Interviewee, *Design and manufacturing of an environmental chamber.* [Interview]. 2018.

[46] G. Goljahi and C. S. Lynch, "Effects of electric field on the fracture toughness (K1c) of ceramic PZT," *Smart Materials and Structures,* vol. 22, no. 9, 2013.

[47] G. R. Anstis, P. Chantikul, B. R. Lawn and D. B. Marshall, "A critical evaluation of indentation techniques for measuring fracture toughness: I, direct crack measurements," *Journal of the American Ceramic Society ,* vol. 64, no. 9, pp. 533-538, 1981.

[48] A. Borger, P. Supancic and R. Danzer, "The ball on three balls test for strength testing of brittle discs-Stress distribution in the disc.," *Journal of the European Ceramic Society,* vol. 22, pp. 1425-1436, 2002.

[49] M. Leoben, "Montanuniversitat Leoben, Institute of Structural and Functional Ceramics," 2018. [Online]. Available: http:/www.isfk.at/de/960/. [Accessed 03 September 2018].

[50] H. A. Barnes, J. F. Hutton and K. Walerr, Introduction to Rheology, Oxford, 1989.

[51] G. Trefalt and M. Borkovec, "Overview of DVLO theory," 29 09 2014. [Online]. Available:

http://www.colloid.ch/grouppage/pdfs/Overview_DLVO_Theory1.pdf. [Accessed 25 10 2018].

[52] R. P. Chhabra, "Non-Newtonian Fluids: An Introduction," in *SERC School-cum-Symposium on Rheology of Complex Fluids*, Chennai, India, 2010.

[53] J. J. Reddy, "Novel method for assessment of critical powder packing during powder forming," *Powder Metallurgy,* vol. 39, no. 4, pp. 281-285, 1996.

[54] K. Hammad and G. Vradis , "Flow of non-Newtonian Bingham plastic through an axisymmetric sudden contraction: Effects of Reynolds and yield numbers.," in *ASME Fluids Engineering Division Summer Meeting.*, 1994.

[55] *EN 843-5. Advanced technical ceramics-Mechanical properties of monolithic Ceramics at room temperature. Part 5: Statistical analysis,* London, UK: British Standard Institute, 2006.

[56] K. Cai, Y. Huang and J. Yang, "Alumina gelcasting by using HEMA system," *Journal of the European Ceramic Society,* pp. 1089-1093, 2005.

[57] A. Tsetsekou, C. Agrafiotis and A. Milias, "Optimization of the rheological properties of alumina slurries for ceramic processing applications. Part I: Slip-casting," *Journal of the European Ceramic Society,* vol. 21, pp. 363-373, 2001.

[58] M. Jabbari, R. Bulatova, A. I. Tok, C. R. Bahl, E. Mistoulis and J. H. Hattel, "Ceramic tape casting: A review of current methods and trends with emphasis on rheological behaviour," *Materials Science and Engineering B,* vol. 212, pp. 39-61, 2016.

[59] A. Szudarska, D. Guryniuk, T. Mizerski and M. Szafran , "Gelcasting of alumina with application of new monomer synthesized from xylitol," *Archives of Metallurgy and Materials,* vol. 58, no. 4, pp. 1299-1303, 2013.

[60] J. F. Roy, M. Descemond, C. Brodhag and F. Thevenot, "Alumina microstructural behaviour under pressureless sintering and hot pressing," *Journal of the European Ceramic Society,* vol. 11, pp. 325-333, 1993.

[61] G. Nicoletto, A. Tucci and L. Esposito, "The effect of microstructure on fracture toughness of polycrystalline alumina," *Fatigue and Fracture of Engineering Materials and Structures,* vol. 19, no. 1, pp. 119-128, 1996.

[62] Y. Sun , S. Shimai, X. Peng, G. Zhou and S. Wang , "Gelacsting and vaccum sintering of translucent alumina ceramics with high transparency.," *Journal of Alloys and Compounds ,* vol. 641, pp. 75-79, 2015.

[63] E. Feilden, G. T. Blanca, F. Giuliani, E. Saiz and L. Vandeperre, "Robocasting of structural ceramic parts with hydrogel inks," *Journal of the European Ceramic Society,* vol. 36, pp. 2525-2533, 2016.

Appendices

Appendix A: Suspension Characteristics

A.1. Cross Modelling

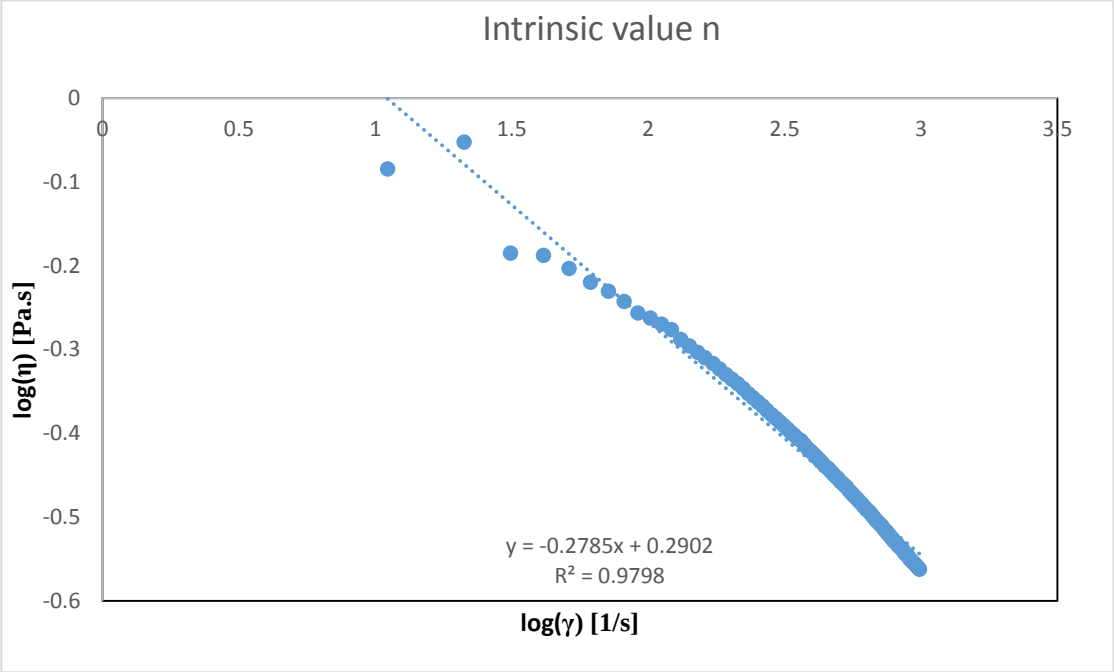

Figure A-1: Determination of flow behaviour index

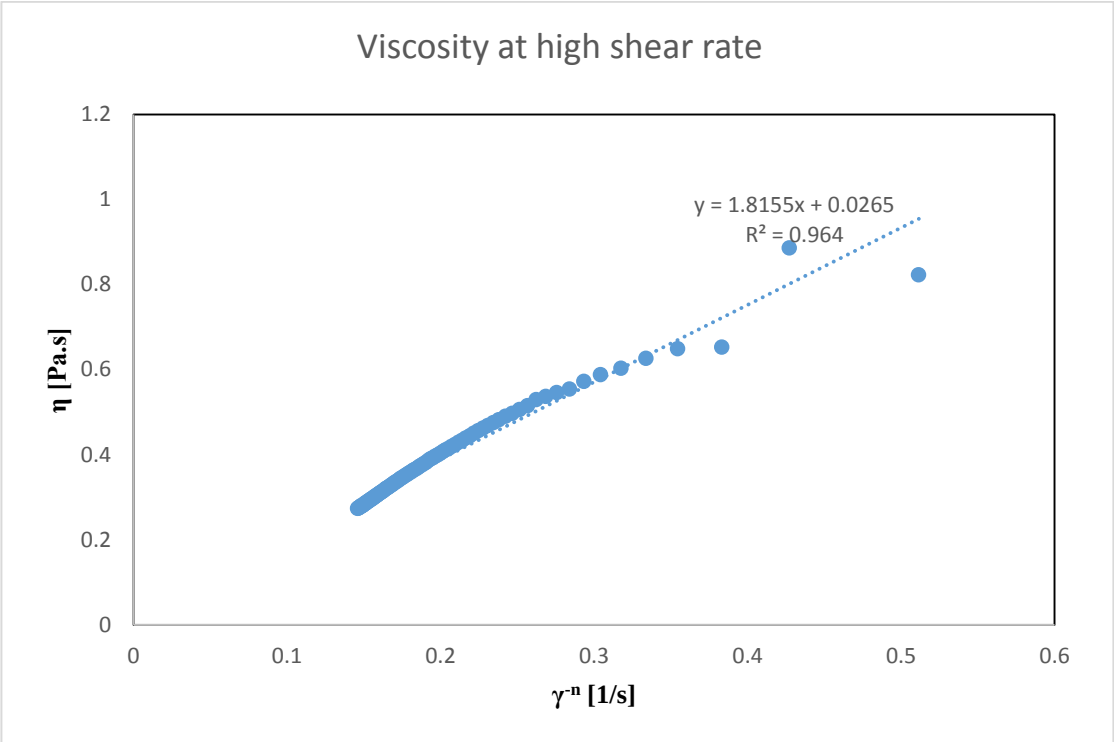

Figure A-2: Determination of Cross parameter, the viscosity at very high shear rates.